MoDOT

Research, Development and Technology Division

RDT 99-004
Final Report

Field Testing and Load Rating Procedures for Steel Girder Bridges

RI 97-3

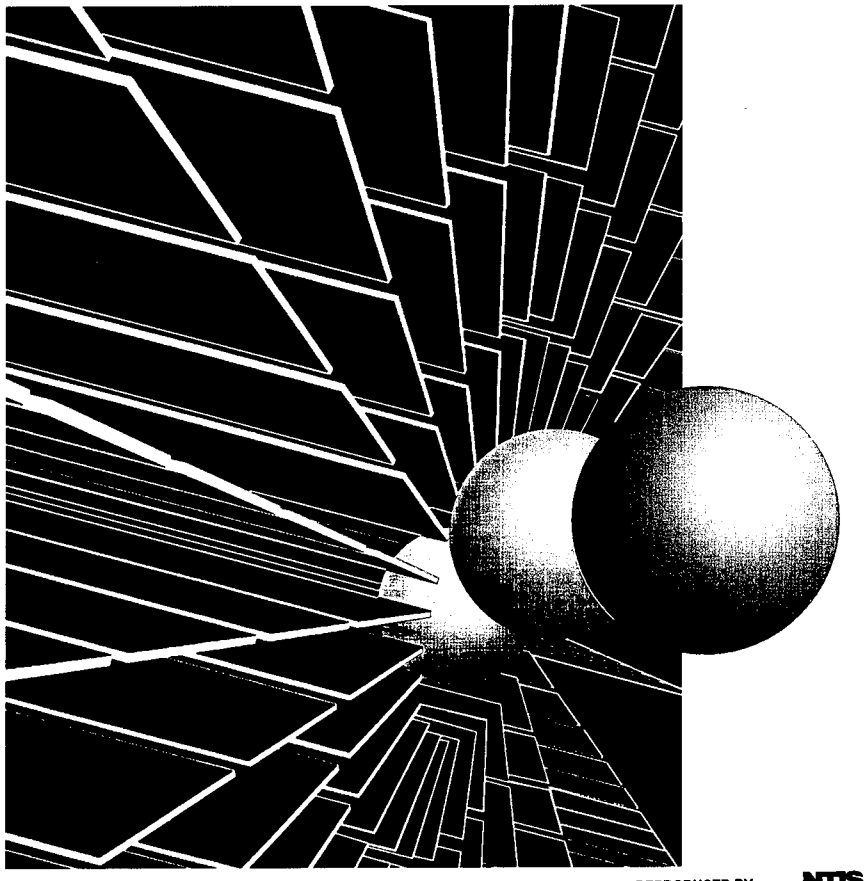

May, 1999

TECHNICAL REPORT DOCUMENTATION PAGE

1. Report No.	2. Government Accession No.	3. Recipient's Catalog No.
RDT 99-004		

4. Title and Subtitle	5. Report Date
FIELD TESTING AND LOAD RATING PROCEDURES FOR STEEL GIRDER BRIDGES	May 1999
	6. Performing Organization Code

7. Authors	8. Performing Organization Report No.
Michael G. Barker, Cory M. Imhoff, W. Travis McDaniel, and Troy L. Frederick	RI 97-3

9. Performing Organization Name and Address	10. Work Unit No.
The Curators of the University of Missouri Office of Sponsored Program Administration 310 Jesse Hall Columbia, MO 65211	11. Contract or Grant No.

12. Sponsoring Agency Name and Address	13. Type of Report and Period Covered
Missouri Department of Transportation Research, Development and technology Transfer P.O. Box 270 Jefferson City, MO 65102	Final Report
	14. Sponsoring Agency Code MoDOT

15. Supplemental Notes

This investigation was conducted in cooperation with the U.S. Department of Transportation, Federal Highway Administration

16. Abstract

Many of the nation's bridges are posted for restricted truck loading. Analytical capacity rating procedures tend to underestimate the true stiffness and overestimate the response of bridges. Research has shown that in most cases, bridges exhibit capacities higher than analytical load capacity rating predictions. These rating procedures are based on conservative design assumptions that do not always represent the true bridge behavior. Testing bridges in the field has demonstrated this additional capacity and bridge field testing has become an acceptable means to determine a more accurate estimate of a bridge's safe capacity.

Many factors not considered in the design process contribute to the response of a tested bridge. Several of these, like the actual load distribution and additional system stiffness from curbs and railings, are welcome benefits and can be used to increase weight limits on bridges. However, there are also contributions from bearing restraint forces and unintended composite action that may not be reliable during the service life of the structure. Determining how much of the increase in capacity is acceptable is difficult.

This report presents systematic field test rating procedures that separate and quantify these contributing factors so that owners may remove unwanted contributors and retain the reliable benefits. An efficient test plan is applied to a three-span steel girder bridge to demonstrate the procedures. The bridge is currently posted for restricted lanes and loads using allowable stress rating procedures. Field test results show that the posted capacity can safely be raised near (opening the bridge to two lanes of traffic) or above (maintaining a single lane) legal AASHTO H20 truck loads.

Even though field testing has become an acceptable means to determine a more accurate estimate of a bridge's safe capacity, field testing can be a time consuming and expensive endeavor. This report presents an efficient modular field testing system and the application of the system to a steel girder bridge. The "plug-and-play" data acquisition vehicle and supporting equipment has great potential for economical field testing.

17. Keywords	18. Distribution Statement
Load Rating, Field testing, Bridge Evaluation, Posting	No Restrictions.

19. Security Classification (of this report)	20. Security Classification (of this page)	21. No of Pages	22. Price
Unclassified	Unclassified	177	

Form DOT F 1700.7 (06/98)

FIELD TESTING AND LOAD RATING PROCEDURES FOR STEEL GIRDER BRIDGES

Prepared For
MISSOURI DEPARTMENT OF TRANSPORTATION

By
Michael G. Barker, PE
Cory M. Imhoff
W. Travis McDaniel
Troy L. Frederick

University of Missouri - Columbia

May 1999

in cooperation with
U.S. Department of Transportation
Federal Highway Administration

ABSTRACT

Many of the nation's bridges are posted for restricted truck loading. Analytical capacity rating procedures tend to underestimate the true stiffness and overestimate the response of bridges. Research has shown that in most cases, bridges exhibit capacities higher than analytical load capacity rating predictions. These rating procedures are based on conservative design assumptions that do not always represent the true bridge behavior. Testing bridges in the field has demonstrated this additional capacity and bridge field testing has become an acceptable means to determine a more accurate estimate of a bridge's safe capacity.

Many factors not considered in the design process contribute to the response of a tested bridge. Several of these, like the actual load distribution and additional system stiffness from curbs and railings, are welcome benefits and can be used to increase weight limits on bridges. However, there are also contributions from bearing restraint forces and unintended composite action that may not be reliable during the service life of the structure. Determining how much of the increase in capacity is acceptable is difficult.

This report presents systematic field test rating procedures that separate and quantify these contributing factors so that owners may remove unwanted contributors and retain the reliable benefits. An efficient test plan is applied to a three-span steel girder bridge to demonstrate the procedures. The bridge is currently posted for restricted lanes and loads using allowable stress rating procedures. Field test results show that the posted capacity can safely be raised near (opening the bridge to two lanes of traffic) or above (maintaining a single lane) legal AASHTO H20 truck loads.

Even though field testing has become an acceptable means to determine a more accurate estimate of a bridge's safe capacity, field testing can be a time consuming and expensive endeavor. This report presents an efficient modular field testing system and the application of the system to a steel girder bridge. The "plug-and-play" data acquisition vehicle and supporting equipment has great potential for economical field testing.

ACKNOWLEDGMENTS

The authors wish to express gratitude to several people and organizations that helped make this work possible. The Missouri Department of Transportation, Pat Martens of the District 6 office, and especially Mr. Paul Porter of the Bridge Division were instrumental in the fulfillment of the objectives. Testing a bridge at a remote location certainly takes a group effort from all involved.

Several undergraduate students spent many hours working setting up for the testing and during the actual tests. These include Suzy Gutshall, Greg Scovitch, Steve Schrage, and Stewart Ludlow. We appreciate their efforts and we hope they learned from the experience.

A special thanks goes to Mr. Delmer Kamper, the property owner surrounding the bridge site. Mr. Kamper allowed us access to the bridge at anytime and he went out of his way to make us feel welcome.

Lastly, research is only as good as the people working on it. Mr. C.H. Cassil and Mr. Richard Oberto, Senior Research Technicians for the college, were instrumental in putting together a very complicated testing system. Many hours of beyond expected effort made this a successful project.

TABLE OF CONTENTS

LIST OF TABLES

LIST OF FIGURES

Page

CHAPTER 1

INTRODUCTION

1.1 BACKGROUND

In Missouri, over one-half off-system bridges and roughly a quarter state-system bridges are posted for restricted loading. The primary reasons for these bridges being classified as structurally deficient are that (1) truck loads have increased since these bridges have been designed, (2) deterioration of the bridge superstructure, and (3) other load capacity controlling aspects. These other aspects may include the condition of the substructure, inadequate design or construction details of off-system bridges at the time of their construction, or the lack of existing "as-built" information. The work contained herein addresses the possibility of using field testing in the evaluation of the superstructure load capacity. Many of the other aspects would need to be studied on a case-by-case basis.

Current load capacity evaluation methods tend to use the same procedures that were used to design the structure. For design of a new bridge, these methods are, and should be, inherently conservative. For evaluating a bridge that has performed successfully in the past, the opportunity exists to "do a better job" of estimating the bridge's performance. This can be accomplished through examining the performance of the bridge (field testing) in conjunction with acceptable analytical procedures. Experimental testing of bridges shows that, in most cases, bridges exhibit greater strengths than current analytical techniques indicate (Lichtenstein 1993). Factors not considered in the analytical models contribute to the strength of the structural system.

Several states have used bridge field testing as an alternative to or supplement to analytical methods for setting load posting limits. Bridge field testing consists of three

features: a calibrated loading system (i.e., truck) or random traffic, a data acquisition system (experimental sensors and support equipment), and bridge modeling, data reduction, and decision/conclusion procedures. Many examples of increased posting limits or total removal of restricted loads have been documented over the last several years (Keeling 1997). Incorporating load testing into the bridge rating process can improve bridge load capacities while maintaining adequate levels of safety. The Missouri Bridge Inspection Rating Manual allows load testing under the direction of qualified registered professional engineers as a means to determine load postings for off-sysem concrete bridges where the details of reinforcement are unknown and an accurate loading history is not available (MHTD 1990). The AASHTO (1994) Manual for Condition Evaluation of Bridges describes field testing as a means of supplementing analytical procedures in determining the live load capacity of a bridge.

The use of standardized or semi-standardized field testing for load capacity evaluation of existing bridges has been in existence in the U.S. for approximately 25 years. Historically, these standardized procedures have been state specific and jurisdictionally limited. The National Cooperative Highway Research Program (NCHRP) realized the importance for using field testing for load capacity rating existing bridges. Research attempting to develop standard procedures on a national level was instigated by NCHRP (Lichtenstein 1993). The resulting report, and the NCHRP Research Results Digest 234 (1998), summarizes field tests for load rating existing bridges and recommends guidelines for using test data in load rating. However, field testing is very subjective and states find they must make policy decisions on how to use test data in rating provisions.

The report also presents a general guideline for nondestructive load testing for bridge evaluation and rating. However, to be incorporated into a state's rating program, state specific detailed procedures and methodologies need to be developed. However, even with standardized procedures, well-qualified engineers must use common sense, good engineering judgment and sound analytical principles to execute a pre-test investigation, set up the test, interpret the data and determine a decision.

When field testing a bridge, the bridge itself is the experimental model. The structural response is exactly what the evaluator is seeking. There are no inaccuracies that plague typical prototype-model experimental tests. A desirable rating procedure would be to use the bridge itself as the "perfect" analog model and determine the structural response and load rating through field testing. However, care must be used in interpreting the results. Factors that increase the load capacity of the structure must be dependable during the remaining service life or at least until the next evaluation. State policy, tempered by the judgment of the bridge engineer managing the test, should be used to address the admissibility of beneficial behavior.

The guidelines presented in NCHRP Research Results Digest 234 (1998) offer a good overview and a considerable amount of practical advice for any state in regard to some of the considerations involved in load testing. The report contains excellent information regarding when and when no to test as well as a number of other topics that should be of interest to any state transportation agency considering its use. However, to adapt field testing as a compliment to analytical bridge rating in Missouri, detailed methods need to be developed specific to Missouri. This means that details for pre-test investigations, testing procedures, and post-test data evaluation techniques need to be developed in such a manner as to be

applicable on an acceptable level. Likewise, testing experience is invaluable for gaining expertise and confidence in a bridge field test load rating system.

Diagnostic and Proof load tests can be used for evaluating a bridge for a load rating. A diagnostic test is one in which a prescribed load, usually significantly lower than the anticipated bridge capacity, is applied to the bridge. A proof load test is one in which a "minimum strength" load is applied. Thus, the bridge has adequate ultimate capacity at least equal to the proof load for the particular configuration being investigated.

Diagnostic tests determine the actual structural response due to the specified loading. These responses can be used to estimate the load and fatigue rating through mathematical models. The models must still consider the limit states as a variable since there is no benefit of a proof loading to determine a "minimum" strength. However, certain dependable factors that indicate greater strength will already be evident. This in itself may make a conventionally analyzed deficient bridge acceptable.

Valuable information concerning the load capacity of existing bridges can be gained through proof loading for load limit states. Diagnostic testing can be very useful in pre-test investigations to estimate the expected behavior and proof load. Using the proof load to load test the bridge removes the question of what is the "minimum" strength. Of course the type of limit state, degree of redundancy, and factors indicating greater strength may affect the resulting rating.

1.2 OBJECTIVES

The objectives of this project are to (1) develop a Bridge Field Test system for use in Missouri, (2) conduct a field test and load rate a steel girder bridge to demonstrate the

benefits, and (3) develop standard steel girder bridge load posting field test procedures for possible implementation.

The field test system will be a powerful state asset for many years, addressing state and national research needs. The initial emphasis of the program was to develop the system and apply it towards standardized field load rating provisions. To accomplish this, the Bridge Field Test system was developed and evaluated on a steel girder bridge in Missouri.

The standard load capacity rating procedures are written in an Allowable Stress rating format. This is because the tested bridge was posted using allowable stress rating. However, the procedures are also applicable to the Load Factor rating method, just the equation changes.

The test plans only use diagnostic field testing techniques. Proof load testing may, and probably will, cause some local or general yielding in the girders, depending on the target capacity. It was decided that the testing should cause no yielding in the girders. This was accomplished by ensuring that the applied stresses did not exceed the yield minus the dead load and residual stresses.

1.3 DEVELOPING THE FIELD TEST SYSTEM

A versatile and mobile bridge field testing system (Imhoff 1998a) was built at the University of Missouri-Columbia for this, current, and future field testing projects. The system was developed to standardize field testing in Missouri. One goal of the system was to reduce the cost, time and effort required to field test bridges. A desire for the test system is to be able to test a bridge in a matter of a couple of days rather than each test being an exhaustive endeavor. A modular "plug-and-play" style system, along with expeditious measurement devices, were developed to allow the quick instrumentation, testing, and clean up of a bridge test. A new experimental field test rating capacity should result within a week. With this time

frame and associated costs, load rating bridges through field testing is economically appealing.

Chapter 3 presents the field testing system and Chapter 4 presents the application of the system to a steel girder bridge. The modular data acquisition vehicle and supporting equipment has great potential for economical field testing. Therefore, it is presented in some detail to demonstrate the effectiveness of such systems. The steel girder bridge is a three-span, four girder structure currently posted for restricted lanes and loads using Missouri allowable stress rating procedures. The testing of the bridge and the field test rating results for an H20 vehicle are presented. The posting levels for other vehicles can be determined in like manner by using the experimental data in conjunction with the analytical procedures for other rating vehicles. The results show that the bridge can safely be posted above H20 legal loads for a single lane bridge. If the bridge is to be opened for two lanes of traffic, the posting can be raised to legal loads (20 tons) for the AASHTO H20 vehicle. However, the field test two-lane posting of 21.9 tons falls short of the Missouri H20 23 ton posting limit.

The system has also been used in three other Missouri Department of Transportation research studies. The studies are all collaborative efforts between the University of Missouri-Columbia and the University of Missouri-Rolla. Two of these are bridge strengthening demonstration projects using Fiber Reinforced Plastics (FRP) bonded to the bottom of concrete slab bridges (MoDOT projects R98-012 and R98-013). The third study (SPR 1998-63) is monitoring the strain demand on signal mast arms in the field. These projects demonstrate the potential and economical benefits of a modular testing system in Missouri.

1.4 FIELD TEST LOAD RATING STEEL GIRDER BRIDGE R-289

Analytical rating procedures are based on conservative design assumptions that do not always represent the true bridge behavior. Therefore, steel girder bridges usually exhibit

capacities higher than analytical load capacity rating predicts. Testing bridges in the field has demonstrated this additional capacity and bridge field testing has become an acceptable means to determine a more accurate estimate of a bridge's safe capacity (Lichtenstein 1993). In many cases, an experimental rating in conjunction with analytical procedures could raise or even remove the bridge's restricted load posting.

The reasons for the increase of capacity can be explained by factors that tend to make bridge responses less than those predicted by design and analysis procedures or adjustments to inputs into the rating equation. Some of these factors include:

1. adjustments in as built parameters such as dead load,
2. actual impact factor,
3. actual section dimensions,
4. unaccounted system stiffness such as curbs and railings,
5. actual lateral live load distribution,
6. bearing restraint effects,
7. actual longitudinal live load distribution, and
8. unintended or additional composite action.

Field testing measures the response of the structure to load. The response contains the aggregate apparent additional capacity from all of the above factors. However, some of these factors may be unreliable during the service life of the bridge. For instance, bearing restraint forces, from friction resistance during movement or frozen in place, tend to reduce measured responses in the structure. Bridge owners may want to remove the capacity increase associated with the bearing restraints given that it may not be dependable at higher load levels over time. Likewise, this may be the case for unintended composite action. Even if a section is built

without mechanical shear connectors, it usually acts at least partially composite (measured response will be reduced). The owner may not be willing to accept a rating based on unintended composite action. Therefore, for field testing to be successful, it is imperative that the unreliable contributions to an experimentally determined load capacity rating be removed.

Chapter 4 presents the field testing, Chapter 5 the data reduction, and Chapter 6 the load posting results for Missouri Bridge R-289. It demonstrates the contributions of the above factors as they pertain to the behavior of the test results in comparison to analytical rating and design procedures.

Missouri Bridge R-289 was selected to develop the field testing capacity rating procedures due to the desirable characteristics it possesses. It has multiple continuous spans, positive moment region composite and noncomposite sections, negative moment region noncomposite sections with cover plates, rocker bearings, substantial curbs and railings, and a one-lane 15 ton single unit truck posting.

1.5 STANDARD FIELD TESTING LOAD RATING PROCEDURES

To implement field test load rating procedures in a state DOT, standardized procedures are beneficial to promote comfortable and uniform application. Chapter 6 presents systematic field test procedures for load rating steel girder bridges. It contains standardized procedures for inspecting, instrumenting, testing, and load rating steel girder bridges through field testing. Six different test plans are offered depending on the factors to be determined. The test plans vary in level of effort and expected results for load rating bridges with experimental test results. For instance, if the owner only wants to determine the benefits of a lower lateral distribution behavior, a medium effort plan can be used. However, if the owner wants to identify and quantify all eight contributing factors, a high effort plan must be used.

A demonstration of the application of Test Plan VI is presented. The plan quantifies each factor and is used to illustrate the procedures for Bridge R-289. All eight factors are determined and removal of unwanted contributions is demonstrated.

1.6 SUMMARY

This report presents standard field test load rating procedures for steel girder bridges in Missouri. The procedures were developed from the comprehensive field test of steel girder Bridge R-289. The load test was intended to (1) develop the testing system (Imhoff 1998) and standardize field testing procedures (McDaniel 1998) and (2) determine a safe capacity for the tested bridge (Frederick 1998). The bridge is a three-span continuous, four girder structure with favorable characteristics for the research. It is currently posted for restricted loads and a single lane using Missouri allowable stress rating procedures. The testing of the bridge and the field testing rating results are presented. The results show that the bridge posting can be significantly improved for a single-lane or two-lane structure. The factors that increase the load capacity are determined by the systematic approach and a discussion of the influence of the factors is presented.

CHAPTER 2

SUMMARY AND CONCLUSIONS

2.1 FIELD TESTING BRIDGES

Some 32% of the interstate, state, and city/county/township bridges in this country are considered substandard. Forty three percent of Missouri's bridges fall in these categories, representing the eighth highest percentage of structurally deficient or functionally obsolete bridges in this country (Keeling 1997). The funds required to replace all of these bridges are not available. An aging and deteriorating bridge inventory results in a large number of bridges posted for lower than original design loads. A posted bridge on a lightly traveled rural road does not pose serious difficulties for the average motorist or trucking company. However, when a structurally deficient bridge serves an important commercial route, serious problems arise in the form of truck traffic detours, increased transportation costs, and higher consumer prices.

Bridges usually exhibit capacities higher than analytical load capacity rating predictions. The rating procedures are based on conservative design assumptions. Testing bridges in the field has demonstrated this additional capacity and bridge field testing has become an acceptable means to determine a more accurate estimate of a bridge's safe capacity (Lichtenstein 1993).

The Civil Engineering Department at the University of Missouri – Columbia has developed a field testing system which is intended to satisfy state research needs as well as providing a mechanism to more accurately load rate Missouri's numerous bridges. This system will provide a tool which could be considered by the state of Missouri to increase the load limits on bridges that are currently restricting truck traffic. Field tests provide the rating

engineer with valuable knowledge of system response, lateral load distribution, longitudinal load distribution, actual section properties, bearing restraint forces, and dynamic impact for the tested bridge. This information allows the rating engineer to reduce the inherent conservatism of current analytical rating methods.

Standardized testing procedures and load posting decision protocols have been developed for steel girder bridges. The procedures and protocols are presented in a step-by-step type format similar to other DOT guidelines. However, a well qualified engineer is necessary to ensure the bridge is a good candidate for field testing. The engineer must examine the capabilities of the substructure, connections and any other aspects with respect to desired benefits from superstructure testing.

The standard methods have been applied to an existing three-span steel girder bridge. Missouri Bridge R-289, posted for restricted lane and weight, was tested thoroughly to develop the field testing system and standardize the methods. The experimental tests verified the standard procedures and resulted in possible significant increases in the safe load carrying capacity of the posted bridge.

2.2 FIELD TESTING SYSTEM

The field testing system was designed from the outset to be mobile, versatile, and reliable. The command center for the field test system is the data acquisition vehicle. A flat-bed truck with a boom and standard steel block weights are used as a calibrated loading.

The goal in developing the system was to reduce the cost, time and effort required to field test bridges. A desire for the test system is to be able to test a bridge in a matter of a couple of days. A modular "plug-and-play" style system, along with expeditious measurement devices, was developed to allow the quick instrumentation, testing, and clean

up of a bridge test. A new experimental field test rating capacity should result within a week. With this time frame and associated costs, load rating bridges through field testing is economically appealing.

The data acquisition system can monitor up to 125 channels of data at distances beyond 200 ft. Diagnostic tools specifically designed for the system allow quick assessment prior to testing. The boom truck and compact steel weights permit variable loading of the structure with total weights up to 50 tons. The weight can be changed and the truck weighed quickly for efficient testing. Crawl speed tests minimize traffic disruption to the public. Test monitoring in real-time is possible with the data acquisition software. Preliminary results can be quickly determined by importing the data into a computer spreadsheet.

The system has also been used in three other Missouri Department of Transportation research studies. The studies are all collaborative efforts between the University of Missouri-Columbia and the University of Missouri-Rolla. Two of these are bridge strengthening demonstration projects using Fiber Reinforced Plastics (FRP) bonded to the bottom of concrete slab bridges. The field test system performed well in that, for Bridge G-270 (R98-012), the elastic deflection tests were executed in 2 hours from start to finish. For the Bridge J-857 tests (R98-103), the field test system was brought to the site just prior to testing, hooked up to the in-place instrumentation, and used to monitor the elastic and ultimate failure tests. The third study (SPR 1998-86) is monitoring the strain demand on signal mast arms in the field. During various wind events, the field test system is driven to the mast arm, hooked up to the instrumentation, and used to collect peak strain measurements. The system can be reading strains within 10 minutes after arrival. These projects demonstrate the potential and economical benefits of a modular testing system in Missouri.

2.3 FIELD TESTING BRIDGE R-289

Bridge R-289 over the Boeuf creek is located on Route ZZ about 6 miles north of Gerald in Franklin County, Missouri. It is a 36 year old, three-span (60 ft, 90 ft, 60 ft) continuous slab-on-steel girder bridge. The bridge consists of four rolled steel girders. It is an ideal candidate bridge for several reasons: it is posted for a restrictive loading, it is in good condition, the substructure appears to be in good condition with no scour, and it has Type D rocker bearings. The bridge was also chosen because it has three continuous spans with the midspan being composite and the end spans being non-composite. This allowed the field testing team to examine such factors as unintentional composite action, bearing restraint forces, actual lateral distribution of live loads, and dynamic impact.

Four separate testing trips were taken to the bridge. The first three were used to set up and diagnose the field testing system. The fourth trip was used to collect the data to develop the standardized procedures and protocols and determine an experimental posting capacity of Bridge R-289.

The bridge was tested to determine the actual elastic behavior. Several different load truck weights and positions were applied. For the rating process, 95 strain gages and 6 deflection devices were used to estimate the lateral distribution, longitudinal distribution, the effects of the curbs and railings, bearing restraint forces, unintentional or additional composite action, and the dynamic impact factor. These properties, with specified values or neglected in design or rating, can have a significant effect on the behavior of the bridge.

The data acquisition software can monitor chosen channels in real time during the test. In addition, near real-time data reduction worksheets in Microsoft Excel were developed to estimate performance and projected ratings immediately after test runs. The

worksheets were used throughout the testing with great success. Linearity checks, maximum response monitoring, and overall bridge behavior along with the ability to project what to do next was a valuable tool.

2.4 STANDARDIZED LOAD POSTING USING FIELD TESTING

Bridges usually exhibit capacities higher than analytical load capacity rating predictions. The main reasons for a lower experimental response than design procedures indicate are that (1) bearings restrain movement or are frozen and tend to oppose the load effects, (2) the actual lateral distributions of live loads, (3) the actual longitudinal distribution of live loads, (4) contributions from the curbs and railings, (5) the actual section properties, (6) and noncomposite sections tend to act composite. Two other reasons why an analytical posting may be lower than possible is that (1) the dynamic allowance for impact may be lower than expected and (2) the available capacity for live load may be underestimated. These factors are the basis of the standard procedures presented in this report.

Past field tests have demonstrated the increase of capacity from the above factors. Experimental data yields a total capacity where the increase over analytical methods is lumped in an aggregate sum. For instance, for Bridge R-289, the experimental single-lane total posting capacity is 26 tons, while the analytical posting is 15 tons. However, some of the factors listed above, such as the bearing restraint forces or unintentional composite action, may not be reliable over the life of the structure. Therefore, if the bridge owner does not want to consider the beneficial increase due to these unreliable sources, the effects must somehow be removed from the experimental total posting capacity.

Standard procedures have been presented in this report to separate and quantify the above contributors so that unwanted benefits can be systematically removed. The procedures

have been verified through the testing of Bridge R-289 and finite element analyses. The owner now has a justifiable procedure to base a decision on field test load ratings.

Six standard test plans have also been developed and presented herein. The plans range in cost, time expended, accuracy, and the ability to quantify the individual factors above. All the test plans arrive at an experimental total posting capacity. However, for the lower effort plans, some of the factors may be combined into a comprehensive factor and be inseparable. This is not necessarily bad. For instance, for a composite simple span bridge, the owner may be satisfied with knowing the actual lateral distribution factor and leaving the remaining factors in a comprehensive form. For a noncomposite bridge, however, the owner may not want to use the increase in capacity due to the unintentional composite action. Therefore, a mid-level test plan may be required.

2.5 FIELD TEST LOAD POSTING RESULTS

Missouri Bridge R-289 is posted for single-lane 15 tons using the allowable stress method and a Missouri H20 truck. This report also uses the allowable stress rating method to determine the experimental posting capacities. However, the procedures are just as applicable to the load factor rating method. This bridge is also posted at 37 tons maximum for combination type vehicles. This report examines the experimental posting for the single unit H20 vehicle. The procedures can be applied for other posting vehicles.

The critical section in Bridge R-289 is the exterior girder in the composite positive moment region of the center span. The experimental total posting for this section for one lane is 26 tons. The bearing restraint forces are responsible for increasing the experimental total posting by 3.8% (bearing restraint factor = 1.038). If the owner does not wish to rely on the bearing restraints over time, the acceptable experimental posting becomes 25 tons (26

tons/1.038). The possible increase to 25 tons (legal H20 loads) is due to a better estimate of the bridge's response to rating vehicle loads.

To open the bridge up to two lanes of traffic, superposition of the diagnostic test results can be used. The experimental total posting using superposition of critical truck positions is 22.6 tons. The bearing restraint factor is 1.032. Thus, an acceptable load posting would be 21.9 tons. This indicates that the bridge could be opened for two lanes of legal AASHTO H20 (20 tons) truck loads and of near legal Missouri H20 (Missouri uses 23 tons as posting limit) truck loads.

2.6 SUMMARY

The standard procedures and decision protocols are presented for steel girder bridges. They are backed by analytical and experimental verification. The results show that significant increases of load capacity can be obtained through field testing. The reason for such is a better estimate of the particular bridge's response to truck loads. There is no lowering of acceptable safety to the public since the rating equations and philosophy are not altered and no material properties are being changed, only the accuracy of the response.

2.7 IMPLEMENTATION AND FUTURE WORK

Clearly it will take experience and several bridge tests to make field testing steel girder bridges an effective program. Although the procedures are standardized, a well qualified engineer is required to manage the tests and produce the load rating. The field test system and test plan procedures have the potential for upgrading the load carrying capacity of many bridges in Missouri. The field test system demonstrated on a state-system bridge could also be applied to the off-system inventory as long as the bridges are determined to be good

candidates. Counties, with limited budgets and rural bridges, should be particularly interested.

The next step in the development phase is to develop standard testing and decision protocols for concrete slab and girder bridges. Preliminary studies are ongoing to determine the requirements as part of the Bridge J857 tests (MoDOT project R98-013).

CHAPTER 3

BRIDGE FIELD TESTING SYSTEM

3.1 INTRODUCTION

The University of Missouri at Columbia, with the support of the Missouri Department of Transportation (MoDOT), has developed a versatile and mobile bridge field testing system (McDaniel 1998). The system was developed to standardize field testing in Missouri. One objective of the project was to reduce the cost, time and effort required to field test bridges. A goal for the test system is to be able to test a bridge in a matter of a couple of days rather than each test being an exhaustive endeavor. A modular "plug-and-play" style system, along with expeditious measurement devices, was developed to allow the quick instrumentation, testing, and clean up of a bridge test. A new experimental field test rating capacity should result within a week. With this time frame and associated costs, load rating bridges through field testing is economically appealing.

This chapter presents the field testing system. The modular data acquisition vehicle and supporting equipment has great potential for economical field testing. Therefore, it is presented to demonstrate the effectiveness of such systems. For a detailed description of the entire system, the reader is referred to McDaniel (1998).

At the heart of the field test system is the data acquisition system. A schematic of the system is shown in Figure 3.1. The figure demonstrates the acquisition system from the measurement devices at the top of the figure to the computer system in the data acquisition vehicle at the bottom.

3.2 DATA ACQUISITION VEHICLE

The field testing system was designed from the outset to be mobile, versatile, and reliable. The command center for the field test system is the data acquisition vehicle. A vehicle had to be selected that could effectively provide transportation and living quarters for the testing team as well as providing a protected and air conditioned housing for the data acquisition computers and hardware.

The data acquisition vehicle selected was a 1992 Fleetwood Tioga Arrow RV. A picture of the data acquisition vehicle is shown in Figure 3.2. The RV was refurbished to meet the requirements of an effective data acquisition vehicle. The front living quarters remained in their original state while the rear living area was completely eliminated. An efficient workspace replaced this area and reduced the maximum occupancy to six people.

The rear workspace houses a data acquisition rack for 95 low level (strain) channels and 25 high level (deflection) channels. The data acquisition CPU, the communications receiver, and an oscilloscope can also be found in the data acquisition rack. Other equipment found in the rear of the data acquisition vehicle are the monitor for the data acquisition CPU, a data reduction computer, uninterruptible power supplies, a printer, and communications equipment. There is enough counter space to provide ample room for two computer or manual work stations.

3.3 DATA ACQUISITION VEHICLE ELECTRICAL SYSTEMS

3.3.1 Onboard and External Generators

The data acquisition vehicle must be capable of providing clean and reliable power to a large number of household devices as well as the data acquisition system. The data

acquisition vehicle's electrical systems were configured for two testing scenarios in an effort to make the vehicle as versatile as possible. The first scenario was a small test that would require minimal equipment and power demand. The second scenario was a large test that would require large amounts of equipment and have a large power requirement. The onboard 4 KW generator can power the living quarters and data acquisition hardware to perform a small test of less than 25 recorded channels. Larger tests, where the full capacity of the data acquisition system is required, is powered by a 12 KW external generator. The external generator can be seen in Figure 3.3.

3.3.2 Data Acquisition Vehicle Wiring

The electrical system is automatically configured for whichever power source may be available by the use of a mechanical relay. When the onboard generator is being used to power the data acquisition vehicle, the circuit is ran entirely through the existing breaker box which also powers the lights, air conditioning, and other appliances. The existing breaker box allows an overall maximum current demand of 30 amps. For this reason, another mechanical relay was installed to disconnect the appliance circuit from the data acquisition hardware circuit when the external generator is in use. Two cables are required when using the external generator. One cable powers the data acquisition hardware the other cable powers the appliances. The dual electrical system provides versatile and dependable power to the data acquisition vehicle.

3.3.3 Uninterruptible Power Supplies

In line with all of the data acquisition equipment are two uninterruptible power supplies (UPS). Two Tripp Lite's Omnipower 2000s were selected as the UPS's for the data

acquisition system. The UPS's provide spike, line noise, and RFI/EMI filtering which eliminates the need for a separate surge protector. The UPS's also provide both brownout (undervoltage) and power surge (overvoltage) line regulation as well as providing a backup power source during a blackout (total power loss) (Tripplite 1997). A picture of the UPS's can be found in Figure 3.4.

3.4 DATA ACQUISITION HARDWARE

3.4.1 Communications Equipment

The testing process is a team effort requiring excellent communication between all members of the testing team. A Telex wireless intercom system was installed in the data acquisition rack to insure good communication of duties and responsibilities during any field test. The system consists of a BTR-200 Base Station Transceiver, base station speakers, a base station microphone, and four TR-200 Belt-Pack Transceivers with headsets. An example of the belt packs and headsets can be seen in Figure 3.5. The Telex communications system provides each member of the testing team with wireless, open channel, two-way communications with any other member of the team. The system has the capability of interfacing a wired intercom system and other auxiliary audio. The BTR-200 Base Station has one transmit and four receive channels which was designed to operate with simultaneous two-way communication with up to four TR-200 Belt Pack transceivers (Telex, 1997).

3.4.2 Oscilloscope

The data acquisition rack is also equipped with a Hewlett Packard 54602B 150 MHz oscilloscope for signal monitoring and system troubleshooting. The oscilloscope is located just above the signal screw terminals allowing easy access to any of the 125 channels of the

data acquisition system. The HP 54602B provides automatic setup of the front panel, automatic and cursor measurements of frequency, time, voltage, waveform storage, save and recall of 16 front panel setups, and peak detect. The oscilloscope is supplied with two 1.5 meter, 10:1 HP 10071A probes (Hewlett Packard 1997). The oscilloscope can be seen in Figure 3.6.

3.4.3 Computers

At the center of the data acquisition system is a Gateway 2000 desktop computer with a 17 in. SVGA color monitor and a 200 MHz Pentium processor. There is a 1.44 MB floppy drive, a CD-ROM drive, and a 100 MB Zip drive for easy backup storage of test data. The computer is mounted on anti-vibration feet to decrease the chance of damaging the computer while in transit. This computer houses the data acquisition card. A Gateway 2000 computer outfitted with a tower CPU, a 17 in. SVGA color monitor, and a 200 MHz Pentium processor serves as the data reduction and general use computer for the testing system. The data reduction computer is equipped similarly to the data acquisition computer except that it does not possess a data acquisition card.

3.4.4 AT-MIO-16E-1 Data Acquisition Card

The AT-MIO-16E-1 board is completely switchless and jumperless and is software configurable. The data acquisition board has three different analog input modes: non-referenced single-ended (NRSE), referenced single-ended (RSE), and differential. The single-ended input mode uses up to 16 channels and the differential input mode uses up to eight channels. A channel configured in NRSE mode uses one analog channel input line, which connects to the positive input of the programmable gain input amplifier (PGIA). The

negative input of the PGIA connects to the analog input sense. A channel configured in RSE mode uses one analog channel input line, which connects to the positive input of the PGIA. The negative input of the PGIA is internally tied to analog input ground. A channel configured in differential mode uses two analog channel input lines. One line connects to the positive input of the PGIA, and the other connects to the negative input of the PGIA. All channels of the data acquisition system were configured for differential mode for best results and noise rejection performance. Differential mode is recommended when measuring low level signals, dealing with long lead wires, and testing in a noisy environment. The AT-MIO-16E-1 has two input polarities, either unipolar or bipolar. The unipolar setting accepts signal between 0 and 10V. The bipolar setting accepts signal between –5V and +5V. The board also has programmable gains of 0.5, 1, 2, 5, 10, 20, 50, and 100 (National Instruments 1996).

3.4.5 SCXI 1001 Chassis

The SCXI 1001 chassis accommodates up to 12 signal conditioning and multiplexing modules. The chassis provides a low-noise environment for signal conditioning and supplying power and control circuitry for the modules. It is a general purpose chassis and can be used with current and future SXCI modules. There are several configurations that can be used with the SCXI 1001 chassis. The chassis in the University of Missouri system has been set up with seven modules installed and five spots available for expansion. Only one of these modules is cabled to the data acquisition board that acquires data from all of the modules. The back panel signal BUS directs signal from all modules to the data acquisition card even though only one is directly cabled to the data acquisition card. The SCXI chassis

is located at the bottom of the data acquisition rack and has been left very accessible for changing settings or adding new modules.

3.4.6 SCXI 1122 Multiplexer-Conditioners

The SCXI 1122 consists of 16 isolated channels with gains of 0.01, 0.02, 0.05, 0.1, 0.2, 0.5, 1, 2, 5, 10, 20, 50, 100, 200, 500, 1000, and 2000, and two isolated excitation channels with voltage and current excitation. Multiple channel scanning is performed by a relay multiplexer that connects only one channel at a time to the PGIA. The SCXI 1122 operates with either a 4 KHz or 4 Hz low-pass filter. The maximum scan rate is 100 scans/sec with the 4 KHz filter and only 1 scan/sec with the 4 Hz filter activated. The SCXI-1122 has digital, automatic control of channel scanning, temperature selection, gain selection, and filter selection (National Instruments 1997). The SCXI 1122 has been configured to read all of the low level strain signals in the University of Missouri system since it is isolated and has superior noise rejection performance. The module is normally configured with the 4 KHz filter and a gain selection of 1000 or 2000 depending on signal offset. A gain setting of 1000 has a range of ±10 mV and a resolution of 4.8 μV. A gain setting of 2000 has a range of ±5 mV and a resolution of 2.4 μV.

3.4.7 SCXI 1322 Terminal Blocks

The SCXI 1322 Terminal Block is mounted to the front of the SCXI 1122 module. The SCXI-1322 provides screw terminals for sixteen differential signal connections as well as external excitation connections. The SCXI 1322 Terminal Block connects the SCXI-1122 to the signals to be acquired. The SCXI-1322 is quite small, inconvenient for making system changes, and does not provide any means of sampling a channel with the oscilloscope. It is

for these reasons that the TBX-24F Feedthrough terminal blocks have been used in the University of Missouri system.

3.4.8 TBX 24F Feedthrough Terminal Blocks

The TBX 24F provides the versatility that was lacking in the SCXI 1322 terminal block. There is a set of screw terminals for signal coming into the terminal block and another set of terminals for signal coming out of the terminal block and into the SCXI 1322. The screw terminals are adequately spaced to provide sufficient room for accessing the signal with the oscilloscope probes. Each TBX-24F provides terminals for 12 differential signals. The University of Missouri system has been designed for up to 95 strain signals. Therefore, there are eight TBX 24F's that provide signal connection to the six SCXI 1322's and SCXI-1122's. The TBX 24F's can be seen mounted in the rack and with all signal connections completed in Figure 3.7.

3.4.9 SCXI 1100 Multiplexer-Conditioner

The SCXI 1100 provides signal conditioning for up to 32 channels. The SCXI 1100 is equipped with jumper selectable low pass filters of 4 Hz and 10 KHz as well as an unfiltered setting. The SCXI-1100 has software programmable gains of 1, 2, 5, 10, 20, 50, 100, 200, 500, 1000, and 2000. The University of Missouri system only has one SCXI 1100 and it is dedicated to reading high level deflection or acceleration inputs. Since the SCXI-1100 is normally reading high level signal from accelerometers or LVDT's, the gain setting is usually set at 1 with a range of ± 5 V resulting in a resolution of 2.4 mV. The SCXI 1100 utilizes a slightly different terminal block to connect signal to the multiplexer.

3.4.10 TBX 1303 Terminal Blocks

The SCXI 1100 does not have a terminal block mounted directly to its face like the SCXI-1122, instead the SXCI-1100 is connected via a 96 conductor shielded cable to the TBX 1303 triple level terminal block. There are three terminals available for each of the 32 possible channels as well as terminals for connection to ground. Two of the three connections are provided for completing a differential signal connection and the third terminal is available for connecting a shield wire to ground. Unlike the SCXI 1322 terminal block, the TBX-1303 provides sufficient access to the signal connections. Therefore, there is no need for the TBX 24F's in this situation. The TBX 1303 can be seen mounted in the rack with all signal connections completed in Figure 3.8.

3.4.11 Data Acquisition Boxes

The signal wires have been routed from the TBX 24F's and the TBX 1303 to a connector panel in the side of the data acquisition vehicle. There are five 52 pin Amphenol connectors located on this panel as well as AC power connections. Each connector has 16 pairs of pins dedicated to the measurement of strain signals. There are 3 pairs of pins allocated to measure either low level or high level signal. Five pairs of pins have been set up to measure only high level signal from LVDT's or accelerometers. One pair has been configured to read the strain circuit's excitation voltage. The last available pair has been dedicated to bringing the ground from the strain gage lead wire shields back to the data acquisition vehicle for connection to the system ground. The connection panel in the side of the data acquisition vehicle can be seen in Figure 3.9.

The signal is carried to the data acquisition vehicle over 26 pair individually shielded cable. Located at the other end of these cables are the five data acquisition boxes. The data

acquisition box is powered by connecting the data acquisition box to the AC connectors on the data acquisition connector panel. Each box has been equipped with sufficient screw terminals for making all signal connections. There is adequate room for up to five Schaevitz LVDT conditioners, up to two DC power supplies for powering the strain circuits, and up to nineteen Wheatstone bridge completion modules. A data acquisition box can be seen in Figure 3.10.

3.4.12 Completion Modules

The data acquisition box contains up to nineteen Wheatstone bridge completion modules. These modules were designed and fabricated at the University of Missouri. The completion module circuit can be seen in Figure 3.11. The primary instrument used in a field test is the strain gage. A strain gage is a grid of resistive material that is manufactured to be extremely sensitive to any increase in length along a primary axis. The resistance of an electrical conductor is proportional to the length if its cross sectional area and resistivity are constant. The strain gage is attached to a location where strain data is required. As the underlying material elongates so does the strain gage. An elongation of the strain gage results in an increase in resistance. The Wheatstone bridge is a circuit that provides two nodes to supply excitation and two more nodes to deliver a strain proportional signal. As seen in Figure 3.12, the Wheatstone bridge consists of four arms with a resistor across each arm. The completion modules located in the data acquisition box provide the other three resistors to form a completed bridge for each strain gage. All nineteen bridges are placed in parallel and powered by a single power supply. The voltage across the power supply (V_P) is normally set at 4 V but could differ from this value. The differential voltage measured at the

other two nodes is recorded as the bridge output (V_S). The strain at the gage location can be found by the following equation:

$$\varepsilon = \frac{V_P * V_S}{4 * GF} \tag{3.1}$$

The variable, GF, is the gage factor. The gage factor is provided for each strain gage by the manufacturer. The gage factor is defined as the proportionality constant between a change in resistance of the gage and the strain required to produce this change in resistance.

3.4.13 Junction Boxes

The data acquisition boxes are large and expensive, especially when they're filled with all of the data acquisition hardware. For this reason, small junction boxes were fabricated. The inexpensive junction boxes can stay at the test site for longer term testing. These junction boxes provide screw terminals for all nineteen strain gage signal wires. The junction box also provides a grounding terminal for sending any shield current back to the system ground. The junction box is connected to the data acquisition box by a 96 pin shielded cable. The wires going into the data acquisition box on this cable are distributed to the appropriate completion module.

Strain gages can have either two wire leads or three wire leads. The two wire leads add extra resistance to one arm of the Wheatstone bridge since the wire itself acts as a resistor. To compensate for lead length effects, the three wire lead can be used and the extra resistance is added to two arms of the Wheatstone bridge. Extra resistance in two opposing arms will not affect the response of the Wheatstone bridge. The junction box and completion modules can accommodate both two and three wire leads.

3.5 DATA ACQUISITION SOFTWARE

The data acquisition software is the instrument used to inform the hardware what to collect and how it is to be collected. The software used to control the data acquisition software is Labview (1997). Labview is a graphical programming language. A program is written in Labview in much the same way as an electrical technician would wire a light switch in a house. Each graphical object has some task or logical operation that it performs. When these graphical objects are placed on the diagramming page of Labview and connected or wired together, a program is formed. The user interfaces with the program through what is called the control panel. This control panel is where the user provides inputs to the program and receives outputs in the form of graphs, numbers, dials, switches, etc.

The data acquisition system required a program that would continuously collect voltage output from up to 125 channels while performing a test. The data acquisition must be performed in a time step manner where, at each time step, a signal from each channel is stored and associated with that time step. These outputs have to be saved to a data file along with the associated time.

The program written to perform the data acquisition is called Daq.vi. Daq.vi has been written entirely within a sequence structure. The sequence structure will run a program as a series of steps. Each step is programmed and then given a step number. The program references the sequence structure until all steps are completed. The first step in the sequence structure is the configuration step. The diagramming page of the configuration step within Daq.vi can be found in Figure 3.13. This step contains a virtual instrument (vi) called Config.vi. The diagramming page for Config.vi can be found in Figure 3.14. Config.vi simply prompts the user for the necessary parameters to perform an acquisition by displaying

the control panel found in Figure 3.15. Once the user enters the necessary information and tells the program to continue, the next step of the sequence structure is performed. The diagramming page of the next step in the sequence structure can be seen in Figure 3.16. This sequence utilizes several vi's which configure the hardware to conform to the input parameters provided by the user in Config.vi. Once the hardware configuration is completed the program enters a while-do loop which will continually read the specified channels and save them and their associated time to a file. The data acquisition process appears to the user on the control panel in the form of a Voltage vs. Time chart, as seen in Figure 3.17. Once the test is completed and the user wishes to terminate the acquisition, the stop acquisition button on the control panel is depressed and the acquisition is completed.

3.6 LOADING SYSTEM

The primary purpose of the field testing system is to experimentally load rate bridges as well as performing worthwhile bridge research. A bridge must be monitored during a known loading event to accurately evaluate member stiffness, load distribution, and various other system characteristics. The method of loading the bridge selected by the University of Missouri was a calibrated load truck. A 1984 Freightliner truck, seen in Figure 3.18, equipped with an M-21-8 Jiffy Lift Classic-Lift Eagle boom was selected. Steel blocks, also seen in Figure 3.18, each weighing an average of 1500 lb were manufactured to increase the axle loads of the truck (Frederick 1997). The boom provides an efficient method of loading and unloading the truck during testing. This efficiency is extremely important since the truck will have to be incrementally loaded several times during a load test. Wheel weights are determined for each load increment through the use of four weighing pads, as seen in Figure 3.19.

3.7 SUMMARY

Field testing is a valuable means of evaluating existing structures. However, typically it is a rather expensive and time consuming task, requiring large efforts in (1) designing the test, (2) instrumenting the structure, (3) loading the structure and (4) reducing the data. One purpose of this project was to develop an economical, efficient and reliable field test system to make testing of structures a common occurrence. This was accomplished addressing the four areas of effort listed above.

Field test guidelines have been developed (Chapter 6 and McDaniel 1998) that guide the engineer in testing steel girder bridges. It contains inspection and instrumentation requirements for six different test plans. The test plans vary in level of effort and expected results for load rating bridges with experimental test results.

A data acquisition system, housed in a command center and living quarters vehicle, has been designed and built to minimize instrumentation effort. The modular data collection hardware can be set up quickly. Weldable strain gages, LVDTs, and the laser deflection device allow quick application and set up with little or no scaffolding. The electronics have been carefully designed to minimize noise and problems associated with collecting up to 125 channels at distances beyond 200 ft. Diagnostic tools specifically designed for the system allow quick assessment prior to testing.

The boom truck and compact steel weights permit variable loading of the structure. The weight can be changed quickly for efficient testing. Crawl speed tests minimize traffic disruption to the public.

Test monitoring in real-time is possible with the data acquisition software. Preliminary results can be quickly determined by importing the data into a computer

spreadsheet. For instance, for the Bridge R289 tests (Chapter 4), a preliminary load capacity rating was determined within a minute after the truck passed over the bridge.

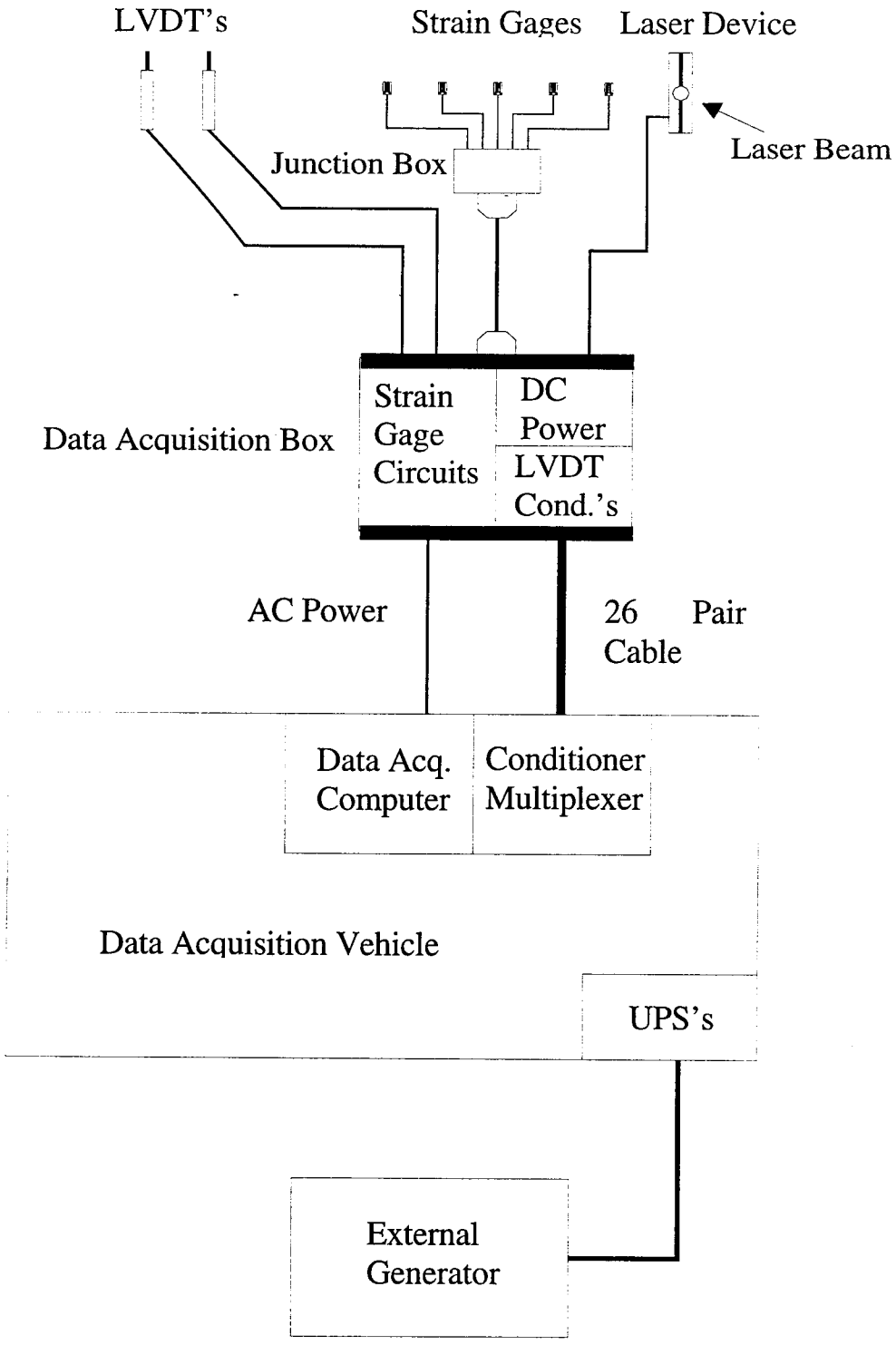

Figure 3.1 Schematic of Data Acquisition System

Figure 3.2 The University of Missouri – Columbia data acquisition vehicle.

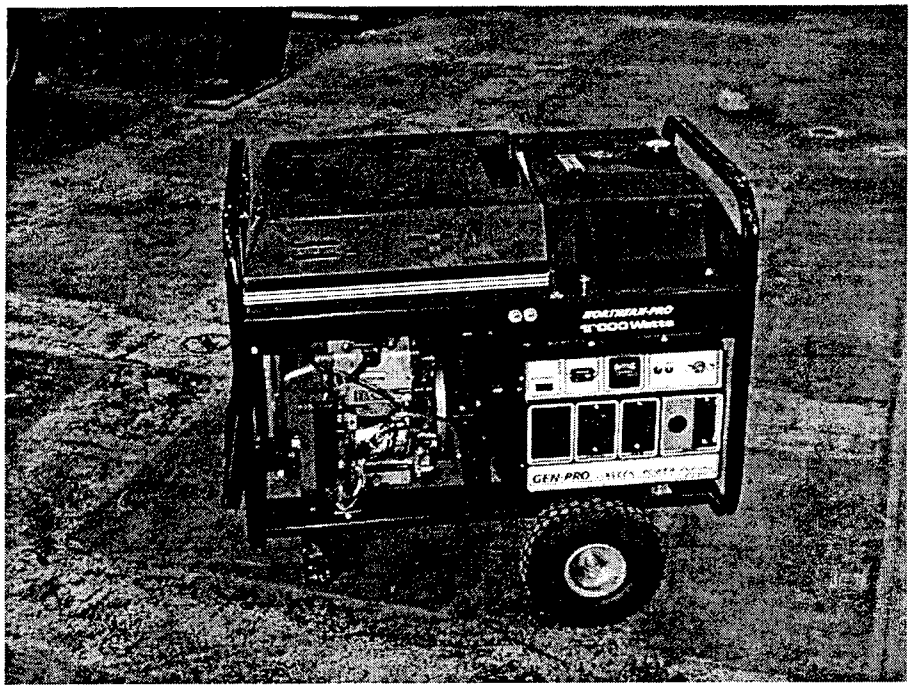

Figure 3.3 Picture of the external generators.

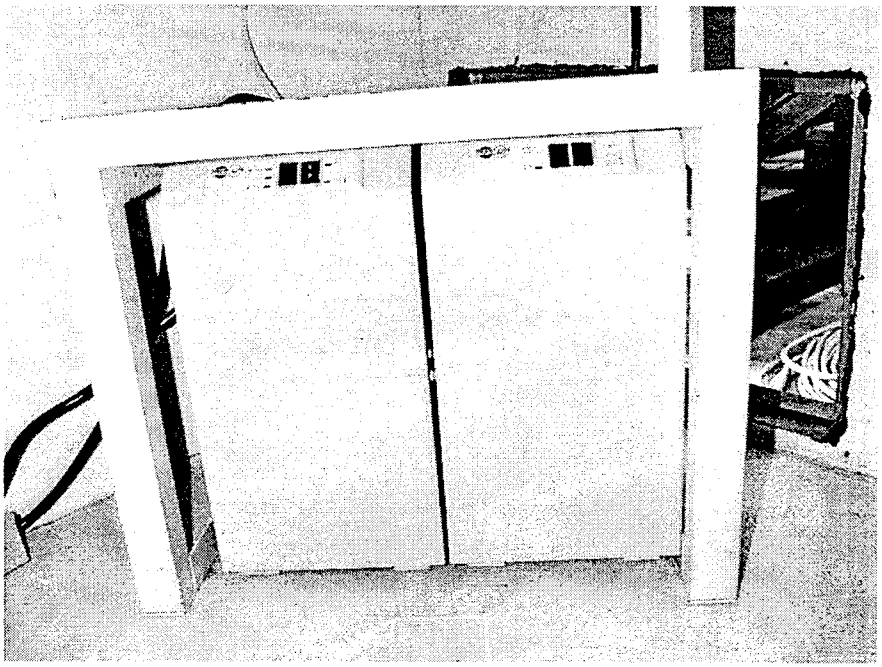

Figure 3.4 Picture of the uninterruptible power supplies.

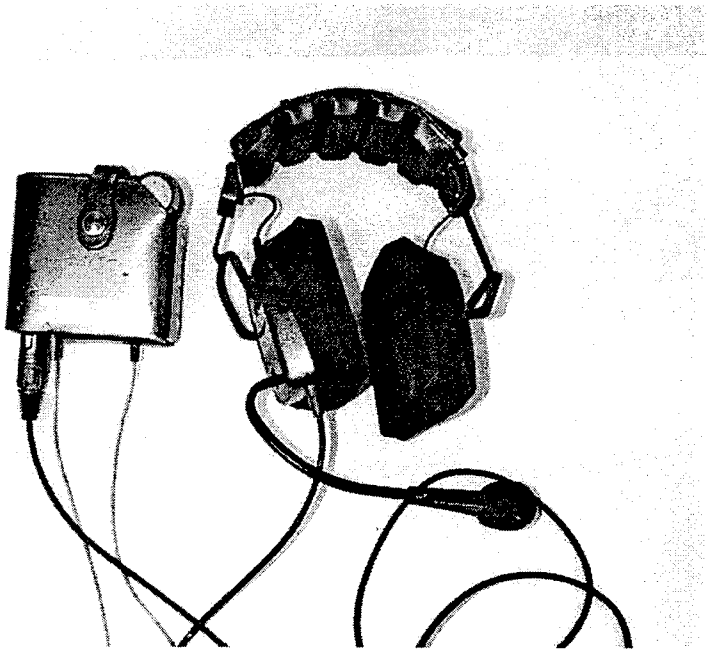

Figure 3.5 The Telex microphone, Belt-Pack, and headsets.

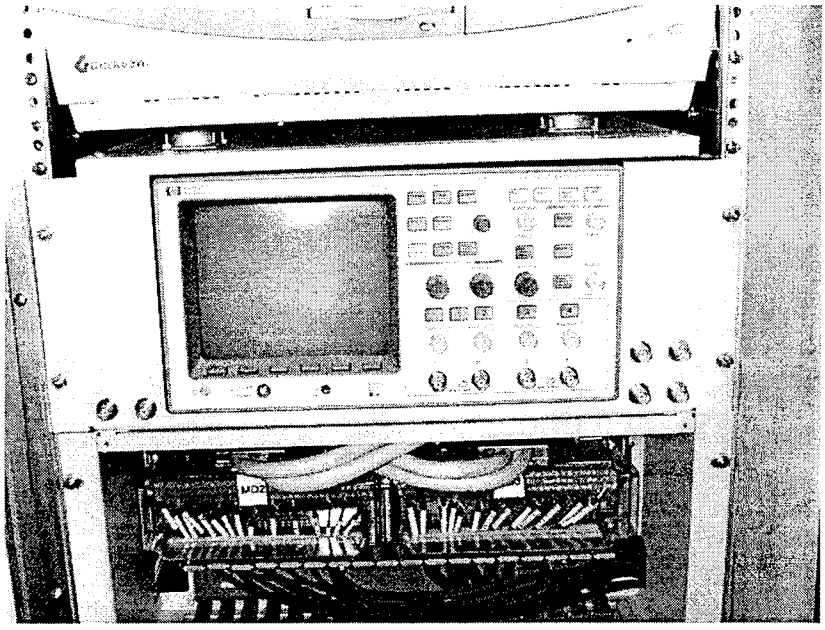

Figure 3.6 Picture of the rack mounted oscilloscope.

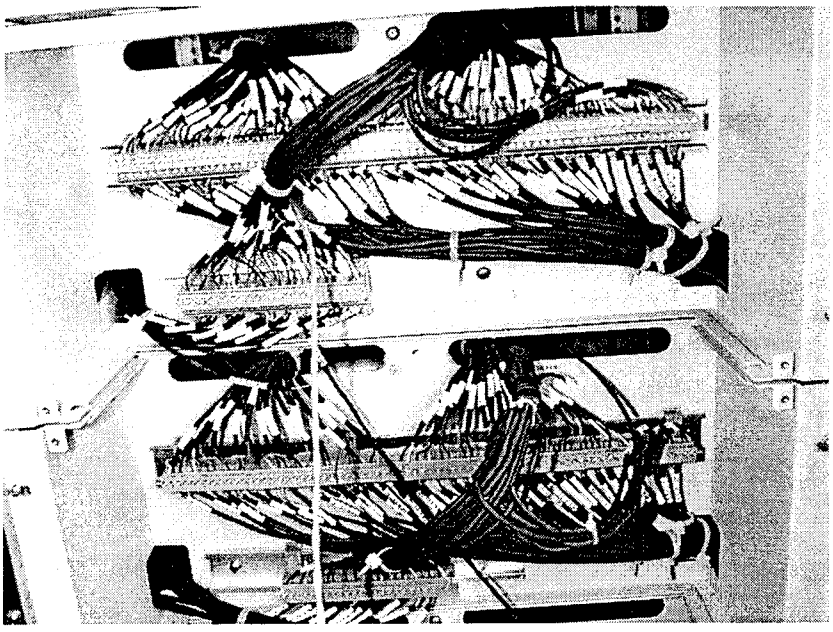

Figure 3.7 TBX-24F's with all signal connections completed.

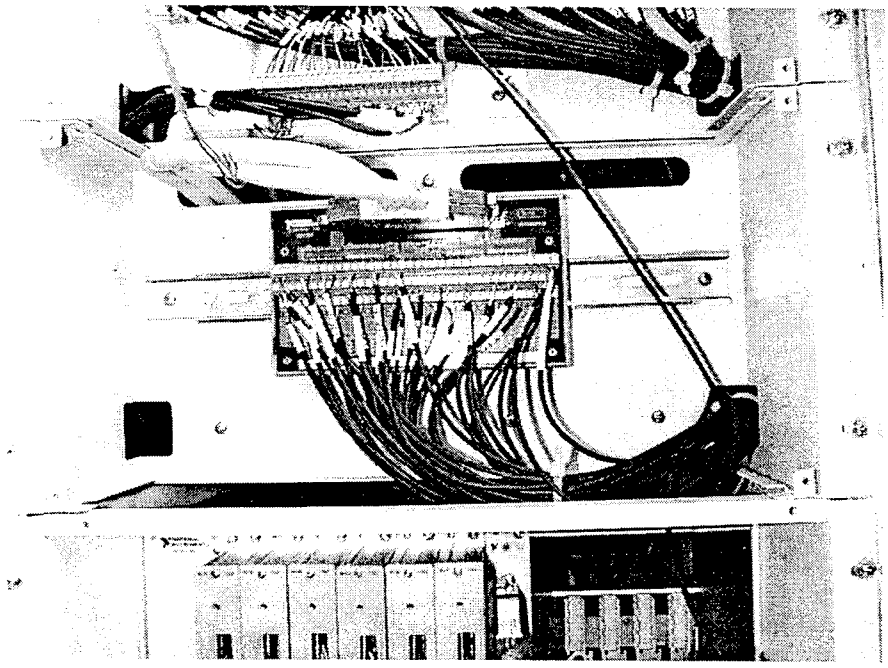

Figure 3.8 TBX 1303 mounted in the rack with all signal connections completed.

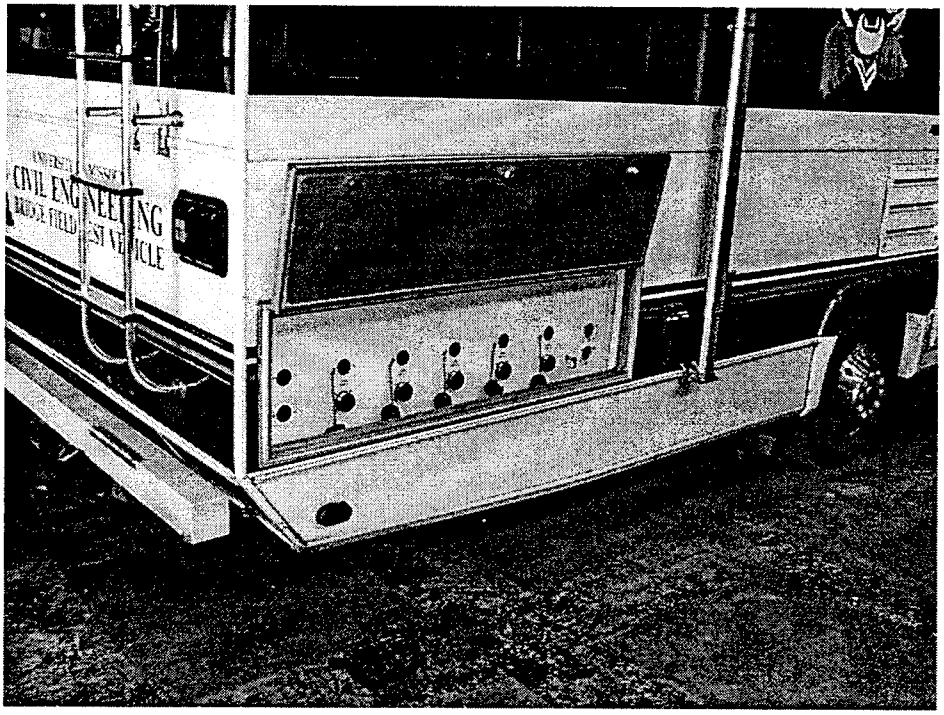

Figure 3.9 Connection panels in the side of the acquisition vehicle.

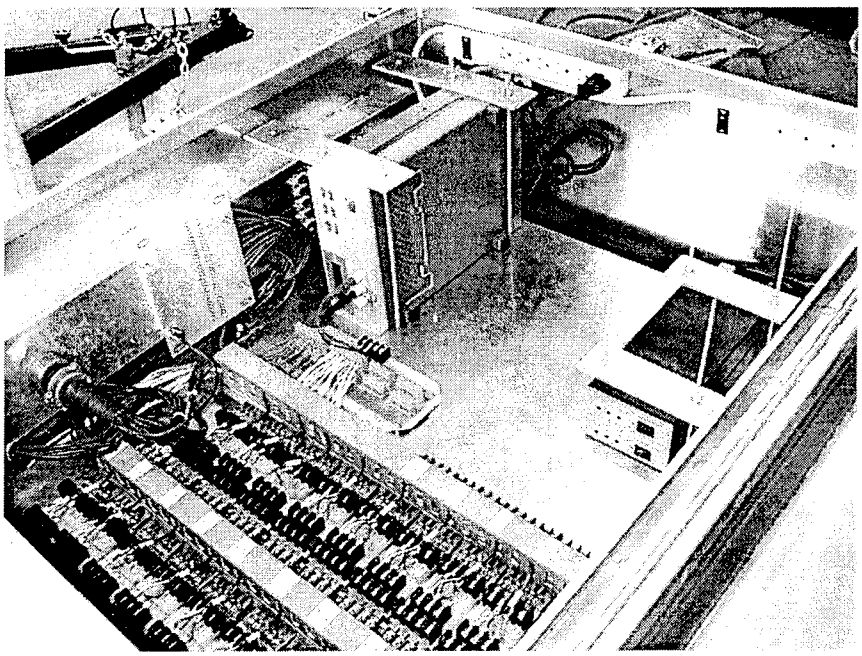

Figure 3.10 A data acquisition box

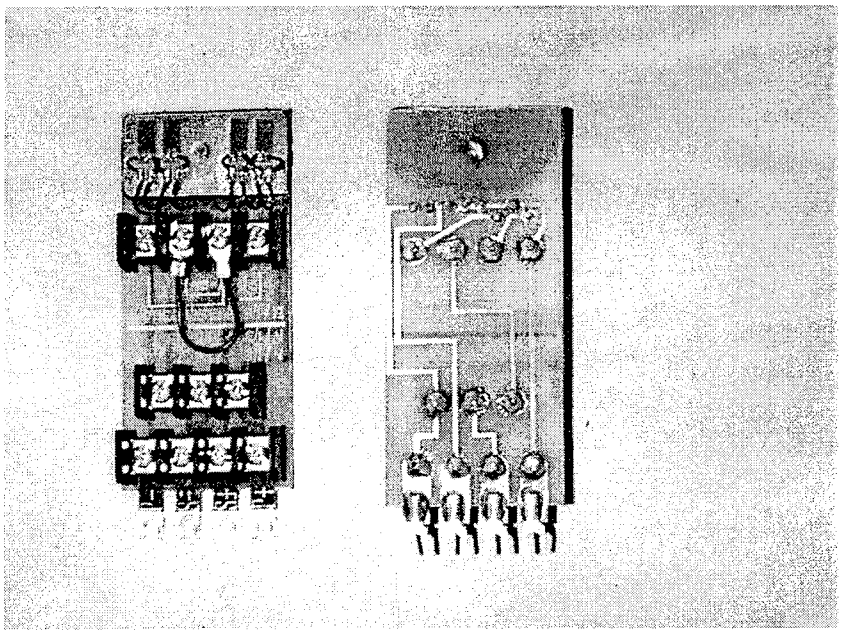

Figure 3.11 Wheatstone bridge completion module.

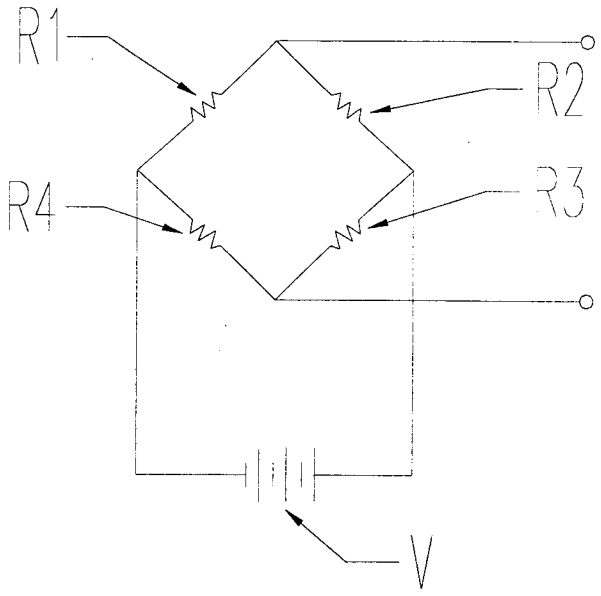

Figure 3.12 Wheatstone bridge circuit.

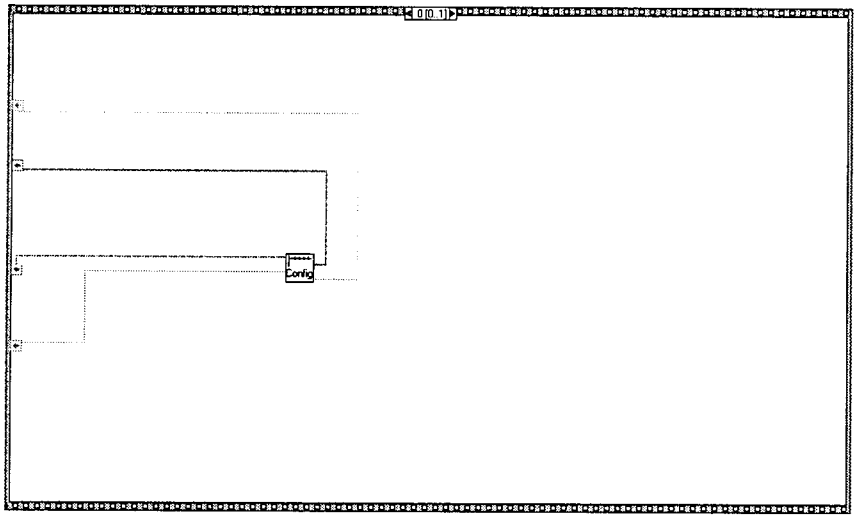

Figure 3.13 Diagramming page of the configuration sequence in Daq.vi.

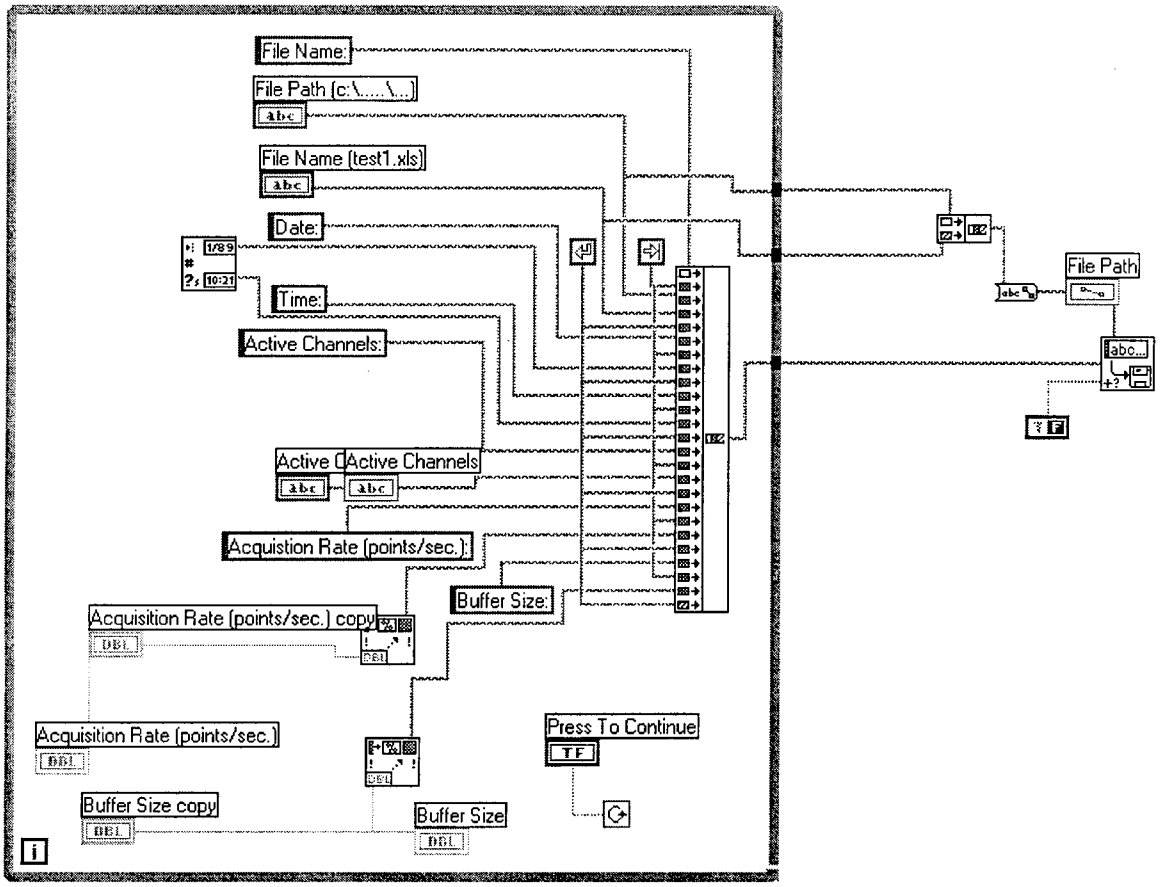

Figure 3.14 Diagramming page of Config.vi.

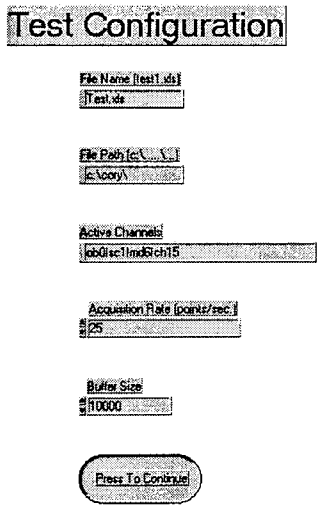

Figure 3.15 Control panel of Config.vi.

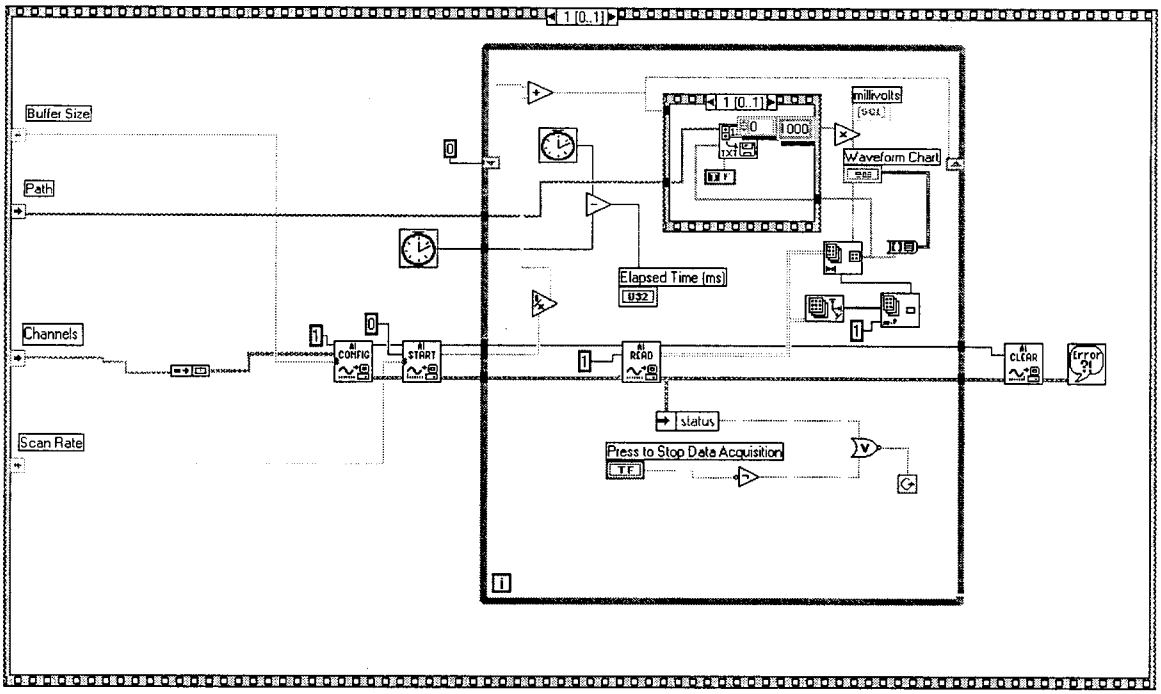

Figure 3.16 Diagramming page of the data acquisition sequence.

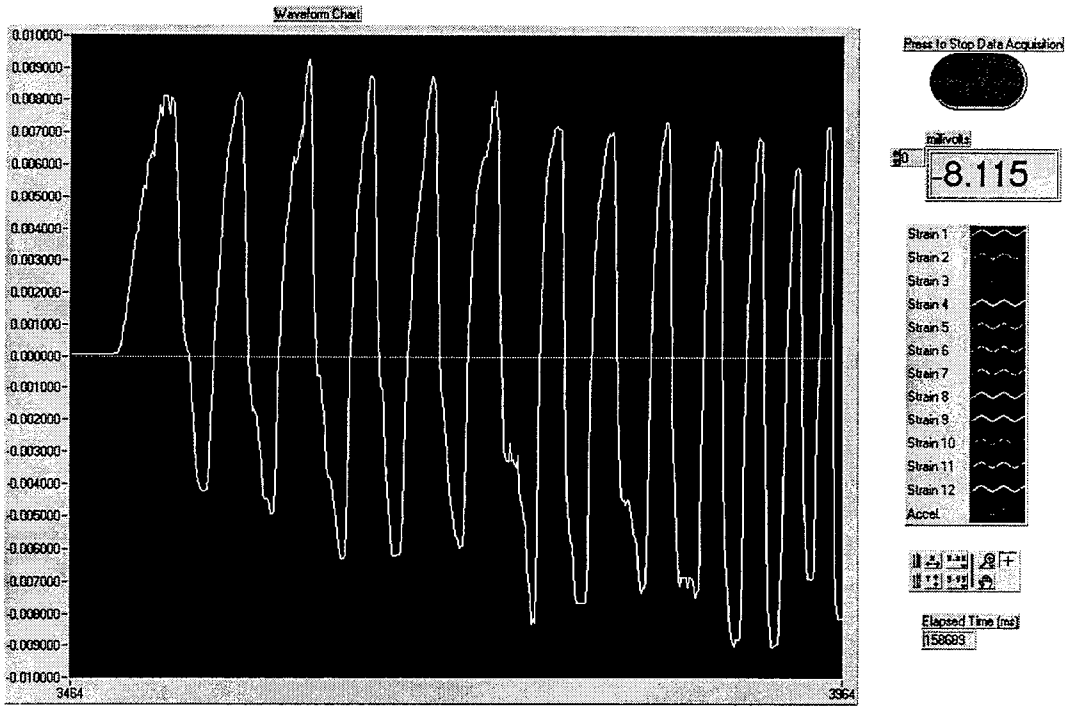

Figure 3.17 Control and output panel of Daq.vi.

Figure 3.18 Load truck and weights.

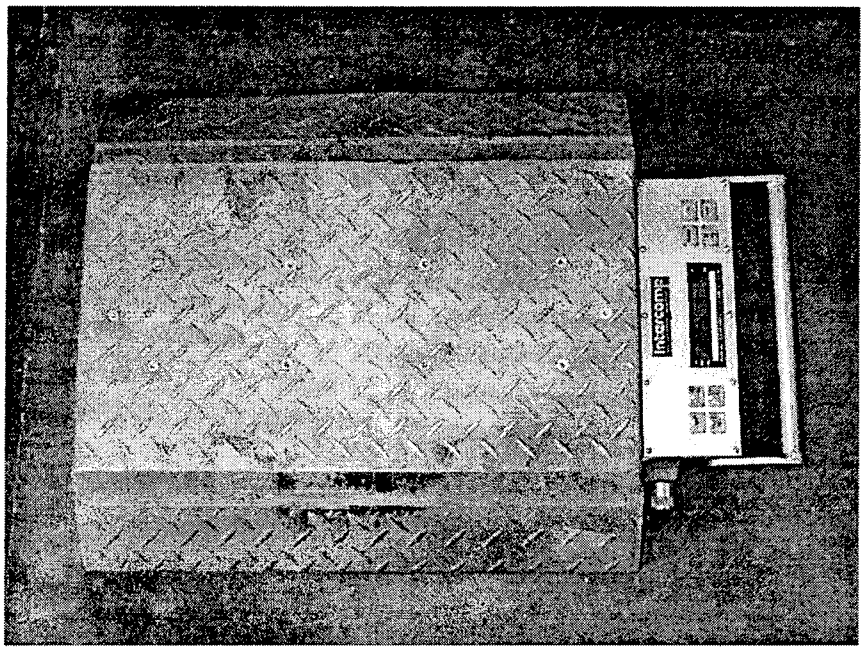

Figure 3.19 Weighing pad.

CHAPTER 4

LOAD TESTING OF BRIDGE R-289

4.1 INTRODUCTION

In September 1997, a letter was sent from the Missouri Department of Transportation (MoDOT) detailing nine candidate bridges in Franklin County, Missouri. Each of the nine bridges were visited and, from these site investigations, Bridge R-289 over the Boeuf creek on Route ZZ was chosen.

Bridge R-289 is a three span, continuous, posted one-lane bridge with a concrete deck and four rolled steel girders. It can be seen in Figures 4.1 and 4.2. It is an ideal candidate bridge for several reasons:

(1) it is posted for a restrictive loading,

(2) it is in a remote location with little traffic (ADT =300),

(3) it has convenient access to the underside of the structure,

(4) it has a good staging area for the load trucks and the data acquisition vehicle,

(5) it is in good condition, with little rust of the girders or deterioration of the concrete slab,

(6) the substructure appears to be in good condition with no scour, and

(7) it has Type D rocker bearings.

The bridge was also chosen because it has three continuous spans with the midspan being composite and the end spans being non-composite. This allowed the field testing team to examine such factors as unintentional composite action, bearing restraint forces, actual lateral distribution of live loads, and dynamic impact. Details on the testing of Bridge R-289 are included in this chapter.

4.2 DESCRIPTION OF BRIDGE R-289

Bridge R-289 over the Boeuf creek is located on Route ZZ about 6 miles north of Gerald in Franklin County, Missouri. It is a 36 year old, three-span (60 ft, 90 ft, 60 ft) continuous slab-on-steel girder bridge. The bridge consists of four rolled steel girders. The north and south exterior girders are W27X84 sections while the interior girders are W27X84 sections at the end spans and then change to W27X94 sections at the splice locations in spans one and three shown in Figure 4.3. The girders are composite with the concrete deck only in the middle span. They are non-composite in spans one and three. However, in spans one and three, the top flanges of the steel girders are partially embedded in the concrete haunch, making the possibility of at least some partial composite action.

Each bridge span is provided with two end diaphragms. Spans one and three have two intermediate diaphragms while span two has three intermediate diaphragms. The locations of the diaphragms can be seen in Figure 4.3. The end diaphragms are C12x20.7 sections as can be seen in Figure 4.4 while the intermediate diaphragms are bent 21x 3/16 inch plates as seen in Figure 4.5.

There are three different splice details for the bridge. The first type of splice attaches a W27x84 to a W27x84, utilizing no filler plates. These are located in all three spans for the exterior girders. The second type of splice connects a W27x94 to a W27x94 in the second span interior girders. The third type of splice attaches a W27x84 to a W27x94, utilizing 3/16x12 x10 inch filler plates for the flanges. This final splice is on the interior girders in spans one and three. A typical splice can be seen in Figure 4.6. Over the two interior piers in the negative moment regions, cover plates are installed on the top and bottom of the girders. These cover plates are 26 ft 6 in long and are composed of 12x5/8 inch plates. A

view of the cover plates can be seen in Figure 4.5. The bridge is supported by standard Missouri Type D bearings that can be seen in Figure 4.7.

The concrete slab is approximately six inches thick and is lined on each side by two concrete curbs and C12x20.7 railings seen in Figure 4.1. The concrete is in excellent condition, with the exception of minor spalling on the overhangs outside the exterior girders.

The concrete piers were observed to be in excellent condition, with no concrete section losses. Also, there appeared to be no signs of scour. The abutments on both the east and west ends are also in excellent condition, with no concrete spalling. A view of the piers can be seen in Figure 4.8. For additional information on the characteristics of this bridge, the reader is referred to Frederick (1998) for the complete MoDOT bridge plans, the most recent analytical rating, and the most recent inspection reports.

4.3 PREPARATION FOR FIELD TESTING

Once the bridge was chosen, the test crew worked to prepare for the field testing of the structure. It is noted that the purpose of this particular field test is two-fold. First, the field test of Bridge R-289 will be used to test theories and the system developed by the University of Missouri-Columbia's Department of Civil Engineering. Second, the field test will be used to propose a new rating and standardized field test procedure for MoDOT. Therefore, Bridge R-289 was instrumented much more heavily than what will be suggested later for implementation.

Four different trips were taken to Bridge R-289 for field testing research. The first visit occurred during January of 1998. This test was the initial outing of the field test system. The goals of this test were to lightly instrument the bridge and take readings that could be analyzed to determine the accuracy of the instrumentation and the system. A total of 18

strain gages were installed on the bridge and a total of five deflections were recorded. However, this test had problems in that data from one of the data acquisition boxes didn't reach the data acquisition vehicle, leaving the testing crew with little data to analyze.

The second visit to Bridge R-289 was early April 1998. This particular time frame was used to instrument the bridge fully for the complete load test that will be discussed below. It took four days to weld and solder 95 weldable strain gages onto the bridge. Details on the placement of these gages are included later in this chapter. After the installation, two days of tests were run with the load truck loaded to a maximum of the posted loading. Encountered with these tests was the presence of signal noise that was greater than desired for the testing system. In addition, some problems with the 26 pair cables (RV to data acquisition box connection) led to some data not reaching the data acquisition vehicle. The system was taken back where the cables were checked for continuity. It was believed that the noise troubles were caused by some leadwires in the cables being shorted to the data acquisition vehicle.

The third test was preformed later in April 1998. The data acquisition boxes and cables were again installed and the instrumentation system was examined. It was determined that a large grounding problem was occurring with the system. After returning from the test, each cable assembly was repaired to ensure no cross talk between wires and no grounding of the system by the connectors. National Instruments Corporation was contacted to determine if the system could be any better than the accuracy the testing crew was observing. It was learned in this conversation that better SCXI modules were available for strain readings. Subsequently, four of the five SCXI-1100 modules in the system were sent back to National Instruments in exchange for six SCXI-1122 modules for low level signals. These new

modules were checked in laboratory settings and found to have much better resolution and noise control. Details of the system performance after the acquisition of the new multiplexers can be seen in Chapter 5.

The fourth and final test of Bridge R-289 occurred in June 1998. The system was set up and calibrated within two days. A few problems with strain gages that were accidentally grounded to the bridge were discovered in the troubleshooting phase. When this was corrected, the noise problems were greatly reduced. After the troubleshooting, three days of field testing followed. This included one day of low load diagnostic testing and two days of higher load testing. The following chapter deals primarily with the execution and results of this fourth and final test.

4.4 FIELD TESTING BRIDGE R-289

The following sections provide information on the instrumentation and testing of Bridge R-289. The gage instrumentation plans and the testing logs can be found in McDaniel (1998).

4.4.1 Preliminary Investigations

In Missouri, MoDOT frequently inspects bridges for signs of deterioration or distress. State system bridges are inspected annually and off-system bridges are inspected on a two-year cycle. Along with the inspection, the bridges have been rated by AASHTO C/E manual standards (AASHTO 1989). During an inspection time, new ratings are determined only if there is a change of the bridge condition from the previous inspection. The following section provides details of the inspection and rating preformed by the state, along with checks made by the University of Missouri's field test team.

4.4.1.1 Inspection

On December 18, 1997, the Missouri Department of Transportation preformed a field inspection of Bridge R-289 located in Franklin County, Missouri. This inspection concluded that the bridge as a whole was in good condition, with a potential for minor repairs. The concrete deck was in good condition, with one minor spall. The steel superstructure was also rated in good condition, with little rust on the steel girders. The substructure was rated in good condition, with little or no scour of the piers and only slight cracking of the east abutment.

The field test crew visited the bridge site and carefully documented the dimensions of the girders, haunches, diaphragms, stiffeners, cover plates, barrier curbs, railings, slab, and wearing surfaces. The only variance between design values and actual values were with the girder measurements. Table 4.1 lists the design dimensions of the girders versus the measured values. From these dimensions, the dead load per linear ft from the measured values for each of the girders was estimated and is used in bridge calculations in subsequent sections. For more complete calculations of the dead load and section properties, the reader is referred to Frederick (1998).

4.4.1.2 Analytical Rating

Along with the most recent field inspection report, MoDOT provided the existing analytical rating information which the department had on file for this bridge. This bridge was also rated analytically by Frederick (1998) using the 1996 MoDOT rating manual. From this, it was determined that the critical section for Bridge R-289 was the 105 ft longitudinal location from the east abutment for the exterior girder. Frederick used the MoDOT bridge

rating information (some was found to be in error as described later) and confirmed the state's single-lane 15 ton posting for the H20 truck.

4.4.2 Test Objectives

After reviewing the as-built plans and the bridge itself, the field testing crew found many attributes that could lead to additional capacity for the structure:

(1) The first and third spans are absent of mechanical shear connectors between the girder and the slab. However, the top flange of the girders is partially imbedded in the haunch, making unintentional composite action a factor to be considered.

(2) The barrier curbs and railings on the top of the bridge have expansion joints, but they are continuous over given lengths or could be frozen in some locations. The testing will therefore include instrumentation to determine if the capacity of the bridge is affected by action due to forces in the railings.

(3) The pin and rocker bearings on the bridge, though they appear in good working order, may in fact be frozen. Also, in working bearings, frictional forces may lead to additional horizontal forces that will act to reduce the applied moment in the girders. Therefore, these phenomena will be instrumented and monitored.

(4) On most slab on girder bridges, the AASHTO lateral distribution factors are often conservative. The bridge will be instrumented at four longitudinal locations (24 ft, 63 ft, 105 ft, 147 ft) to assess the actual lateral distribution of forces.

(5) Impact factors can be conservative in AASHTO design calculations. Thus, the field testing crew will attempt to measure the impact factor for Bridge R-289 with the same gages that are installed for lateral distribution.

The above factors were tested by the use of diagnostic testing. Several truck load levels were applied to the bridge to ensure the results are consistent and linear and to help establish testing protocol for future load tests.

4.4.3 Diagnostic Testing

Due to the availability of as-built bridge plans, Bridge R-289 can be accurately tested with diagnostic testing procedures. This type of testing will ensure that the researchers will be able to verify assumptions used in load rating calculations and will help to establish the extent to which the load carrying capacity has been enhanced by the additional factors listed above. This will provide sufficient information to develop a new load rating.

4.4.4 Instrumentation

Due to the purpose and objectives of the field test of Bridge R-289, the bridge was carefully instrumented for diagnostic load testing. For the diagnostic test, several factors that can lead to additional capacity were found to be present on this bridge. Each of the factors will have instrumentation placed in a way that will allow for adequate data to determine the effects. The gage logs for this test can be found in McDaniel (1998).

4.4.4.1 Bearing Restraint Force Instrumentation

One of the main factors tested on Bridge R-289 was the presence of bearing restraint forces. Due to the multi-span nature of this bridge, several gages are needed on the critical south exterior girder to accurately test this phenomena. Gages were placed at a distance of

six inches from the bearing and on each side of the bearing, when applicable. Though only the critical south exterior girder needed to be instrumented for bearing restraint, each girder was instrumented with bearing restraint gaging to help the researchers develop testing protocols. Figure 4.9 illustrates the positions of the bearing restraint strain gages at 0.5 ft, 59.5 ft, 60.5 ft, 149.5 ft, and 150.5 ft from the east abutment. A typical girder instrumentation for bearing restraint is shown in Figure 4.10. However, since the west interior pier contained the pinned bearing, little axial bearing restraint force was expected to pass through the support. Therefore, the bearing at the west abutment was not instrumented for bearing restraint because it will do little to the axial rigidity of the bridge in spans one and two.

At two locations on the critical south exterior girder, 0.5 ft and 60.5 ft from the east abutment, the girder was further instrumented for bearing restraint by placing gages at two web locations and one flange location. Views of these gage placements can be seen in Figures 4.11 and 4.12. These gage placements were done mainly to compare results with experimental results of an earlier bearing restraint test performed by the University for MoDOT (MCHRP 97-4) and to help in further understanding bearing restraint in existing structures (Barker and Hartnagel 1997). A detailed log of the gages used for bearing restraint is included in McDaniel (1998).

4.4.4.2 Railing Instrumentation

Another factor that could influence the rating of the bridge is the presence of concrete barrier curbs and 12 inch C-channel railings. However, with the limitations of the field test system, strain gage placement became limited. Therefore, the instrumentation of the railings was limited to two gages on the web of each railing at the 105 ft critical location, which was

the positive moment region in the second span. These gages can be used to show if a large compressive force develops in the railing, indicating a contribution to the load carrying capacity. The layout of these gages can be seen in the gage logs in McDaniel (1998). A view of the gage placement on the railings can be seen in Figure 4.13.

4.4.4.3 Moment Section Instrumentation

The remainder of the gages installed on the bridge serve a variety of functions. These include the determination of the lateral distribution factor, determination of the impact factor, determination of composite action, and determination of maximum strain. The critical girder was heavily instrumented at maximum moment sections in order to be able to monitor the behavior carefully. The three other girders were also instrumented at the maximum moment locations to get a better confirmation of the behavior of the bridge.

For span one, the bridge was instrumented at the four-tenths point (24 ft) from the east abutment for the maximum positive moment in this section. The instrumentation at the four-tenths point was to study behavior of non-composite sections in positive moment regions. For each of the four girders, two strain gages were installed: one on the top flange and one on the bottom flange. The placement can be seen in Figures 4.14 and 4.15. The bottom gages on each section will help to determine the maximum stress at this section and can be used to determine a lateral distribution factor at this section. The top gages can be used with the bottom gages to draw cross section strain diagrams for the steel, thus showing the researcher the amount of unintended composite action.

The second span of the bridge is critical for the analytical rating. Therefore, the bridge was instrumented at three cross sections: at midspan for the maximum positive moment and near both of the pier supports for the maximum negative moment. Gage

placements at the supports is prohibited by bearings and diaphragms and is unwise due to local support compression effects. Near the piers, the gages were placed at 63 ft and 147 ft from the east abutment, 3 ft away from both piers. The positive moment was also shifted 0.5 ft away from an intermediate diaphragm and is located at 105.5 ft from the east abutment. The gage placements listed above can be seen in Figure 4.9.

At both 63 ft and 147 ft from the east abutment, each critical south exterior girder was instrumented with seven gages. Two gages were located on the bottom of the bottom flange, three gages in the web, and two gages on the bottom of the top flange. Figures 4.16 and 4.17 show the layout of these gages. The bottom flange gages were averaged to determine a bottom flange strain. This was one of the stress quantities used to monitor the bridge for signs of distress. The top two gages were also averaged to determine the top flange stresses. The remaining gages were useful in determining an accurate strain diagram for this cross section. On the non-critical girders at these locations (north exterior and interior girders) four gages were used. One gage was located on the bottom of the bottom flange, two gages in the web, and one gage on the bottom of the top flange. The bottom flange gages were used in conjunction with the south exterior bottom flange gages to determine lateral distribution factors and impact. The other gages were used to determine the strain diagrams for each of the girders. A detailed view of this placement can be seen in Figures 4.18 and 4.19.

At the 105.5 ft positive moment location, the critical south exterior girder was instrumented with seven gages. Two gages were located on the bottom of the bottom flange, three gages in the web, and two gages on the bottom of the top flange. The gages at this section were crucial because this was the critical location for rating the bridge. The bottom

flange gages were again averaged and used to monitor if the bridge was showing any signs of distress. The remaining gages were used to get an accurate strain diagram. Figures 4.20 and 4.21 show the layout of these gages. On the other girders at this location, four gages were used. One gage was located on the bottom of the bottom flange, two gages in the web, and one gage on the bottom of the top flange. Again, these bottom flange gages were used in conjunction with the bottom flange gages on the south exterior girder to determine the lateral distribution factor for the span and to determine the impact factor. The remaining gages were used with the respective bottom flange gages to give an accurate strain diagram. Figures 4.22 and 4.23 show the layout of these gages.

As was for the first span, the gage placements on the girders in the middle span were multifunctional. The bottom flange gages were used to determine the maximum stress on each cross section, and the impact on each cross section. Also, when used in conjunction with each other, they can determine a lateral distribution of forces. The remaining gages are also used to study the amount of composite action and to determine if the cross sections are behaving in a linear elastic fashion.

4.4.4.4 Deflection Instrumentation

In addition to strain, deflection devices were set up for the testing. Four LVDT's were set up at the 24 ft location from the east abutment and are hooked into a data acquisition box. A view of an LVDT on Bridge R-289 can be seen in Figure 4.24. The laser deflection device is used at the critical location, 105 ft from the east abutment, on the critical south exterior girder. A view of the laser deflection device on Bridge R-289 can be seen in Figure 4.25.

4.4.4.5 Data Acquisition Boxes

The boxes were arranged to minimize lead wire lengths. Box 1 was located on the diaphragm between the south interior and exterior girder at the 24 ft location from the east abutment. This box serviced the gages at the 24 ft cross section locations and some bearing restraint gages. It also serviced the four LVDT's. Box 2 was located on the top of the east pier at the 60 ft location between the interior girders. It serviced the gages at the 63 ft location. Box 3 was located on the diaphragm at the 105 ft location between the south exterior and interior girder. It serviced the gages at the 105 ft location as well as the laser deflection device. Box 4 was located at the top of the west pier and serviced the gages at the 147 ft location. Box 5 was located on the diaphragm at the 105 ft location between the interior girders. It serves the remaining bearing restraint gages. It was put at the center of the bridge so that leadwires from the bearing restraint gages over the interior piers would have the same length.

4.4.5 Measurement Devices

From the instrumentation plan described in the previous section, several decisions were made as to the types of instruments to be used on the structure. In general, most of the strain gages that were used are 120 ohm CEA-06-W250A-120 gages. However, for some of the bearing restraint gages in boxes 1 and 5, significant lengths of leadwire are needed to connect the gage to the data transfer box. Therefore, these strain gages were 350 ohm CEA-06-W250A-350 gages. Both types of gages come from Measurements Group, Inc (1993).

For deflections, four 3002 XS-D LVDT's from Schaevitz engineering were used at the 24 ft from the east abutment location. The laser deflection instrumentation was on the south exterior girder in the center of the second span. Due to the height of the girder from

the ground, coupled with the flow of the creek, it was decided that an alternative deflection measurement device be used. Thus, the laser deflection device, mentioned earlier, was used on the exterior of the girder. The helium neon laser installed on a tripod was about 150 ft from the girder at about a ten ft lower elevation than the girder.

4.4.6 Loadings, Load Postings, and Load Steps

The truck weight and configuration used for the diagnostic tests should roughly resemble the H20 rating truck from AASHTO (differences are taken care of by adjusting H20 and load truck moments). This allows for an easier analysis from the theoretical behavior of the bridge to the actual behavior. It was decided that this truck should be placed on 2 ft transverse locations across the entire bridge. The worst case scenario for the critical south exterior girder is driving the truck's wheel line directly next to the south curb. Figure 4.26 and 4.27 show the different south and north tandem axle wheel line positions (transverse paths) that were used on Bridge R-289, respectively. The truck was driven at crawl speeds from the east side of the bridge to the west side. The dynamic tests were administered with the loading truck driving directly down the center of the bridge at crawl speed, then at 10, 20, 30, 40, 50, and 55 miles per hour. The bottom flange girder strains for the moving cases were divided by the strain for the crawl speed case to estimate the impact factor for the bridge. A full list of testing runs for Bridge R-289 is found in McDaniel (1998).

The design impact factor for Bridge R-289 in the second span is 1.23, dead load stresses in the south exterior girder section are approximately 14.0 ksi, and residual stresses can be assumed to be 10 ksi. Thus, for the 36 ksi steel girder, the amount of live load stress that can be applied to the bridge before the onset of yielding is 12.0 ksi. The 12.0 ksi limit was used as the "cease test" criteria examined during each of the tests performed. Thus, no

yielding occurred during any of the tests. For future field tests, a practical 'cease test" stress level could be that the calculated dead load stress plus the measured live load stress not exceed 0.70Fy ((Fy-residual)/Fy).

The diagnostic testing began at the 21.75 ton load level and the structure was put through a full cycle of tests. After it is determined that the bridge behaved elastically, the loadings were increased to show that the bridge will behaved linearly and that values could be extrapolated from lower load levels. This was also used to show repeatability of results.

4.4.7 Personnel Requirements

From setup and installation of the instrumentation to the actual field tests, qualified personnel must be present. The University of Missouri –Columbia field testing team consisted of Travis McDaniel, Troy Frederick, Cory Imhoff (Graduate Students), Dr. Michael Barker (Associate Professor), Dr. Bryan Hartnagel (Research Assistant Professor), and C.H. Cassil (Senior Research Technician). Each of these members worked in unison to instrument, troubleshoot, and test the bridge. All members are qualified to handle the instrumentation, troubleshooting, and testing of the bridge. During the actual field testing, the loading truck was driven by C.H. Cassil while T. McDaniel, T. Frederick, and Dr. Hartnagel handled the traffic duties. C. Imhoff and Dr. Barker handled the data acquisition duties in the data acquisition vehicle.

4.4.8 Sequence of the Load Testing

For most field tests, three days will be adequate for instrumentation, troubleshooting, testing, and clean-up. However, due to the expanded nature of this project, several trips were

made to the bridge for instrumentation and troubleshooting as well as for testing (see Section 4.3).

4.4.8.1 Instrumentation and Troubleshooting

The setup of the instrumentation and the troubleshooting for final testing took place over four different testing intervals at the bridge as discussed earlier in Section 4.3. During the second visit to the testing site, the 95 strain gages were completely installed and leadwires were run to the data junction boxes that remained at the test site until completion. It took approximately four days to install the gages, solder the leadwire tabs, run leadwires to the data junction boxes, and connect the leadwires into the data junction box.

Once all of the gages and deflection devices were attached to the bridge, the troubleshooting process began. This included a few days from the second site visit, five days from the third visit, as well as three days from the final testing visit. Problems encountered were due to faulty cables, incorrect signal conditioning modules, broken Wheatstone bridge completion modules, and grounding problems. After the cables had been repaired and the proper modules were installed in the data acquisition system, each data acquisition box was checked with a shundt calibrator to test for linearity. From these tests it was found that two gages on the girders were shorted to the bridge at the gage location, making the entire system common to the bridge and allowing the bridge to act like a large antenna for noise. This problem was corrected and, afterward, most of the gages performed with the accuracy that was expected. However, a few problems were encountered with two completion circuit signals between the data acquisition box and the data acquisition rack. Thus, these two signals were hard wired into the data acquisition rack from the completion module, bypassing

the acquisition box and the cables. After this rearrangement, the noise that the system was encountering was greatly reduced.

On June 7th, 1998 all of the problems with grounding and noise in the data acquisition system were fixed and the data acquisition system was ready for testing.

4.4.9 Load Application

The truck was loaded with 12 steel blocks on the rear of the vehicle. After weighing the truck with the portable scales, the total weight of the truck was found to be 21.75 tons, deemed close enough to the AASHTO H20. Figure 4.27 shows the axle loads for the load truck at 21.75 tons.

The data acquisition power was left on throughout the entire stay at the bridge, ensuring that the system was properly warmed up. On June 7th tests included eight runs at crawl speed heading west over the bridge in the eight different transverse locations listed in Figures 4.26 and 4.27. Next, three runs over the centerline at speeds of 20, 35, and 45 miles per hour were preformed to assess the dynamic characteristics of the bridge.

On June 8th, the majority of the diagnostic test runs were preformed. This included starting with the exact same eight runs that had been tested for on the previous day to test whether the system was giving reliable and consistent results over time. After a few minutes of analysis, it was determined that the system was giving the same results as the previous day. Knowing this, the next six tests preformed were dynamic tests ran at speeds of 10, 20, 30, 40, 50, and 55 miles per hour.

The truck was turned around and the same eight tests were preformed at crawl speeds with the truck heading east. Then the same six dynamic tests were preformed over the center of the bridge at the previous speeds.

After careful data analysis, it was determined that the bridge was only being subjected to about 6150 psi of stress in the critical location, far less than the distress value of 12,000 psi. Therefore, through careful calculations using bridge rating techniques shown in Imhoff (1998), it was decided that the truck could be conservatively loaded to over 30 tons with absolutely no damage. Figure 4.29 shows the maximum stress placed on the bottom flanges of all the girders at the critical longitudinal location due to the 21.75 ton load truck. The truck was loaded further with 11 more steel blocks in front of the crane, bringing the total weight to 29.93 tons. Figure 4.30 shows the axle weights for the 29.93 ton load truck. The concrete deck was checked with the larger axle loads to ensure the transverse bending did not produce stresses above the modulus of rupture for the concrete.

After the new loading, the same eight runs heading west over the bridge were performed. After the truck crossed the bridge heading west, the deflections and strains did not return back to exactly zero. This is expected with a system "resting" position after loading. The bridge was shifting when the truck crossed east to west and then reset to the original position when the truck backed over it to prepare for a new test. To study this behavior, the truck was run down the six ft south of centerline location, remained off the west side of the bridge for a period of five seconds, and then was backed across the bridge over the same location. From this run, called a full cycle run, the deflections should return to zero if no damage has occurred. Figure 4.31 shows the full cycle test run. Figures 4.32 and 4.33 are enlargements of Figure 4.31. Figure 4.32 shows how offset stresses are left after the truck crosses the bridge heading west while Figure 4.33 shows how the stresses return to zero after the truck is backed across the bridge.

The maximum stress that the bridge girders were subjected to with the 29.93 ton truck was 8662 psi as can be seen in Figure 4.34. Thus, it was again determined similar to that done for the 21.75 ton truck that the bridge would conservatively behave elastically above 35 tons. This demonstrated linear elastic behavior for varying truck weight. The truck was subsequently loaded with an extra 5 steel blocks in the front of the crane and three blocks behind the crane for a total weight of 34.96 tons. Figure 4.35 shows the axle loadings for this truck. Again, the transverse concrete deck maximum stress was checked.

On June 9th, testing began by running the truck from east to west over the eight transverse positions as shown in Figures 4.26 and 4.27. Some tests were run in half cycles while others were run in full cycles. After these eight runs, two more full cycle runs were made over the critical six ft south of centerline location for repeatability.

On June 10th, three more runs with the 34.96 ton truck were made over the six ft south of centerline location for repeatability. It can be shown from Figure 4.36 that the bridge was subjected to about 10,000 psi, but was below the distress value of 12,000 psi. At this point, it was decided to not increase the load due to possibilities of localized yielding.

The truck was lowered near the initial testing weight, this time weighing 21.77 tons and driven across again to confirm repeatability.

The final test was performed with the truck on the six ft south of centerline transverse position. The truck was stopped at locations on the bridge that maximized moment at 24 ft, 60 ft, 105 ft, and 150 ft to take static readings. This was done to insure that the crawl speed tests caught the maximum stresses. Imhoff (1998) shows that the crawl speed tests did in fact catch the maximum responses of the bridge. This is important since using crawl speeds greatly reduces traffic disruptions.

4.4.10 Evaluation of Load Test Results

Imhoff (1998) developed near real-time data reduction worksheets in Microsoft Excel to estimate performance and projected ratings immediately after test runs. His worksheets were used throughout the testing with great success. Linearity checks, maximum response monitoring, and overall bridge behavior along with the ability to project what to do next was a valuable tool.

Once the field testing crew returned to Columbia, work began to reduce the vast amount of data obtained at the field test. The reduction of the data and the results can be found in Imhoff (1998). This included deriving equations that reduce the measured strain data into moments and calculating the bearing restraint forces. These values can be added or subtracted back into the elastic moment as needed.

4.4.11 Experimental Rating Results

Frederick (1998) developed an experimental rating based on the results of the field testing and the subsequent reduction by Imhoff (1998). Table 4.2 shows the results of the experimental rating. Notice that the experimental rating was 11 tons over the analytical. This experimental rating contains additional capacity from a dead load stress adjustment (2.93 tons), the experimental lateral distribution (4.85 tons), unintentional composite action (0.78 tons), contributions from curbs and railings (0.72 tons), and other attributes (1.72 tons). Frederick (1998) shows procedures that separated and quantified these contributions (Chapter 6).

Table 4.1 Measured Girder Dimensions

	W27x84		W27x94	
	Specified	Measured	Specified	Measured
Flange Width, inches	9.96	10.19	9.99	10.06
Flange Thickness, inches	0.64	0.65	0.75	0.76
Web Thickness, inches	0.46	0.50	0.49	0.56
Depth, inches	26.71	26.74	26.92	26.96
Area, inches^2	24.80	25.96	27.70	29.60

Table 4.2 Experimental versus Analytical Rating (Frederick 1998)

Rating Vehicle	Analytical Rating	Experimental Rating
H20	15 tons	26 tons

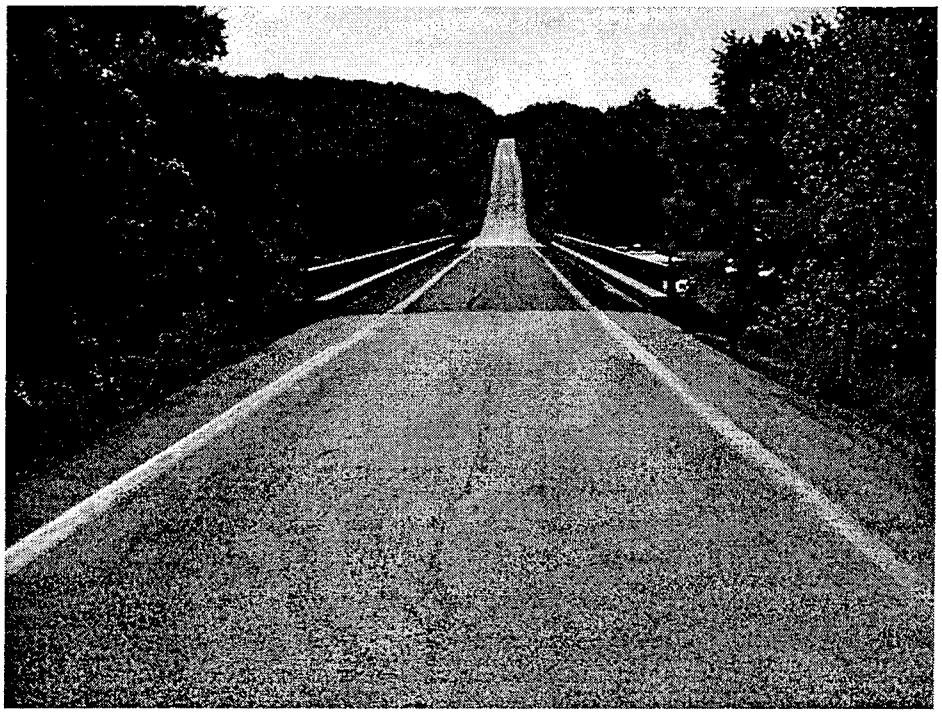

Figure 4.1 Bridge R-289

Figure 4.2 Profile of Bridge R-289

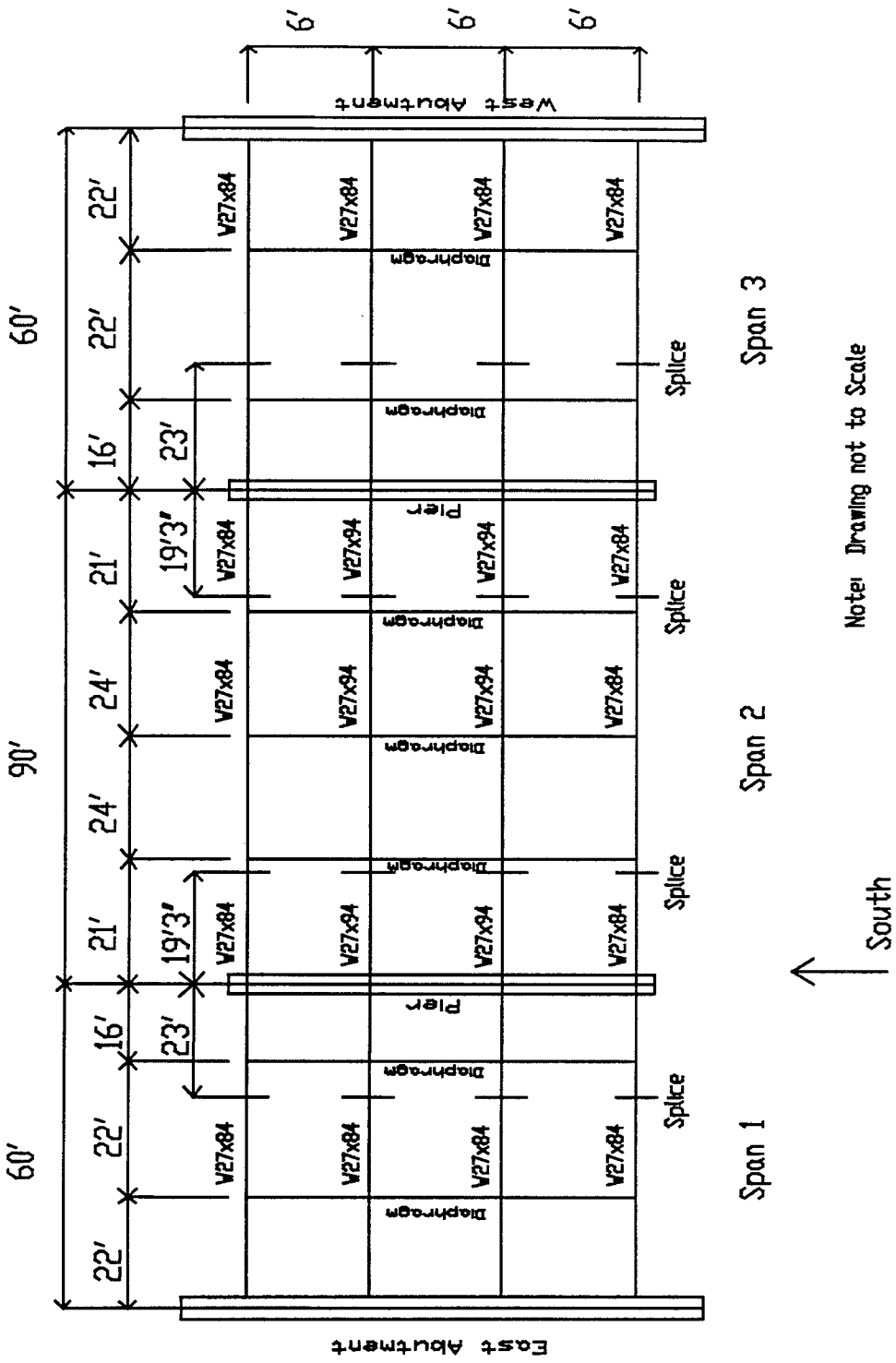

Figure 4.3 Layout of Superstructure

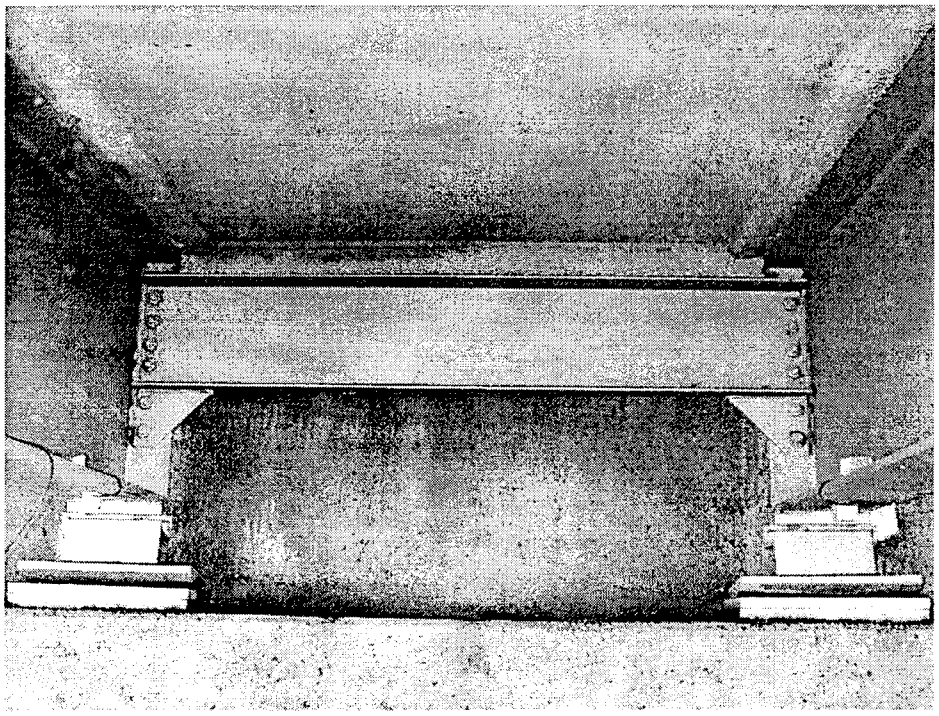

Figure 4.4 End Diaphragm

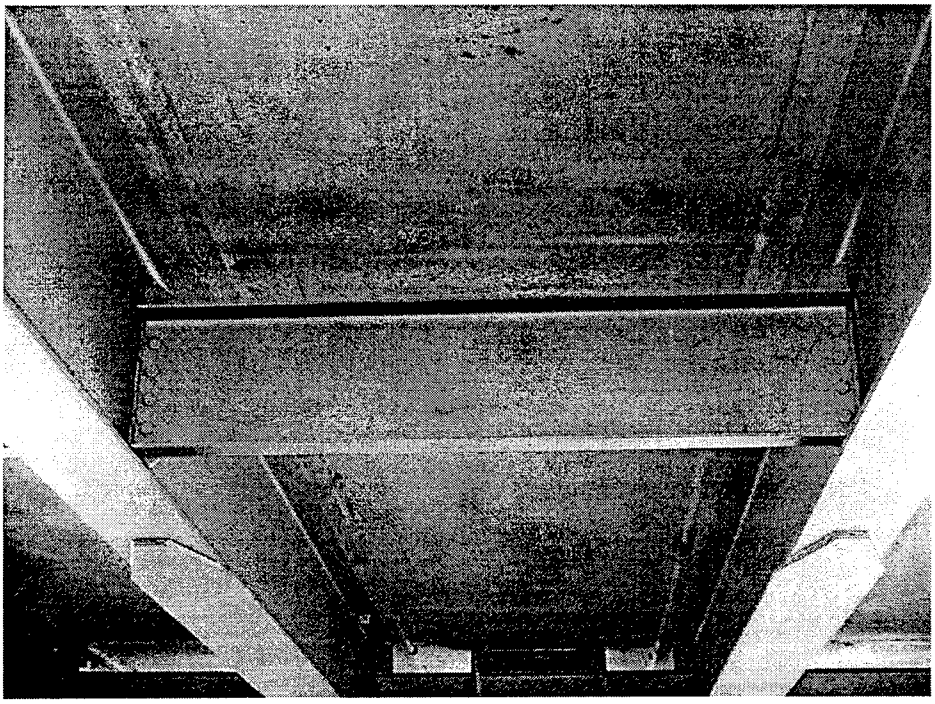

Figure 4.5 Intermediate Diaphragm and Cover Plates

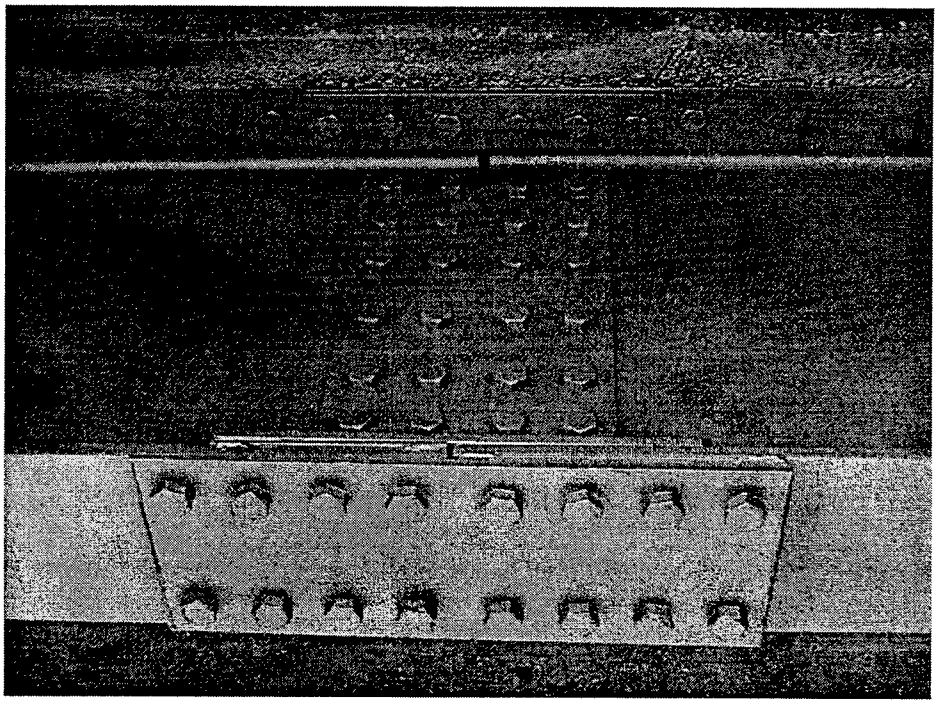

Figure 4.6 Field Splice

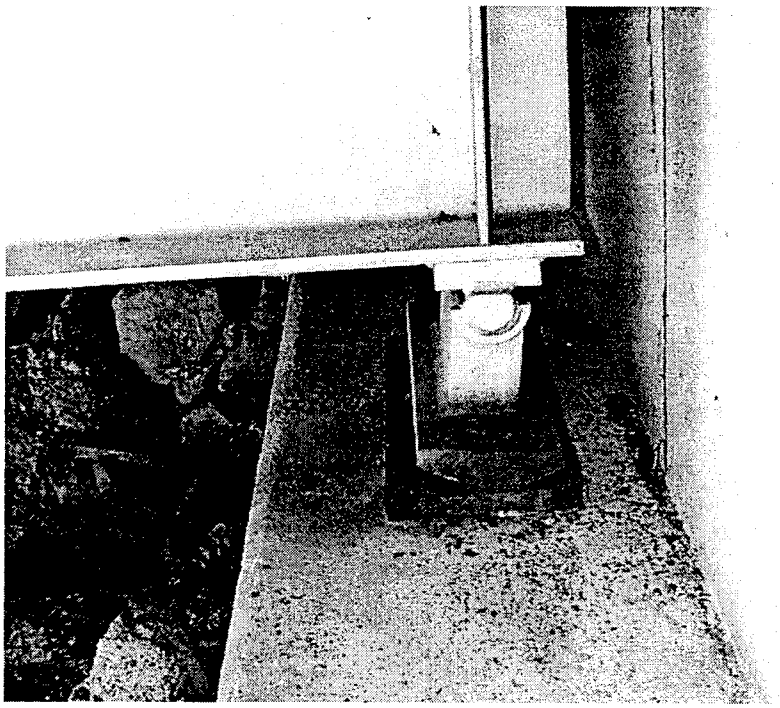

Figure 4.7 Type D Bridge Bearing

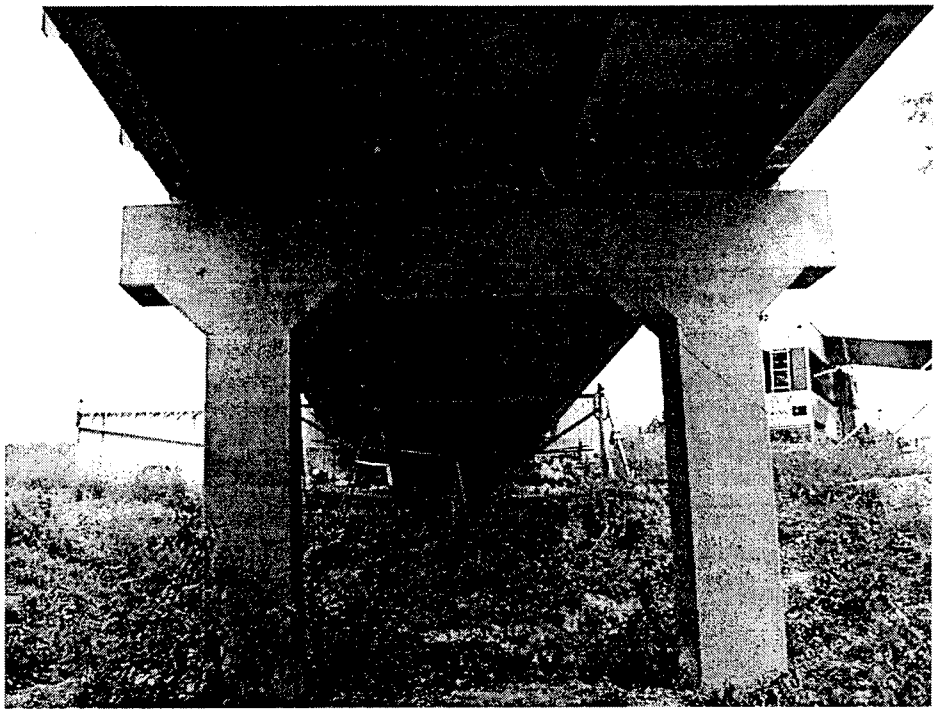

Figure 4.8 Bridge Pier

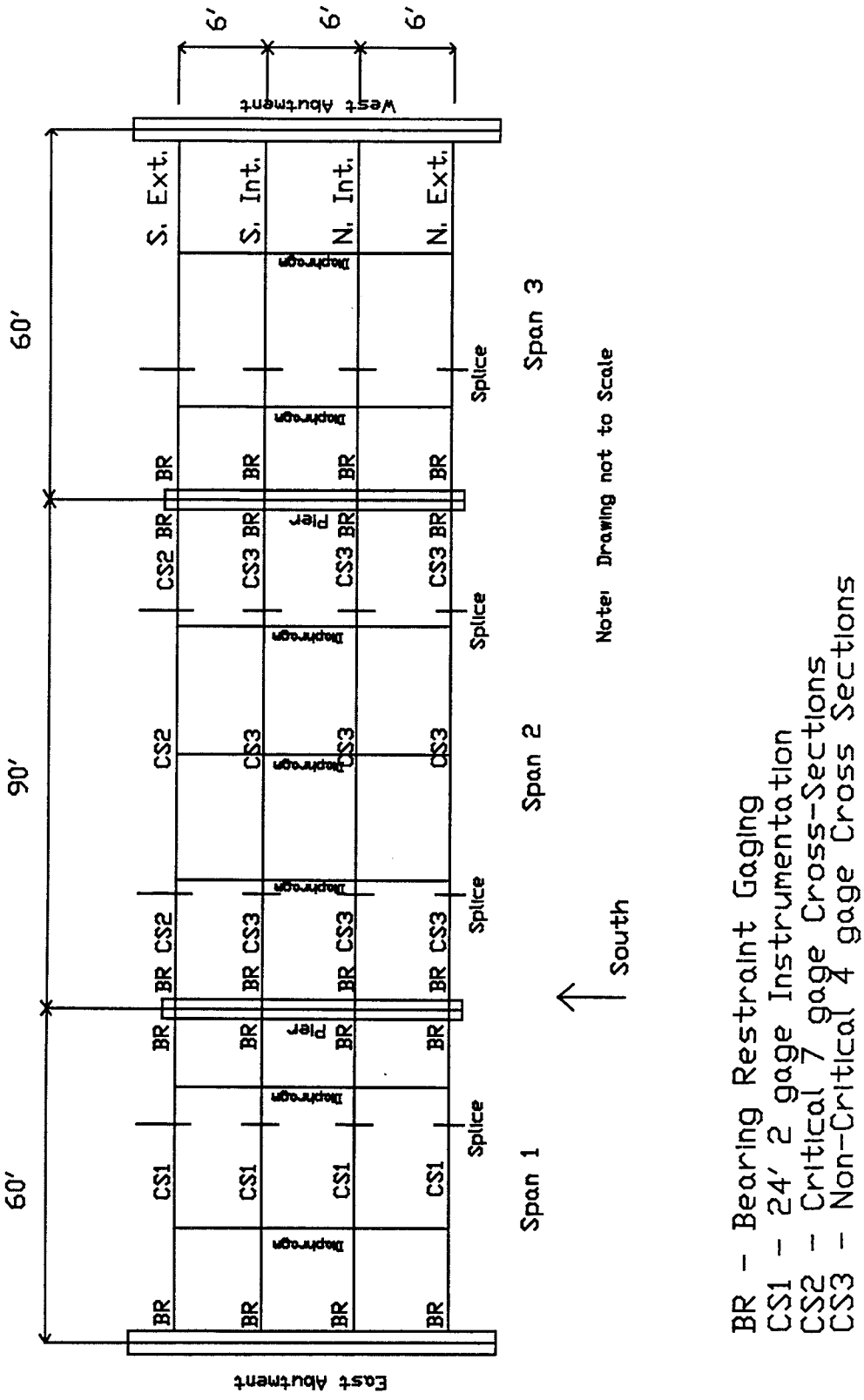

Figure 4.9 Instrumentation Plan for Bridge R-289

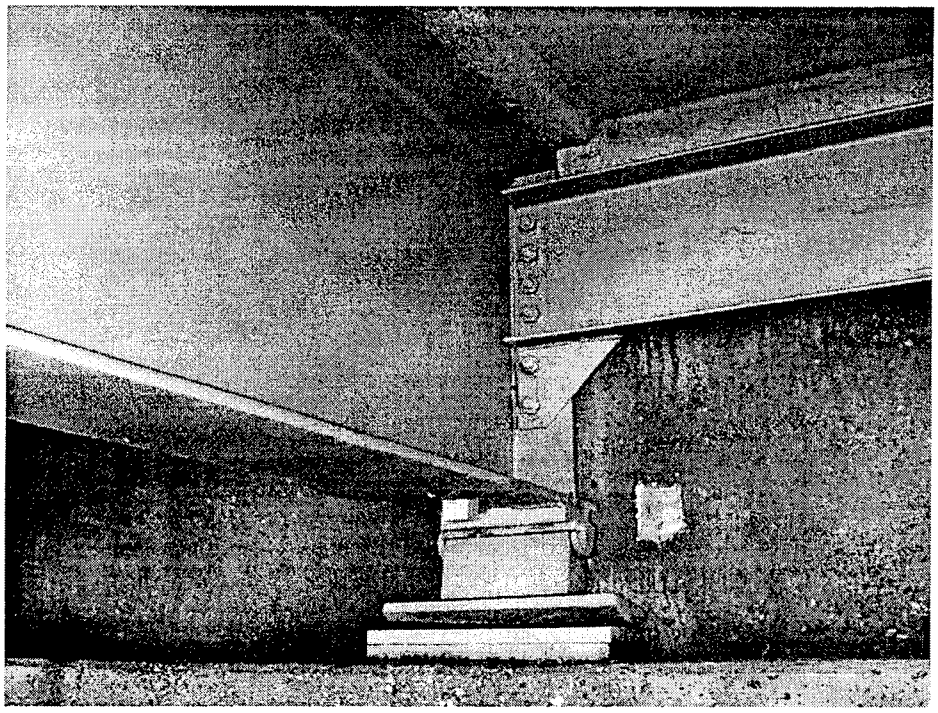

Figure 4.10 South Interior Girder at 0.5 ft

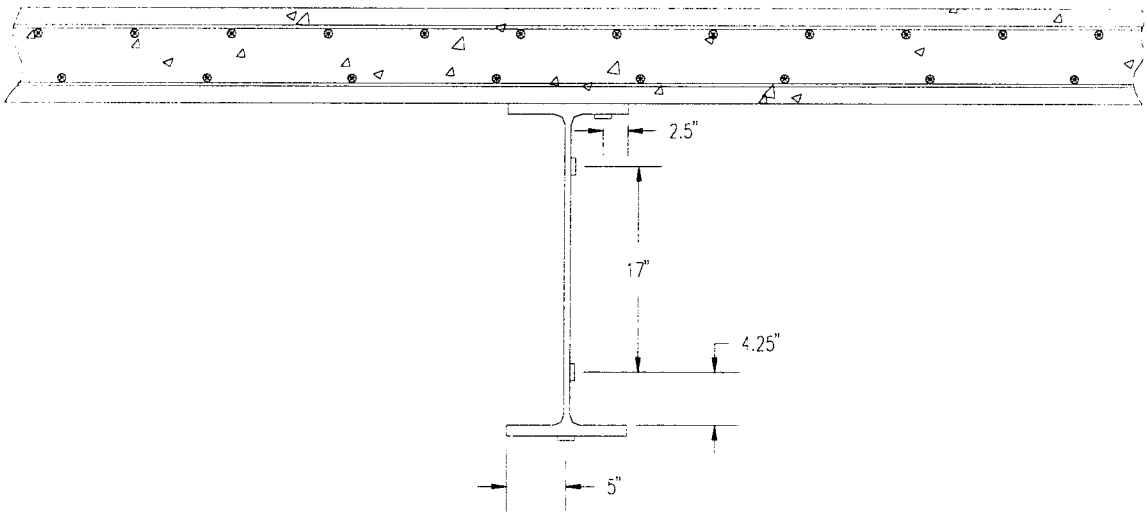

Figure 4.11 South Exterior Girder at 0.5 ft and 60.5 ft

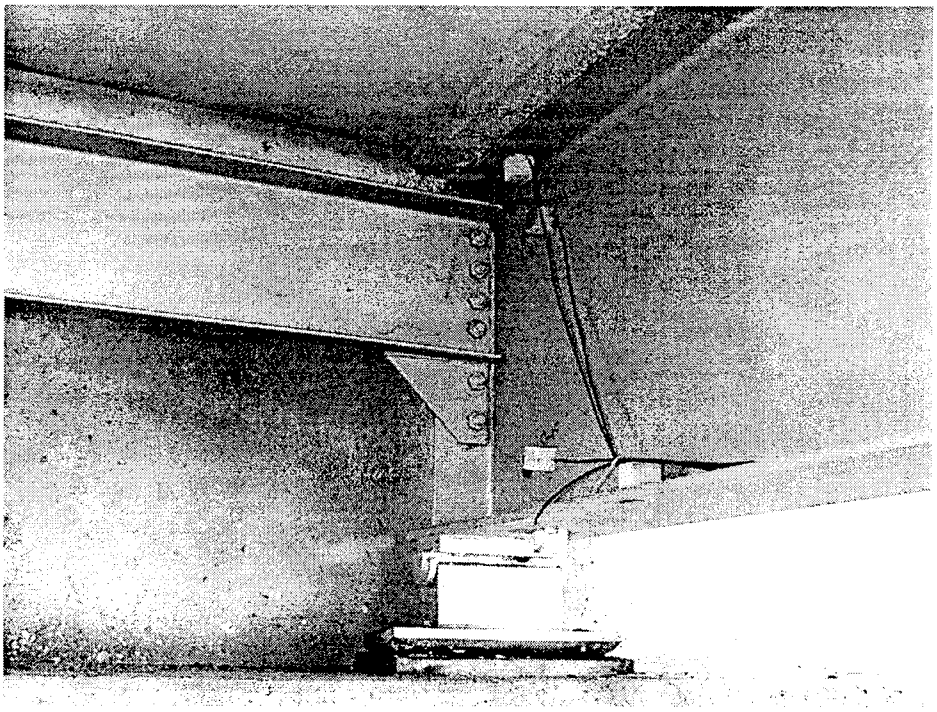

Figure 4.12 South Exterior Girder at 0.5 ft

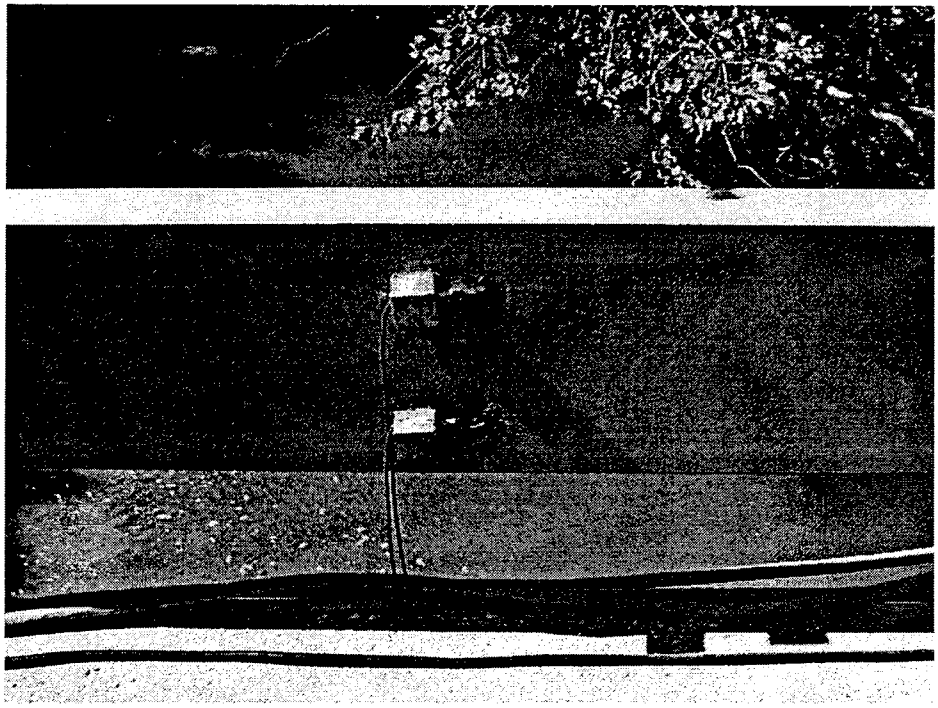

Figure 4.13 North Railing at 105.5 ft

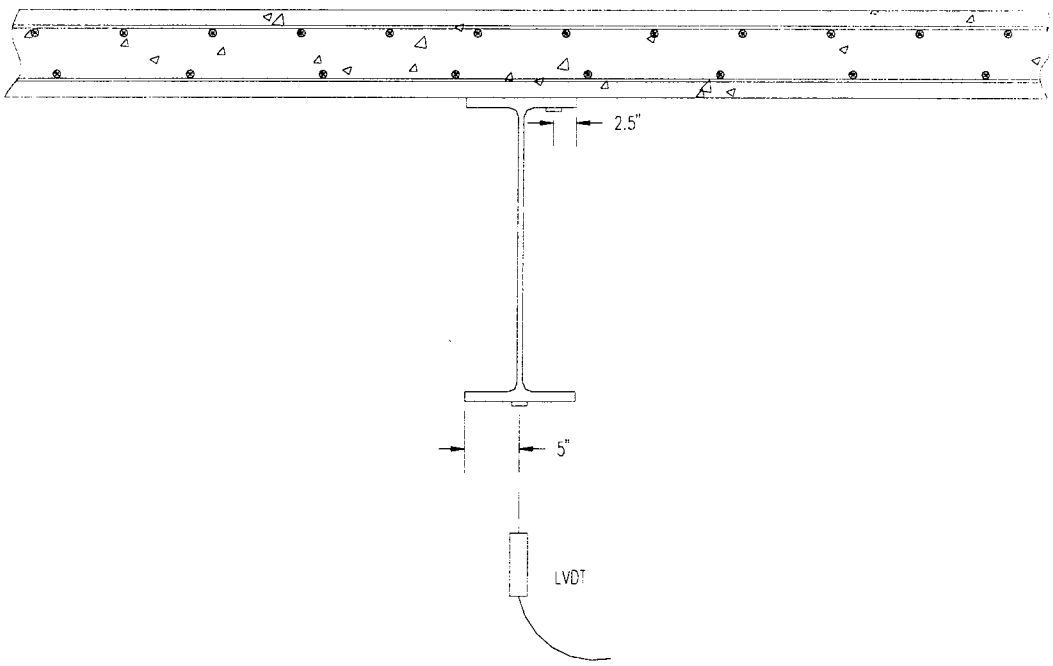

Figure 4.14 Girder Instrumentation at 24 ft

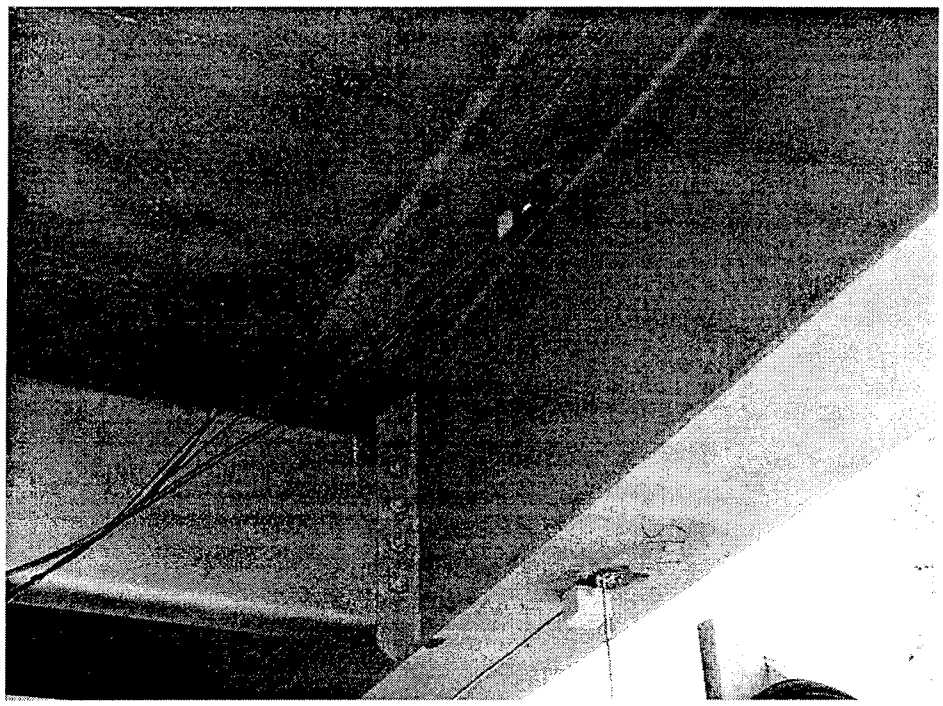

Figure 4.15 South Exterior Girder at 24 ft

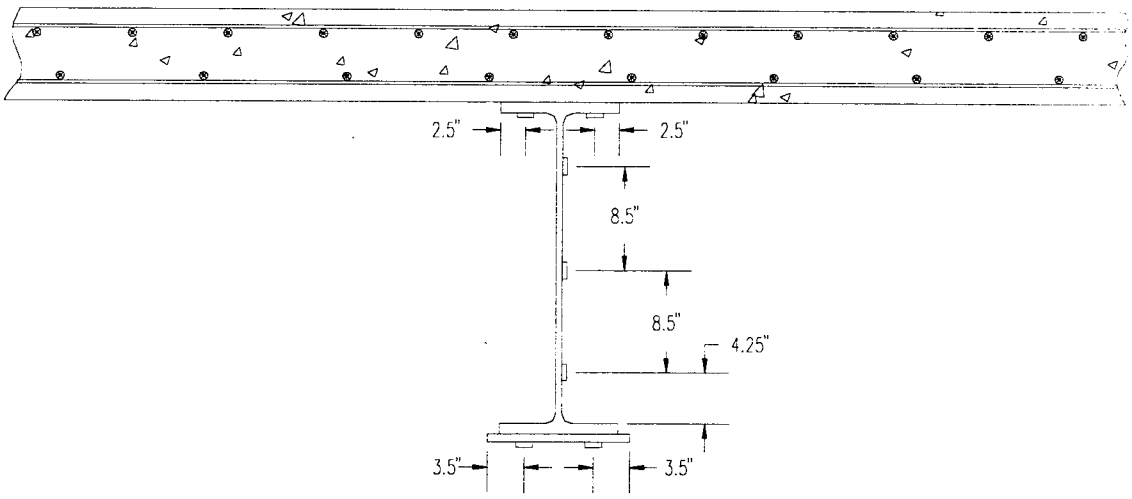

Figure 4.16 South Exterior Gage Placement at 63 ft and 147 ft

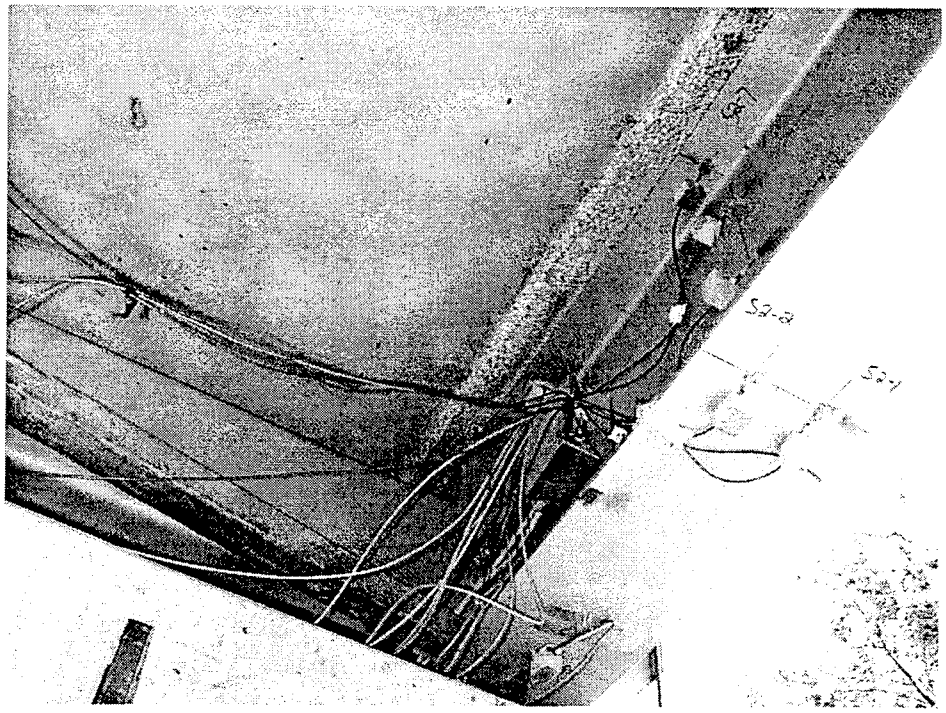

Figure 4.17 South Exterior Girder at 63 ft

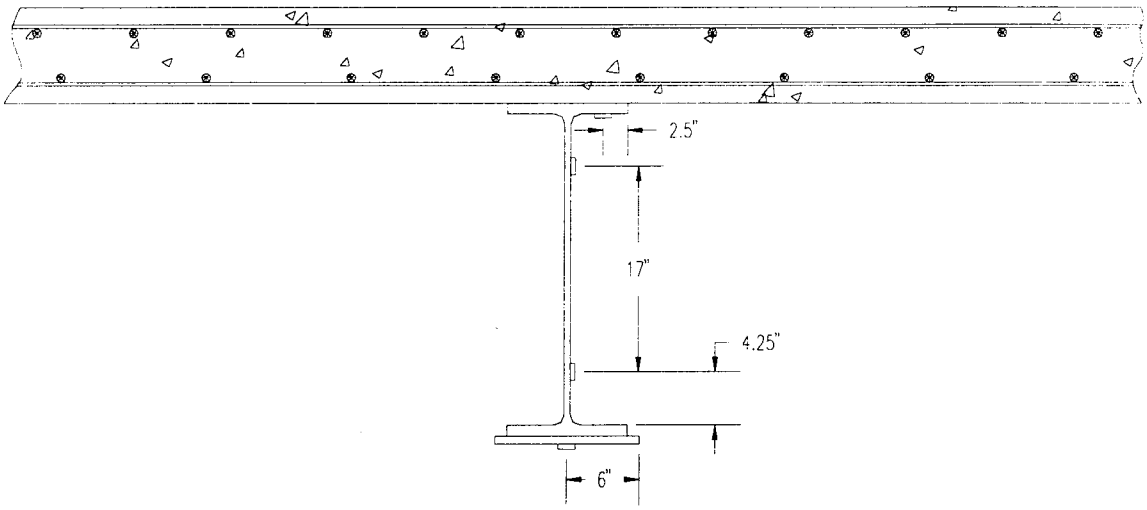

Figure 4.18 Non-Critical Girders Gage Placements at 63 ft and 147 ft

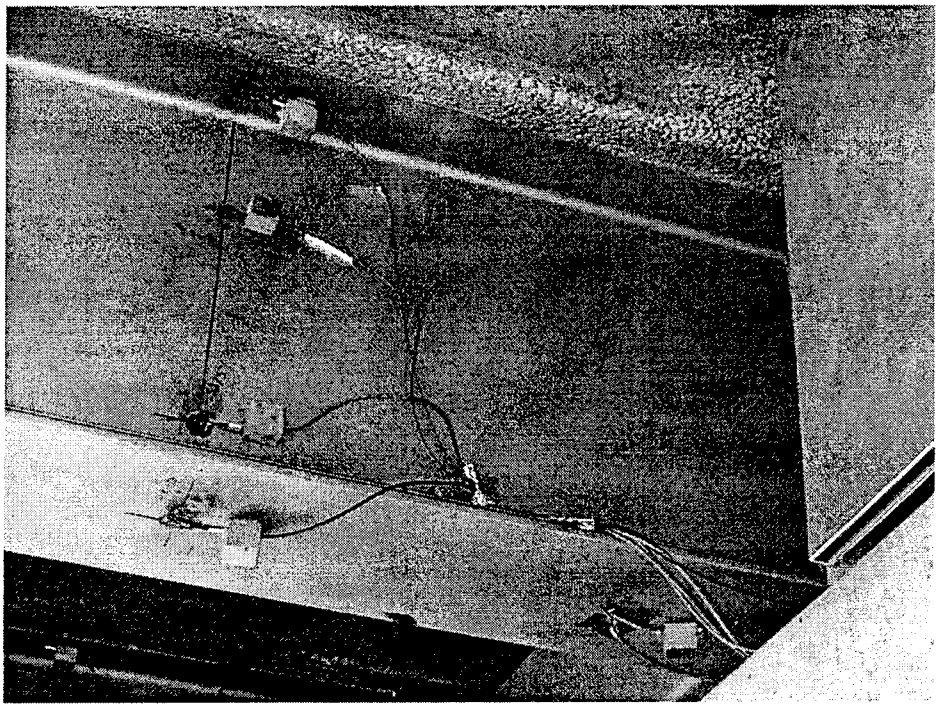

Figure 4.19 Non-Critical Girder Gage Placement at 63 ft

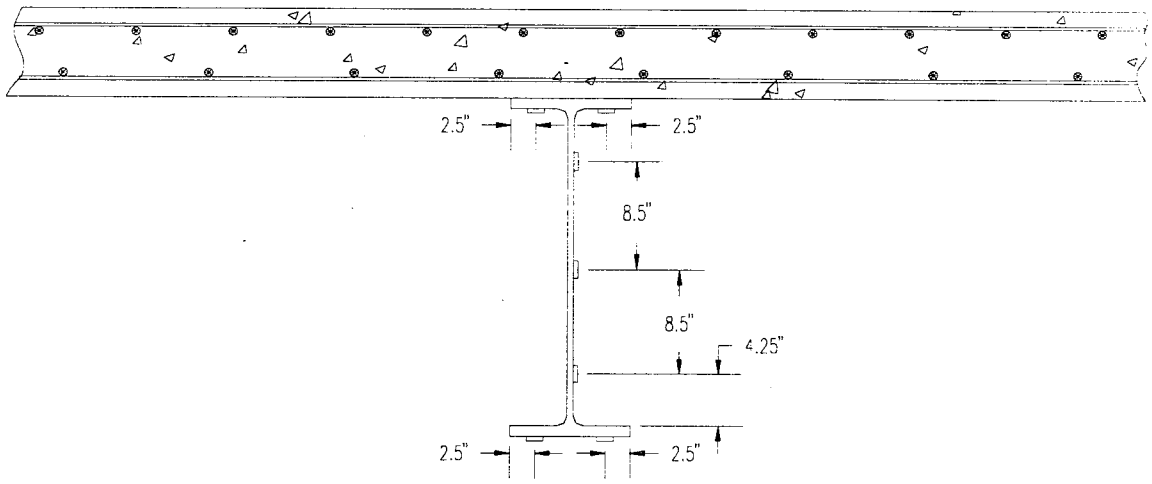

Figure 4.20 South Exterior Girder Gage Placement at 105.5 ft

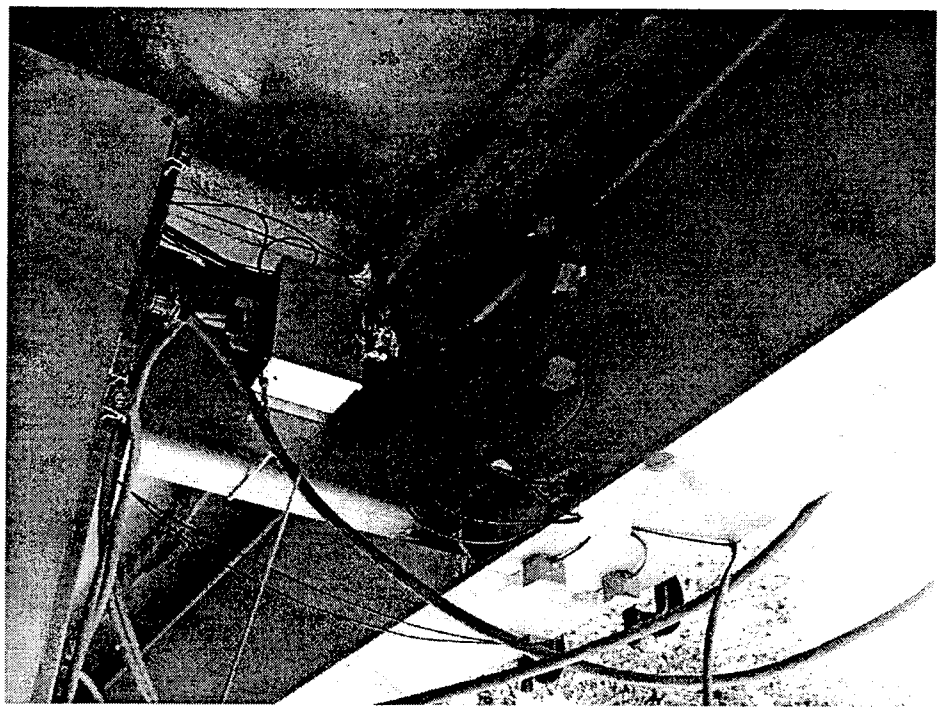

Figure 4.21 South Exterior Girder at 105.5 ft

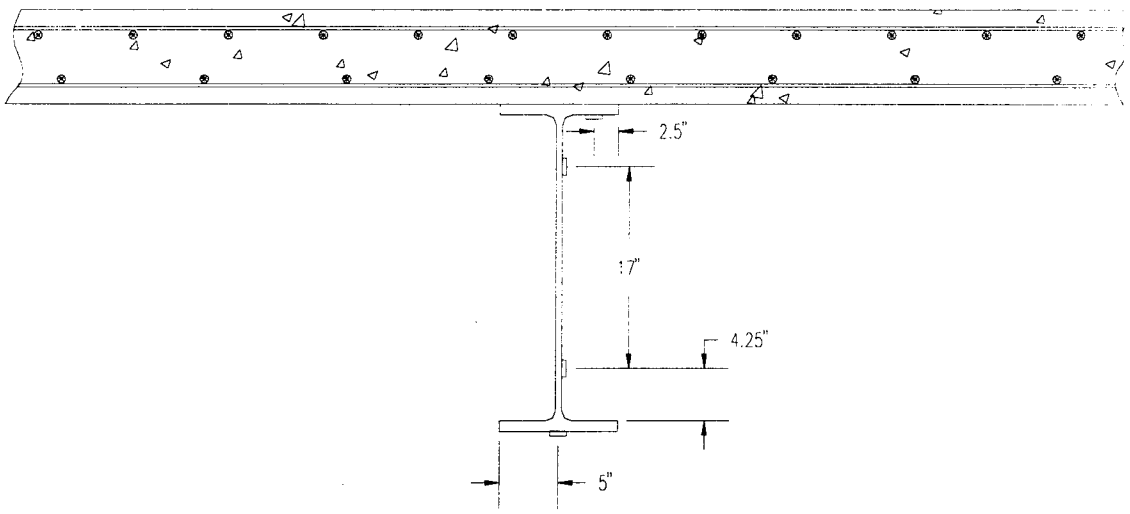

Figure 4.22 Non Critical Girders Gage Placements at 105.5 ft

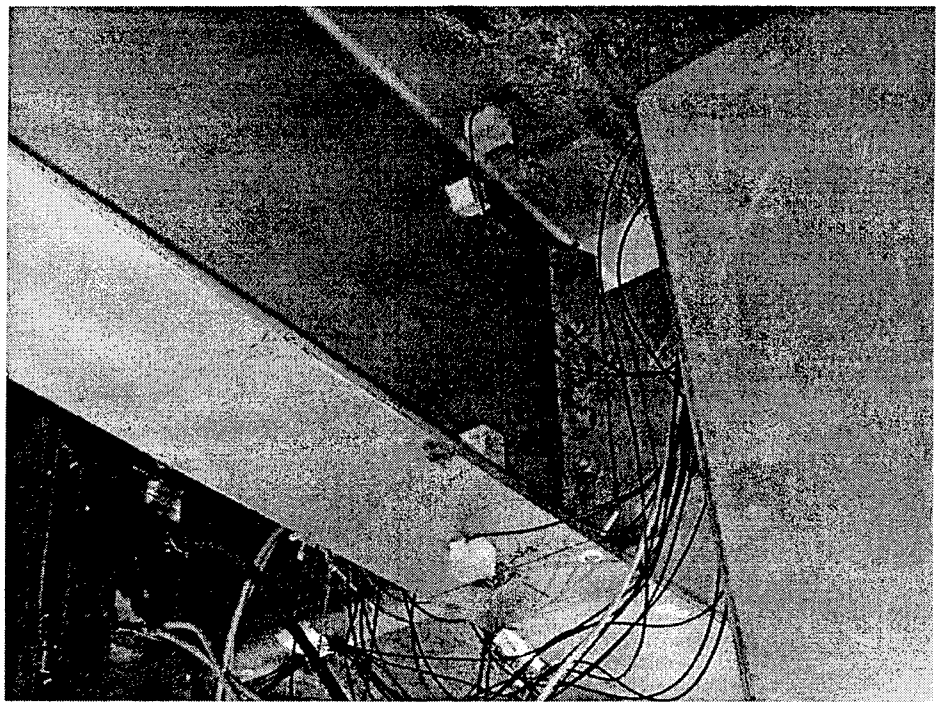

Figure 4.23 Non Critical Girders at 105.5 ft

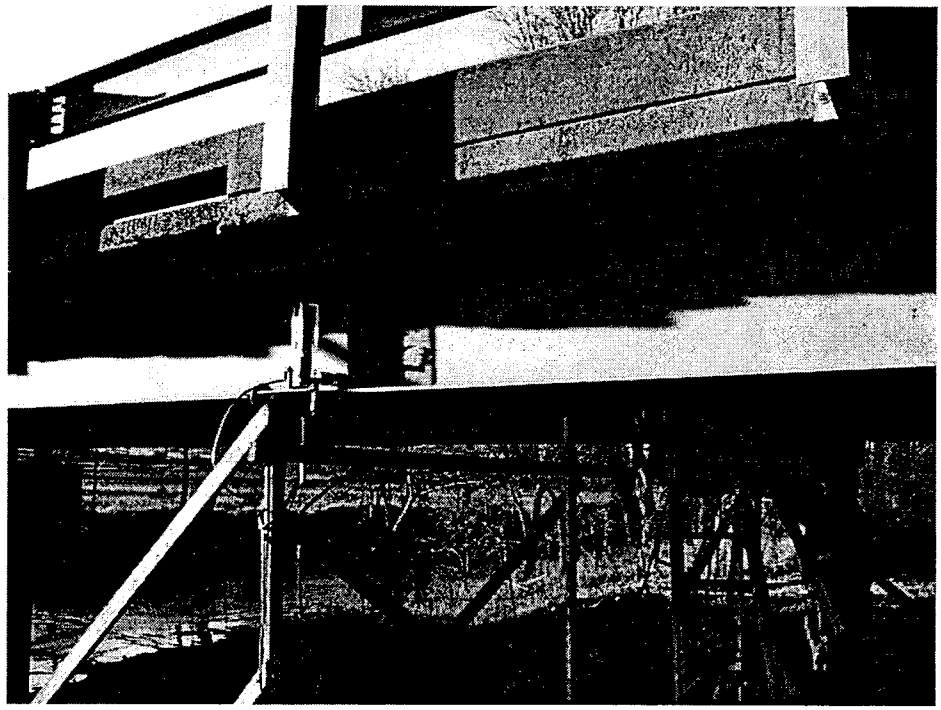

Figure 4.24 LVDT Placement at 24 ft

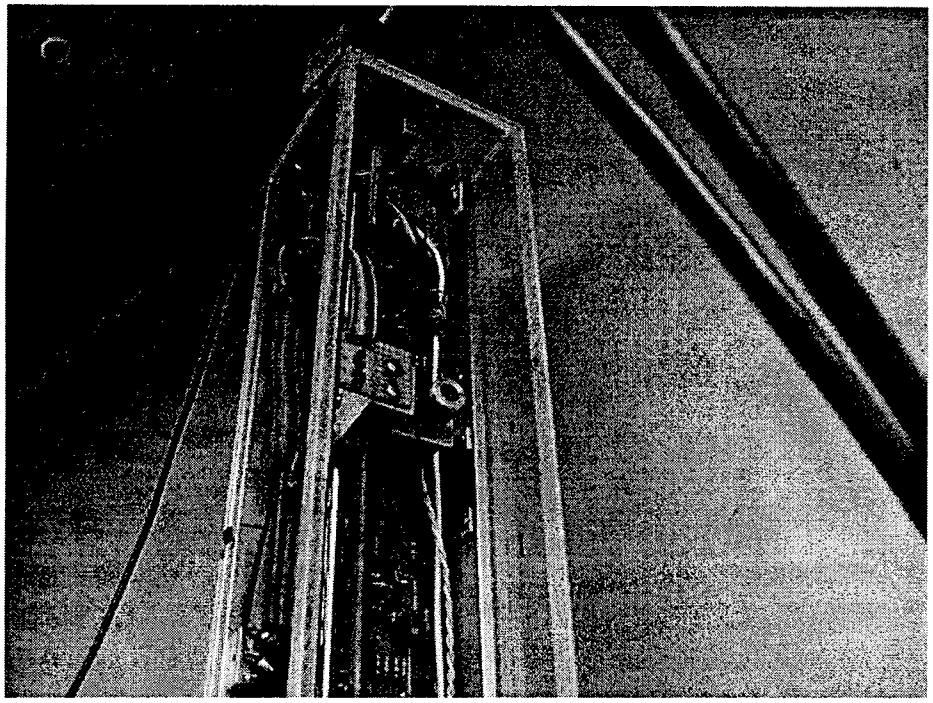

Figure 4.25 Laser Deflection Device

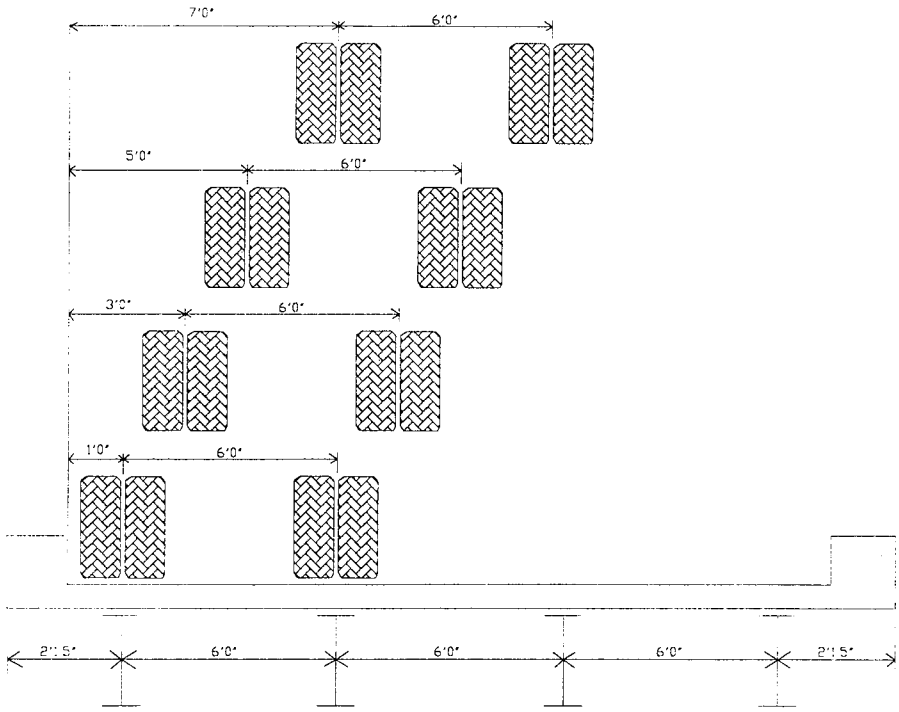

Figure 4.26 South Transverse Loading Positions

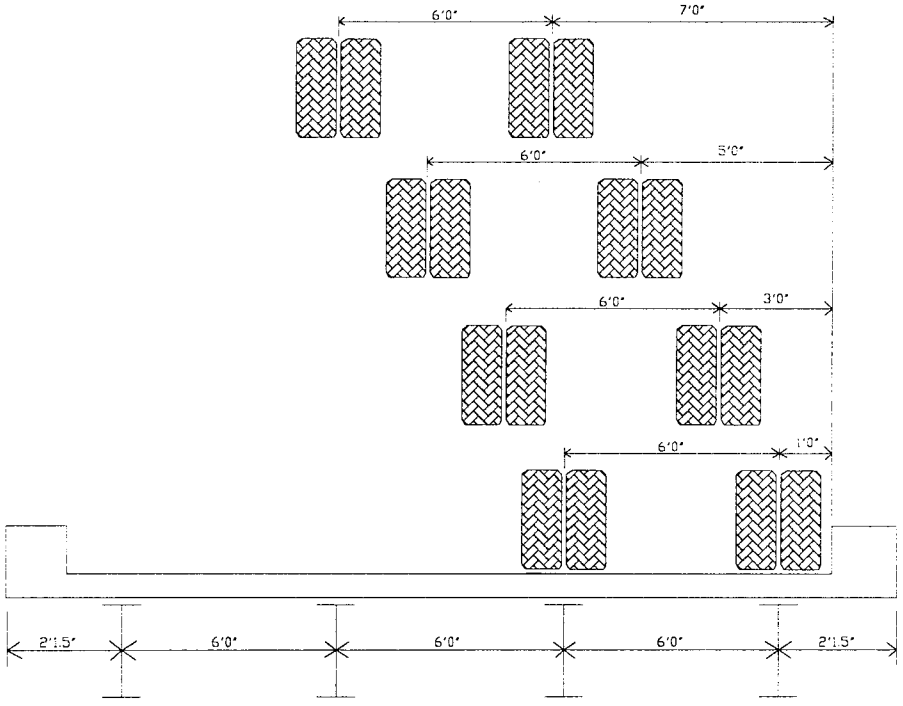

Figure 4.27 North Transverse Loading Positions

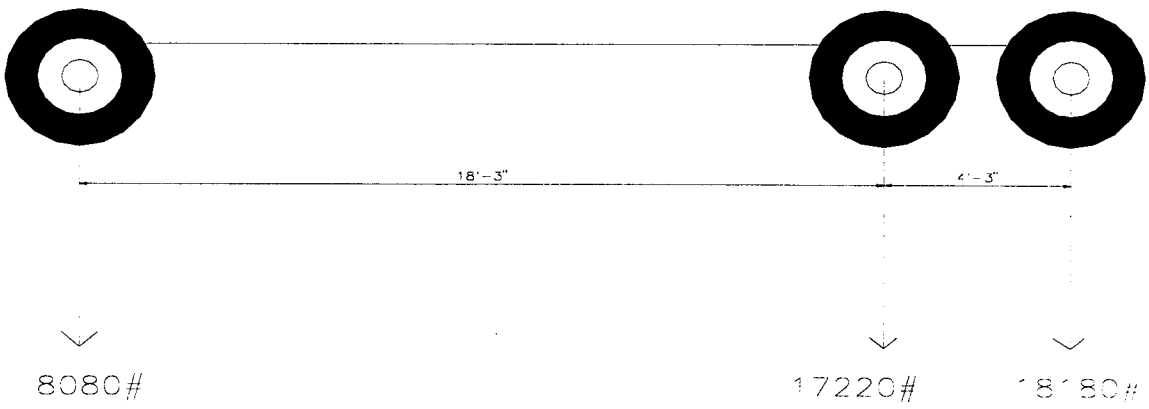

Figure 4.28 Axle Loads for 21.75 Ton Load Truck

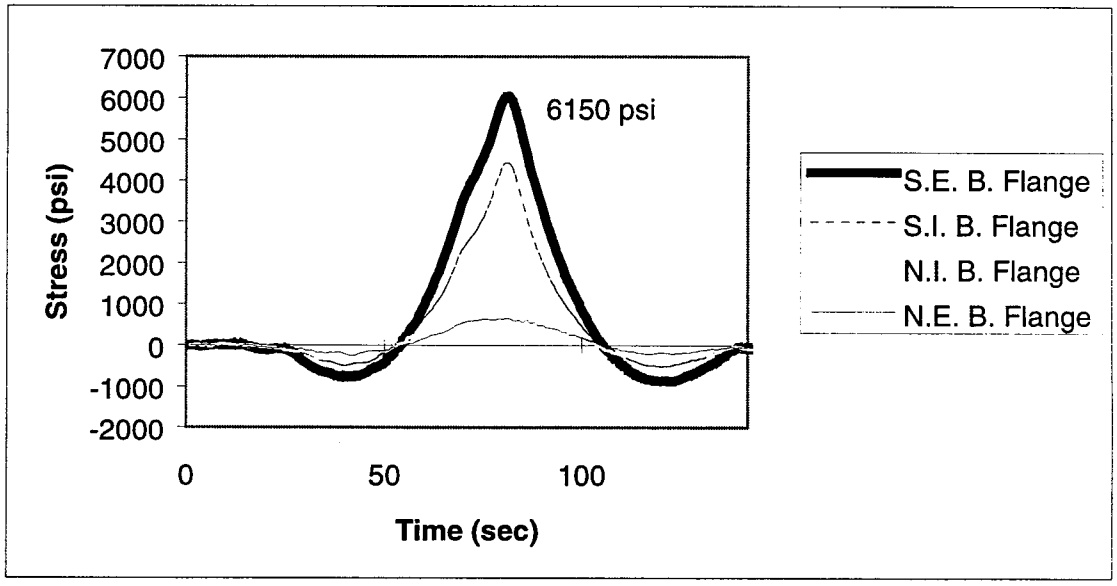

Figure 4.29 Averaged Maximum Stress for 21.75 Ton Load Truck (R-289-6-8-5)

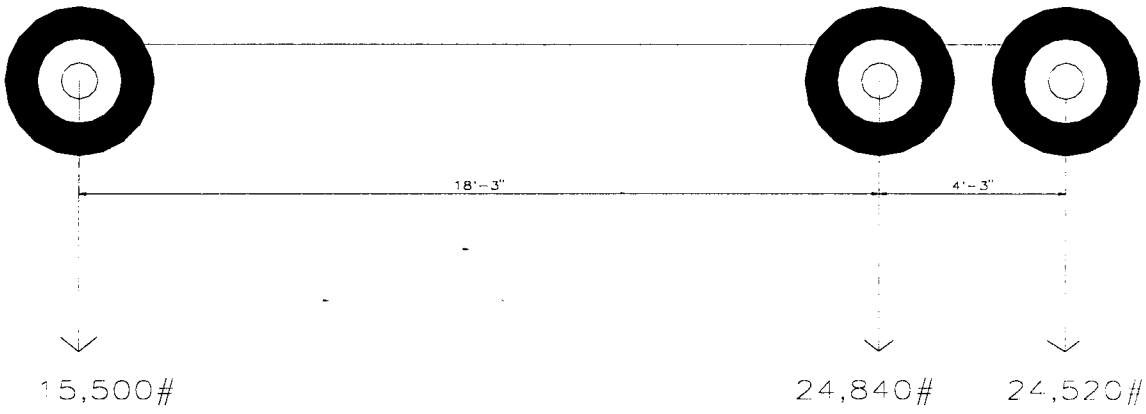

Figure 4.30 Axle Weights for 29.93 Ton Load Truck

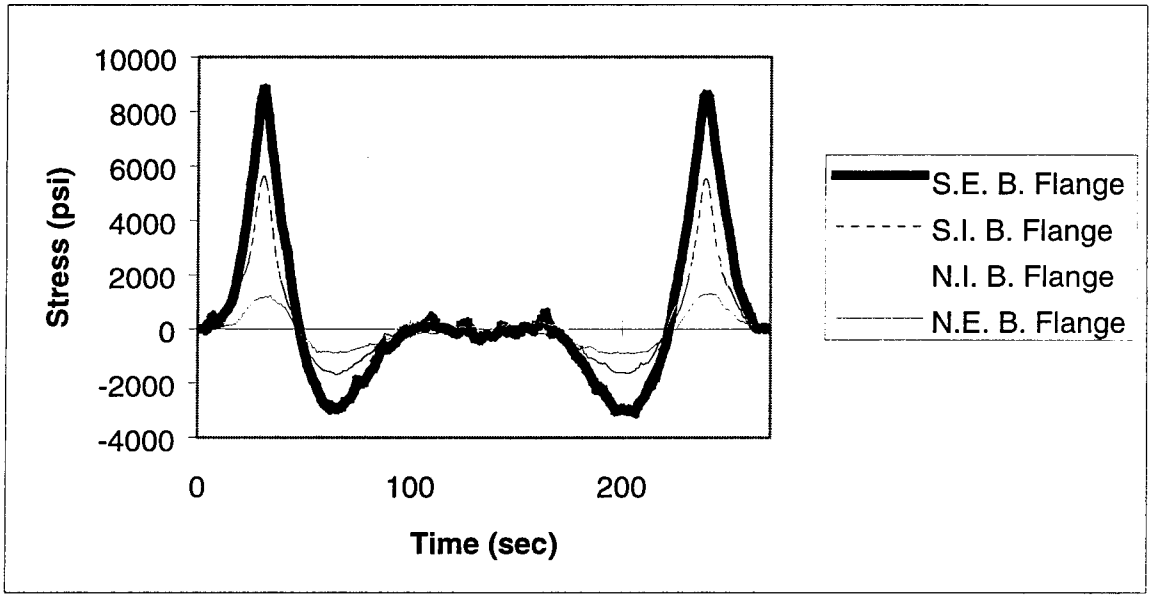

Figure 4.31 Full Cycle Test Run at Six Ft South of Centerline (R-289-6-8-33)

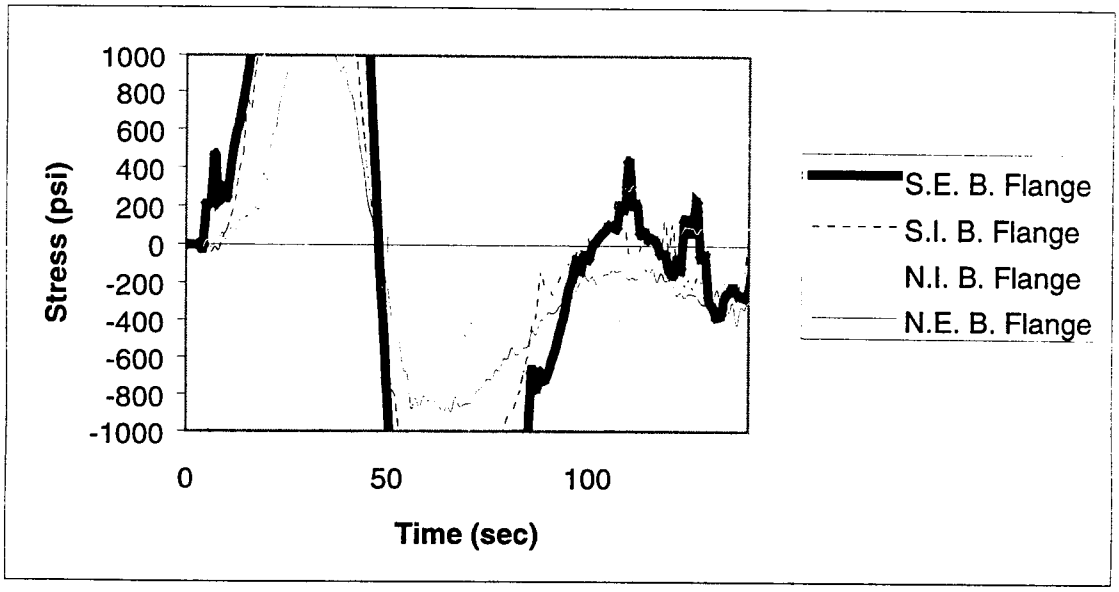

Figure 4.32 Residual Stress after Truck Initially Drives off Bridge (R-289-6-8-33)

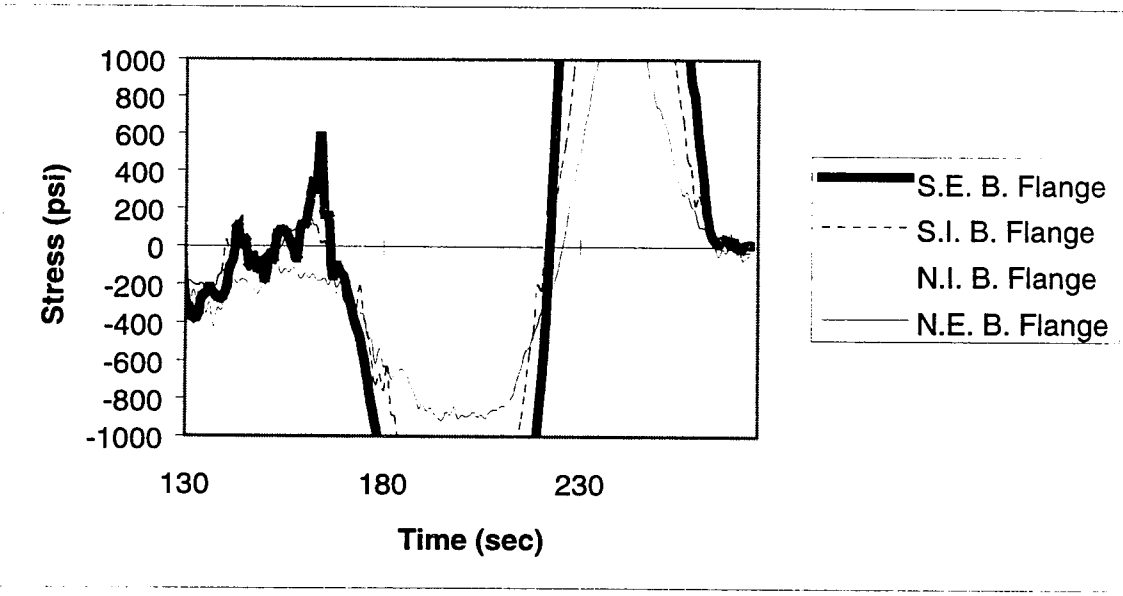

Figure 4.33 Residual Removed after Truck Backs Across Bridge (R-289-6-8-33)

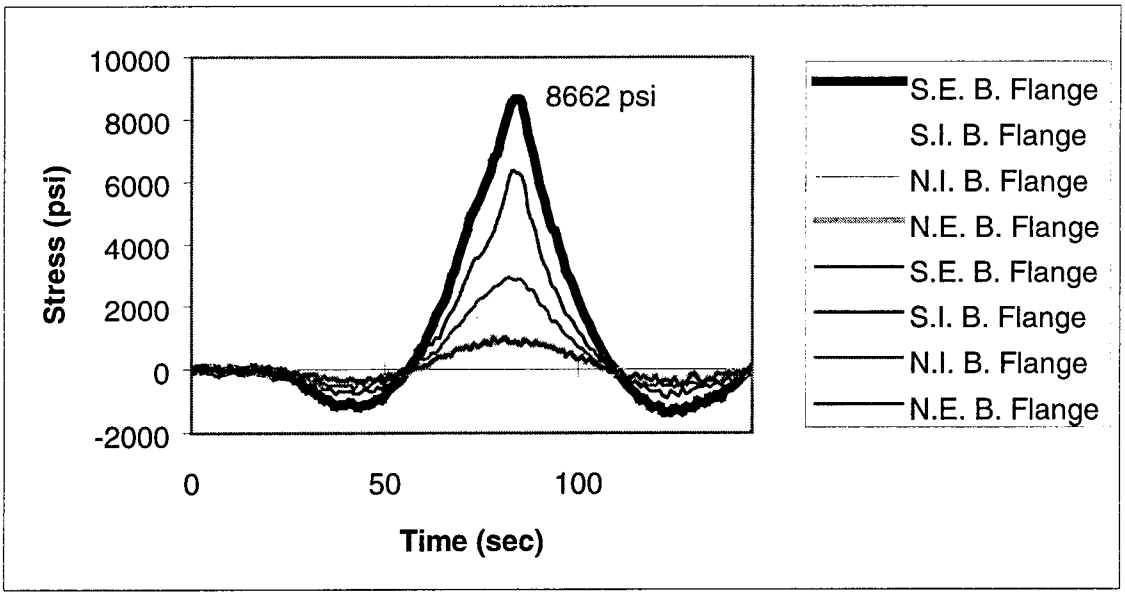

Figure 4.34 Averaged Maximum Stress for 29.93 Ton Load Truck (R-289-6-8-33)

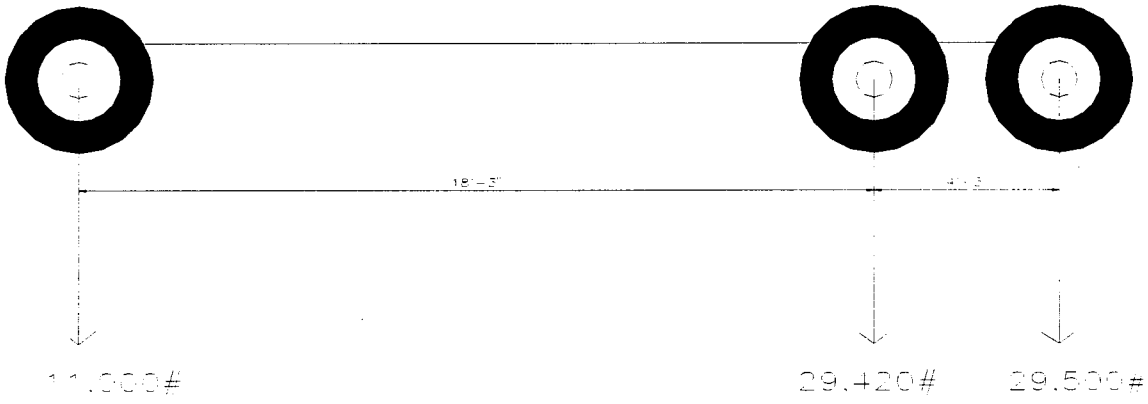

Figure 4.35 Axle Loads for 34.96 Ton Load Truck

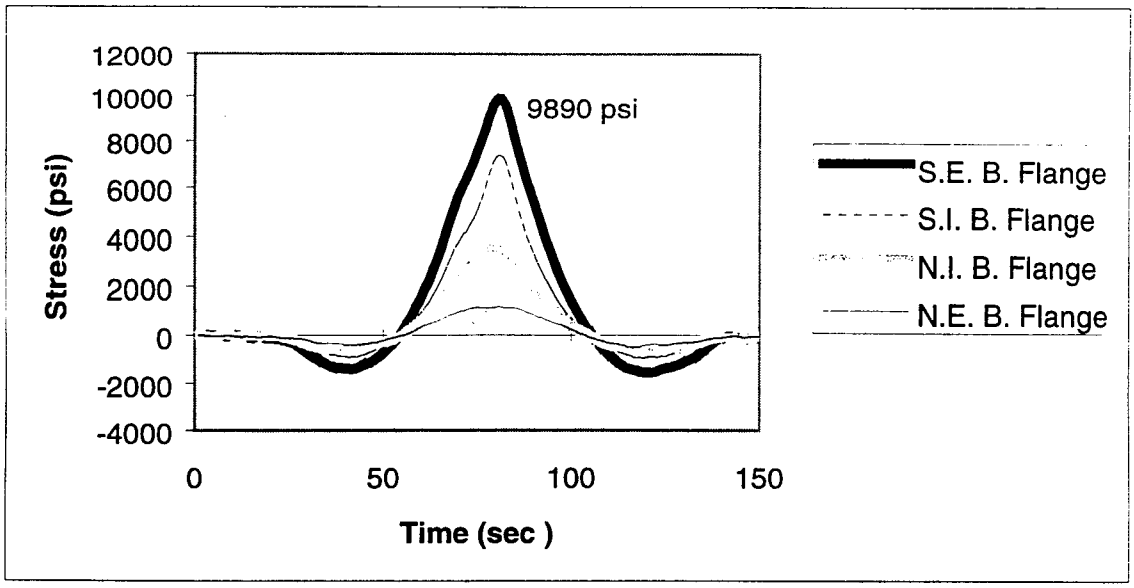

Figure 4.36 Averaged Maximum Stress for 34.96 Ton Load Truck (R-289-6-9-5)

CHAPTER 5

DATA REDUCTION AND PRESENTATION OF RESULTS

5.1 INTRODUCTION

This chapter presents the methods used to reduce experimental voltage readings to several engineering parameters. These parameters include stress distributions, deflections, neutral axes, moments, and moments of inertia. All of the assumptions made within this method will be explained. The data reduction procedure will attempt to identify all of the contributors to the measured strains. The engineering parameters obtained from this chapter are used for the standard field test procedures and have been verified by experimental results (Imhoff 1998).

Verification of experimental results is important to insure that the testing system and reduction methods are accurately assessing the structural response of Bridge R-289. The field test results will be used to calculate Bridge R-289's experimental capacity in Chapter 6. Imhoff (1998) compares the experimental results to a finite element model to verify the behavior and the procedures used to load rate Bridge R-289.

5.2 DATA REDUCTION PROCESS

The results from each test were stored in a tab delimited text file that could be easily imported to a Microsoft Excel spreadsheet. A template was created in Excel that would automatically zero the readings from each channel and apply the appropriate factors to convert the voltage readings into meaningful engineering units. The following equation, which is only valid when excitation is equal to 4 Volts, was applied to all of the strain channels to get the voltage readings into the stress unit of pounds per square inch:

$$\sigma(\text{psi}) = \frac{(V_i - V_0) * E}{GF} \tag{5.1}$$

where:
σ = Stress,
V_I = Voltage reading at i seconds,
V_0 = Initial voltage reading, taken when the truck is off of the bridge,
E = Modulus of Elasticity (29000000 psi), and
GF = Gage factor (2.08).

Deflections are obtained from the LVDT's and the laser device in nearly the same way as stress is obtained from the strain gages. The following equation is applied to all deflection channels to convert the voltage readings to deflection in inches:

$$\delta = \frac{V_i - V_0}{F} \tag{5.2}$$

where:
δ = Deflection in inches,
V_0 = Initial voltage reading, taken when the truck was off of the bridge,
V_I = Voltage reading at i seconds,
F = Calibration Constant with
LVDT#2= 2.4578,
LVDT#3= 2.2884,
LVDT#4= 2.4596,
LVDT#5= 2.8045, and
Laser= 1.0000.

The data reduction template has five stress versus time plots for the strain channels in the five data acquisition boxes. It also plots deflection versus time for the five deflection channels. The plots produced from the R-289_6-8-5 run (21.75 ton truck, 6 ft south load line) can be seen in Figures 5.1, 5.2, 5.3, 5.4, 5.5, and 5.6. These plots were used to determine the time at which a maximum loading condition was reached at 24 ft, 63 ft, 105.5 ft, and 147 ft from the East abutment. The deflection plots provided information that can effectively demonstrate that the bridge is responding elastically to load application.

5.3 EXPERIMENTAL MOMENTS AND SECTION PROPERTIES

5.3.1 Example Calculations

The elastic response of Bridge R-289 is quite different than that assumed in accepted design analysis procedures. Several factors must be accounted for when comparing an experimental moment to theoretical moment calculations. These factors must also be accounted for when obtaining an experimental member stiffness. The Type D bearings have been found to apply an eccentric axial force which is assumed to be applied through the bottom flange at the bearing locations (Bakht 1988). When this eccentric axial force is resolved to the neutral axis of the member, there is an axial force and a moment that is applied at that location. There is also extra section acting either in the form of extra material in the girder and slab itself, due to unintended composite action, or due to additional stiffness from the deck, curb, and railing.

At any instant during a test, the moments and section properties can be determined at 24 ft, 63 ft, 105.5 ft, and 147 ft. If the moment is known at these points, a reasonably accurate moment diagram can be developed for the entire bridge. The following is a list of steps that describe the method used to obtain moments and section properties from experimental results. Each step can be seen in detail in the sample calculations found in Imhoff (1998):

Step 1: Curve fitting a line to the measured stresses for each cross section,
Step 2: Calculate bearing restraint forces,
Step 3: Remove axial forces due to the bearing restraints,
Step 4: Calculation of total moment due to bearing and truck moments,
Step 5: Calculation of bearing restraint moments,
Step 6: Calculation of elastic moments,
Step 7: Calculation of lateral distribution factors, and
Step 8: Calculation of moments of inertia.

5.3.1.1 Curve Fitting

The strain response from multiple gages on a cross section provides the necessary information to fit a curve that represents a linear strain profile of a plane of material at that location. The least squares method can be used to fit a line to the experimental results. This method states that the summation of the squares of the residuals will be a minimum. This statement can best be described with the following equation:

$$\begin{bmatrix} \sum \sigma_i^2 & \sum \sigma_i \\ \sum \sigma_i & n \end{bmatrix} * \begin{Bmatrix} a \\ b \end{Bmatrix} = \begin{Bmatrix} \sum d_i * \sigma_i \\ \sum d_i \end{Bmatrix} \tag{5.3}$$

where:
σ_i = Experimentally determined stress,
d_i = Depth from the bottom of the bottom flange,
a = Slope, and
b = Intercept, or Neutral Axis.

The two unknowns in the above equation are the slope, a, and the intercept, b, of the stress diagram in the section.

The above equation is a system of two equations which can be solved for the unknown coefficients a and b. These coefficients can be obtained for each cross section that has been instrumented. The cross sections have two, four or seven strain gages depending on their location. While reviewing some preliminary test results an interesting and unanticipated response was noticed. When the truck is at a maximum loading condition at either 24 ft or 105.5 ft, one of the tandem axles is directly over the instrumented sections while the other tandem axle is 4.3 ft away. When the heavy axles are close to an instrumented location, the compressive stress zone formed by contact between the wheels and the slab appear to be interfering with the strain gages that have been placed near the top of the girder. This theory is depicted in Figure 5.7 and supported by observing the effect on

the stress histories in Figure 5.8. To insure that this local compressive zone does not interfere with the curve fitting process, several gages near the top have been neglected. The South Exterior girders at 63 ft, 105.5 ft, and 147 ft are fitted using the two bottom flange gages and the first two web gages. The other girders at these locations are fitted using the bottom flange gage and the first web gage. The 24 ft cross sections are fitted using both gages on each girder since a minimum of two data points are required to get a linear fit.

5.3.1.2 Bearing Restraint Forces

Bearing restraint forces are applied by the bearing to the bottom flange of the girder it is supporting. The bearing restraint force is normally assumed as the bearing restraint measured stress acting on the bottom flange area (Bakht 1988). A typical stress profile produced by a bearing at 60 ft while the truck is at 105 ft is presented in Figure 5.9. This stress distribution shows that compressive stresses are primarily found only in the bottom flange of the girder at the point where the bearing is located.

The rate of change of stress with depth is extremely high and the bottom flange thickness is twice as large over the piers due to the additional cover plate. For this reason, calculation of bearing restraint forces at the interior piers is accomplished by assuming that the compressive stress will be a maximum at the extreme bottom fiber and that it will go to zero at the top of the bottom flange (Imhoff 1998). The difference between the assumed stress distribution and the actual stress distribution will change the calculated bearing restraint force from that of Bakht (1988). However, this difference and its effect on the overall analysis has been found to be negligibly small (Imhoff 1998). This assumption, basically a triangular stress distribution through the bottom flange, produces the following equation for the calculation of bearing restraint forces at 60 ft and 150 ft:

$$FBR = \frac{\sigma_{BR1} * A_{bf}}{2} \tag{5.4}$$

where:
FBR = Bearing restraint force,
σ_{BR1} = Experimental bottom flange stress, and
A_{bf} = Area of the bottom flange (including cover plate).

The rate of change of stress with depth is similar at the abutments but the flange thickness is only the bottom flange of the W shape. Therefore, it is assumed that the measured stress is constant through the thickness of the bottom flange in agreement with Bakht (1988). This assumption produces the following equation for the calculation of bearing restraint forces at the abutments:

$$FBR = \sigma_{BR2} * A_{bf} \tag{5.5}$$

FBR = Bearing restraint force,
σ_{BR2} = Experimental bottom flange stress, and
A_{bf} = Area of the bottom flange.

The bearing restraint stresses, σ_{BR1} and σ_{BR2}, in the above equations are obtained differently. As seen in Figure 5.10, the bearing restraint stress at the abutment is simply the negative of the stress ($\sigma_{BR2} = -\sigma_1$) obtained from the gage at that point. The negative is used to preserve the positive sign convention for bearing restraint forces set forth in Figure 5.10. However, the gages at the pier are measuring primarily compressive strains due to bending. To obtain the bearing restraint force present at the pier, the difference between two gages, one on each side of the bearing, must be used as the bearing restraint force ($\sigma_{BR1} = \sigma_2 - \sigma_1$), being sure to preserve the positive sign convention. This assumes that the rate of change of

moment is the same on both sides of the pier, or that the effect from a different rate of change of moment is negligible.

5.3.1.3 Removal of Axial Forces due to Bearing Restraint

The axial forces applied by the bearings will effectively shift the stress distributions created by bending. Since the largest bearing restraint forces are applied as compressive forces to the girder in the span where the load truck is located, tensile stresses will be underestimated, compressive stress will be overestimated, and the neutral axis will be shifted down. Subtracting out the axial stresses caused by bearing restraint forces will leave a stress distribution composed of elastic moment from the truck load and the moment caused by the eccentrically applied bearing restraint force. The superposition of stresses due to the elastic moment caused by the load truck and bearing restraint moment, and the axial stress caused by the bearing restraint force can be seen in Figure 5.11. The objective of removing the axial stresses is to obtain an intercept, y_2, for the fitted curve which can be used to calculate section properties for bending only and to calculate the total moment, M_T, which is present at each instrumented cross section.

The axial force due to bearing restraint in the East span is equal to the negative of the bearing restraint force that is calculated at 0 ft ($FBR_{24} = -FBR_0$). The axial force due to bearing restraint in the interior span is equal to the negative of the summation of the bearing restraint forces that were calculated at 0 ft and 60 ft ($FBR_{63} = FBR_{105} = FBR_{147} = -(FBR_{60} + FBR_0$). The negative sign is again the result of the selected sign convention of positive bearing forces to the West. The axial stress due to these forces is obtained by assuming that the area over which they act is equal to the area of steel and the equivalent area of concrete deck. The steel area is simply the steel area at the point of interest. The equivalent concrete

is equal to the area of the slab and curb divided by the modular ratio (n=8). Subtracting the axial stress from the experimentally determined stress distribution results in the following equation (Imhoff 1998) which calculates the neutral axis, y_2, due to total bending alone:

$$y_2 = y_1 * \left(1 - \frac{\sigma_{axial}}{\sigma_{bf}}\right) \tag{5.6}$$

where:
y_2 = Bending neutral axis,
y_1 = Measure neutral axis,
σ_{axial} = Axial stress due to bearing restraint, and
σ_{bf} = Experimental cross sectional bottom flange stress.

5.3.1.4 Total Moment

The total moment (elastic moment and bearing restraint moment) is calculated by breaking the load carrying mechanism into three parts (Bakht 1998). One part is the steel girder bending about its own neutral axis, M_L. The second part is the concrete area bending about its own neutral axis, M_U. The third component is a couple that is a function of the amount of composite action between the concrete area and the steel section, Na. Figure 5.12 shows how the experimental stresses are transformed into the three components described above.

$$M_L = (\sigma_{bf} - \sigma_a) * S_{stl} \tag{5.7}$$

$$M_U = M_L * \left(\frac{E_c * I_c}{E_s * I_s}\right) \tag{5.8}$$

$$Na = (\sigma_a * A_{stl}) * a \tag{5.9}$$

where:
σ_{bf} = Bottom flange stress after compensating for axial stresses,
σ_a = Stress after compensating for axial stresses at the steel section neutral axis,
S_{stl} = Section modulus of the steel alone,
E_c = Modulus of elasticity for 4000 psi, normal weight concrete (3600000 psi),

I_c = Moment of inertia of the concrete alone,
E_s = Modulus of elasticity for steel (29000000 psi),
I_s = Moment of inertia of the steel section alone, and
A_{stl} = Area of the steel section.

This method is important because it provides a convenient method of dealing with a partially composite section. The use of this method is relatively simple and it has the ability to quantify the amount of composite action for any member with the Na term.

5.3.1.5 Bearing Restraint Moments

The applied bearing restraint moments are found by multiplying the bearing restraint forces by the neutral axes. The neutral axes used in this calculation are the result of the axial stress correction. The sign convention selected for the bearing restraint force is transferred to the bearing restraint moments. A positive applied bearing restraint moment will result in a right hand rule resultant that points to the North. The positive sign convention is shown in Figure 5.13.

The next step in removing bearing restraint moments is to convert the external applied moments into internal moments. This is done by assuming that a positive internal moment produces tension on the bottom flange, which is also the sign convention used in the method of calculating total moments. The conversion of applied bearing restraint moments into internal moments at 0 ft, 60 ft, and 150 ft is presented in Figures 5.14, 5.15, and 5.16. The equation at the bottom of each figure is simply the results of summing moments at that point with the appropriate sign conventions for applied moments and internal moments. The calculation of internal moments at the piers requires distribution of moment based on member and joint stiffness. The ratio of member stiffness to joint stiffness is defined as the moment distribution factor, MDF. By assuming constant moment of inertia in all spans, a

distribution factor of 0.6 should be used for the exterior side of the pier, and a distribution factor of 0.4 should be used for the interior side of the pier.

The internal moments due to bearing restraint at 0 ft, 60 ft (left and right of support), and 150 ft (left and right of support) provides enough information to construct an entire moment diagram due to the applied bearing restraint moments. An example of what this moment diagram may look like can be found in Figure 5.17. Internal moments due to bearing restraint can be found at 24 ft, 63 ft, 105.5 ft, and 147 ft by linear interpolation.

The following equations are simply the linear interpolations used to get the necessary moments at 24 ft, 63 ft, 105.5 ft, and 147 ft:

$$M_{24}^{Int} = 0.6 * M_{0}^{Int} + 0.4 * M_{60m}^{Int} \tag{5.10}$$

$$M_{63}^{Int} = 0.9667 * M_{60p}^{Int} + 0.0333 * M_{150m}^{Int} \tag{5.11}$$

$$M_{105.5}^{Int} = 0.4944 * M_{60p}^{Int} + 0.5056 * M_{150m}^{Int} \tag{5.12}$$

$$M_{147}^{Int} = 0.03 * M_{60p}^{Int} + 0.9667 * M_{150m}^{Int} \tag{5.13}$$

5.3.1.6 Elastic Moments

The elastic moments that can be compared to theoretical moment calculations are obtained by subtracting the internal moments due to bearing restraint from the total moments calculated earlier. By subtracting negative moments, this process will effectively add the bearing restraint moments onto the total calculated moment in the positive moment region.

5.3.1.7 Lateral Distribution Factors

The elastic moments provide the necessary information to calculate lateral distribution factors for each girder. The distribution factor is defined as the number of wheel lines of the load truck that is being supported by the girder for which the distribution factor is being calculated. The distribution factor is only valid if obtained from a maximum loading

condition at that location. The following equation can be used to calculate distribution factors from experimentally determined elastic moments:

$$DF_i = \frac{2 * M_i^{girder}}{\sum_{i=1}^{4} M^{girder}} \tag{5.14}$$

where:
DF_i = Distribution factor for the i^{th} girder, and
M^{girder} = Girder elastic moments.

5.3.1.8 Moments of Inertia

The moments of inertia of the various cross sections can be easily obtained from information already available from previous data reduction of the experimental results. The axial corrected depth vs. stress curve and the flexural stress equation σ=Mc/I can be utilized to produce a convenient equation for the calculation of moment of inertia. Since the axially corrected depth vs. stress curve is based upon the total moment, this total moment must be used when arriving at this equation for moment of inertia. The following equation is the result of combining the aforementioned equations:

$$I = -M_T * a \tag{5.15}$$

where:
I = Moment of inertia,
M_T = Total moment, and
a = Slope of the depth vs. stress curve.

5.3.1 Data Reduction Program

As can be seen from the previous section, an appreciable amount of calculations is required. The data reduction procedure has been written into a computer program which will perform the previously mentioned calculations in an efficient and timely manner (Imhoff

1998). The program written to perform these calculations is called Bridge.c and it was written in the C programming language. The program follows the same logic that was presented in the previous section. The program was basically written to obtain the elastic moments. The full code to Bridge.c can be found in "Field Test of State Bridge R-289: Presentation of Results" (Imhoff 1998b).

5.4 PRESENTATION OF RESULTS

A volume of results, "Field Test of State Bridge R-289: Presentation of Results" (Imhoff 1998b), has been prepared for the Bridge R-289 tests. This volume contains the data reduction, moment calculations, and properties obtained from the output of the Bridge.c program. The volume contains experimental results for maximum loading at 24 ft, 60 ft, 105 ft, and 150 ft. To keep the information to a manageable amount, four sets of runs, based on truck weight, truck position, and truck direction, were included in the volume. It includes one set of runs for each of the truck weights of 21.75 tons, 29.93 tons, 34.96 tons, and 21.77 tons. These sets were all run from East to West and all except for the 21.77 ton runs have output for each possible transverse position. The 21.77 ton runs were only performed on the South loading lines.

Table 5.1 is a list of all runs contained in the testing results volume. Although the data reduction results are not repeated here, specific references are cited for documentation. The results contained in the data volume (Imhoff 1998b) provide a large amount of information that characterizes the response of Bridge R-289. The volume presents the experimental results in a tabular format. The neutral axes, total moments, elastic moments, lateral distribution factors, and moments of inertia are tabulated for the four cross sections at

24 ft, 63 ft, 105.5 ft, and 147 ft from the East abutment. The load ratings are discussed in Chapter 6.

5.4.1 Neutral Axes

The neutral axes are an important result of the data reduction process that must be considered to fully understand the behavior of Bridge R-289. The axially corrected neutral axes along with the experimentally determined moments of inertia provide the necessary information to correctly determine section properties. Imhoff (1998) Tables B1 through B4 summarize the axially corrected neutral axes found in the testing results volume (Imhoff 1998b).

5.4.2 Total Moments

The total moments are the actual bending moments that the girders are supporting during each test. These moments were used to arrive at the elastic moments and the moments of inertia.. Imhoff (1998) Tables B5 through B8 summarize the total moments for each girder at 24 ft, 63 ft, 105.5 ft, and 147 ft.

5.4.3 Elastic Moments

The elastic moments are comparable to the moments obtained from standard design and analysis. These standard designs and analyses assume that the bearings supporting the girders are frictionless. To compare the response of Bridge R-289 to a standard analysis, the bearing effects must be removed from the calculated bending moments. Therefore, the elastic moments are obtained by removing the bearing restraint moments from the total moments. The elastic moments have been tabulated and can be found in Imhoff (1998)

Tables B9 through B12. The global moments resulting from the elastic moments have also been tabulated, and they can be found in Tables B13 through B16.

5.4.4 Lateral Distribution Factors

The lateral distribution factors have been calculated for each girder, at each location, for each of the maximum loading conditions, for all of the runs. Imhoff (1998) Tables B17 through B20 summarize the lateral distribution characteristics of Bridge R-289 at 24 ft, 63 ft, 105.5 ft, and 147 ft.

5.4.5 Moments of Inertia

As stated earlier, the total moment has a component that is due to bearing restraint and one due to the load truck. Therefore, this moment must be used when calculating the moment of inertia since the slope of the depth vs. stress curve was determined from data that still contained the bearing restraint moment. Imhoff (1998) Tables B21 through B24 summarize the moments of inertia that were found for each girder.

5.4.6 Impact

Series of 21.75 ton runs were performed at various speeds. The first series was run with the truck traveling West and the second set was performed with the truck traveling East. The speeds at which these tests were performed ranged from 10 mph to 55 mph. All impact runs were performed on the 4 ft South wheel line. These tests were performed to experimentally determine an impact factor. The impact factor for each truck speed is found by taking the ratio between the stress measured during the truck passage at the given speed to the stress measured at the same location during a static test. The final impact factor for Bridge R-289 will be found by taking the maximum factor found from all of the dynamic

runs. As seen in Figure 5.18 the maximum impact factor from both sets of tests turned out to be 0.25. This means that the crawl test data must be increased by 25 percent to convert the static results to dynamic results.

5.5 SAMPLE CALCULATIONS

5.5.1 Introduction

The steps described in Section 5.3 will be reviewed by presenting a numerical example of each step in the data reduction process. The same run will be used for all calculations. The run selected for the example calculation is run 6-8-33. This run is for a 29.93 Ton load truck positioned on the six foot South loading line. The results from each calculation will be referenced to a corresponding value in the tables found in Imhoff (1998). These values may not match exactly because of rounding differences. All calculations will be performed for the South exterior girder at 105 ft from the East abutment. This includes bearing restraint calculations at each of the instrumented bearings on the South exterior girder.

5.5.2 Curve Fitting

The measured strains at the section are:

X-Data - σ_i

3-S1 (psi)	3-S2 (psi)	3-S3 (psi)	3-S4 (psi)
8254.0	9070.1	7683.0	4650.5

Y-Data - d_i

D1 (in)	D2 (in)	D3 (in)	D4 (in)
0.0	0.0	4.9	13.4

$$\sum \sigma_i^2 = 8254.0^2 + 9070.1^2 + 7683.0^2 + 4650.5^2 = 2.31 \times 10^8$$

$$\sum \sigma_i = 8254.0 + 9070.1 + 7683.0 + 4650.5 = 29657.6$$

$n = 4$

$$\sum d_i * \sigma_i = 0.0*8254.0 + 0.0*9070.1 + 4.9*7683.0 + 13.4*4650.5 = 99963.4$$

$$\sum d_i = 0.0 + 0.0 + 4.9 + 13.4 = 18.3$$

$$\begin{bmatrix} 2.31\times10^8 & 29657.6 \\ 29657.6 & 4 \end{bmatrix} * \begin{Bmatrix} a \\ b \end{Bmatrix} = \begin{Bmatrix} 99963.4 \\ 18.3 \end{Bmatrix} \rightarrow a = -.003216 \rightarrow b = 28.4$$

$$d = -.003216 * \sigma + 28.4$$

$y_1 = 28.4\text{in.}$

5.5.3 Bearing Restraint Forces

The measured bearing restraint stresses are (from east to west):

1-S9 (psi)	1-S16 (psi)	5-S1 (psi)	5-S12 (psi)	5-S16 (psi)
-13.58	-3223.91	-5054.95	-6635.48	-4142.01

$$\sigma_{BR}^{0} = -(-13.58) = 13.58\text{psi}$$

$$\sigma_{BR}^{60} = -3223.91 - (-5054.95) = 1831.04\text{psi}$$

$$\sigma_{BR}^{150} = -6635.48 - (-4142.01) = -2493.47\text{psi}$$

$$F_{BR}^{0} = \frac{13.58 * 6.374}{1000} = .09\text{k}$$

$$F_{BR}^{60} = \frac{1831.04 * (13.874/2)}{1000} = 12.7\text{k}$$

$$F_{BR}^{150} = \frac{-2493.47 * (13.874/2)}{1000} = -17.3\text{k}$$

5.5.4 Remove Axial Force Effects

$$F_{BR}^{24} = -F_{BR}^{0} = -.09\text{k} \qquad F_{BR}^{63} = F_{BR}^{105} = F_{BR}^{147} = -(F_{BR}^{60} + F_{BR}^{0}) = -(12.7 + .09) = -12.79\text{k}$$

$$\sigma_{axial}^{24} = \frac{-.09}{90.1} * 1000 = -1.0\text{psi} \qquad \sigma_{axial}^{63} = \sigma_{axial}^{105} = \sigma_{axial}^{147} = \frac{-12.79}{90.1} * 1000 = -142.0\text{psi}$$

$$y_2^{105} = 28.4 * \left(1 - \frac{-142.0}{(28.4/.003216)}\right) = 28.9\text{in.} \rightarrow \qquad d_{105} = -.003216 * \sigma_{105} + 28.9$$

Reference Table B3, Column: y2_105se, Row: 6-8-33, Value: 29.05 in.

5.5.5 Total Moment

$$\sigma_a = \frac{((26.74/2) - 28.9)}{-.003216} = 4829.0\text{psi}$$

$$\sigma_{bf} = \frac{-28.9}{-.003216} = 8986.3\text{psi}$$

$$S_{stl} = 220.1\text{in}^3$$

$$M_L = \frac{(8893.0 - 4735.7) * 220.1}{12000} = 76.3\text{k} - \text{ft}$$

$$I_c = 11224.9\text{in}^4 \qquad I_c = 2942.5\text{in}^4$$

$$M_U = 76.3 * \left(\frac{3.6 \times 10^6 * 11224.9}{29 \times 10^6 * 2942.5}\right) = 36.1\text{k} - \text{ft}$$

$$A_{stl} = 25.97\text{in}^2 \qquad a = 22.26\text{in}$$

$$Na = \frac{(4829.0 * 25.97) * 22.26}{12000} = 232.6\text{k} - \text{ft}$$

$$M_T = 76.3 + 36.1 + 232.6 = 345.0\text{k} - \text{ft}$$

Reference Table B7, Column: MT_105se, Row: 6-8-33, Value: 347.6 k-ft.

5.5.6 Removal of Bearing Restraint Moments

$$F_{BR}^{60} = 12.7\text{k}$$

$$F_{BR}^{150} = -17.3\text{k}$$

$$y_2^{60} = 24.58$$

$$y_2^{150} = 19.71$$

$$M_{BR}^{60} = \frac{12.7 * 24.58}{12} = 26.0\text{k} - \text{ft}$$

$$M_{BR}^{150} = \frac{-17.3 * 19.71}{12} = -28.4k - ft$$

$$M_{60p}^{Int} = -0.4 * 26.0 = -10.4k - ft$$

$$M_{150m}^{Int} = 0.4 * (-28.4) = -11.36k - ft$$

$$M_{105}^{Int} = 0.4944 * (-10.4) + 0.5056 * (-11.36) = -10.9k - ft$$

$$M_T = 345k - ft$$

$$M_E^{105} = 345 - (-10.9) = 355.9k - ft$$

Reference Table B11, Column: ME_105se, Row: 6-8-33, Value: 358.5 k-ft.

5.5.7 Lateral Distribution Factor

$$M_E^{105se} = 355.9k - ft$$

$$M_E^{105si} = 238.94k - ft$$

$$M_E^{105ni} = 96.96k - ft$$

$$M_E^{105ne} = 26.98k - ft$$

$$DF_{105}^{se} = \frac{355.9 * 2}{355.9 + 238.94 + 96.96 + 26.98} = 0.99$$

Reference Table B18, Column: ME_105se, Row: 6-8-33, Value: 0.99

5.5.8 Moment of Inertia

$M_T = 345k - ft \qquad a = -.003216$

$$I_{105}^{se} = -(345) * (-.003216) * 12000 = 13314.2in^4$$

Reference Table B23, Column: I_105se, Row: 6-8-33, Value: 13404 in

5.6 SUMMARY

This chapter presents the data reduction requirements for load rating a steel girder bridge using field test data. The procedures are theoretical in nature and have been verified

through field testing of Bridge R-289 for this project and other tests (Imhoff 1998). The procedures can be computerized with ease. Sample calculations for Bridge R-289 are provided to demonstrate the procedures.

Table 5.1 List of runs contained in the testing results volume.

Run Name	Run Type	Speed	Load Line	Truck Wt. (tons)
R-289_6-8-2	Half Cycle	0	South Centerline	21.75
R-289_6-8-3	Half Cycle	0	2 ft. South	21.75
R-289_6-8-4	Half Cycle	0	4 ft. South	21.75
R-289_6-8-5	Half Cycle	0	6 ft. South	21.75
R-289_6-8-6	Half Cycle	0	North Centerline	21.75
R-289_6-8-7	Half Cycle	0	2 ft. North	21.75
R-289_6-8-8	Half Cycle	0	4 ft. North	21.75
R-289_6-8-9	Half Cycle	0	6 ft. North	21.75
R-289_6-8-30	Half Cycle	0	South Centerline	29.93
R-289_6-8-31	Half Cycle	0	2 ft. South	29.93
R-289_6-8-32	Half Cycle	0	4 ft. South	29.93
R-289_6-8-33	Half Cycle	0	6 ft. South	29.93
R-289_6-8-34	Half Cycle	0	North Centerline	29.93
R-289_6-8-35	Half Cycle	0	2 ft. North	29.93
R-289_6-8-36	Half Cycle	0	4 ft. North	29.93
R-289_6-8-37	Half Cycle	0	6 ft. North	29.93
R-289_6-9-2	Half Cycle	0	South Centerline	34.96
R-289_6-9-3	Half Cycle	0	2 ft. South	34.96
R-289_6-9-4	Half Cycle	0	4 ft. South	34.96
R-289_6-9-5	Full Cycle	0	6 ft. South	34.96
R-289_6-9-6	Half Cycle	0	North Centerline	34.96
R-289_6-9-7	Half Cycle	0	2 ft. North	34.96
R-289_6-9-8	Full Cycle	0	4 ft. North	34.96
R-289_6-9-9	Full Cycle	0	6 ft. North	34.96
R-289_6-10-4	Half Cycle	0	South Centerline	21.77
R-289_6-10-5	Half Cycle	0	2 ft. South	21.77
R-289_6-10-6	Half Cycle	0	4 ft. South	21.77
R-289_6-10-7	Full Cycle	0	6 ft. South	21.77

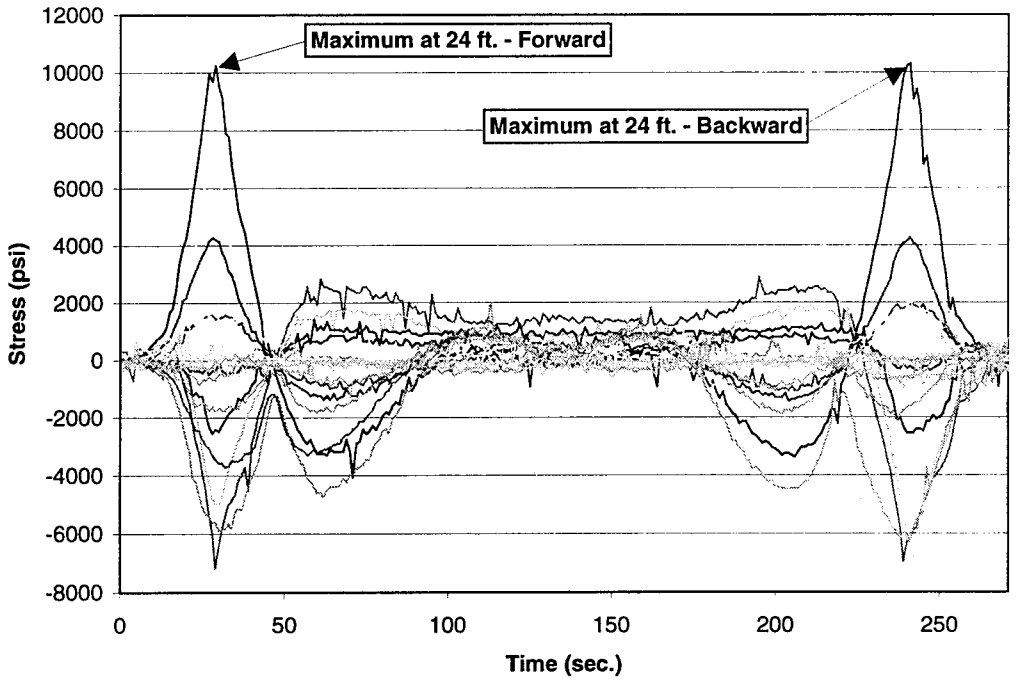

Figure 5.1 Stress vs. Time plot for Box #1, R-289_6-9-10.

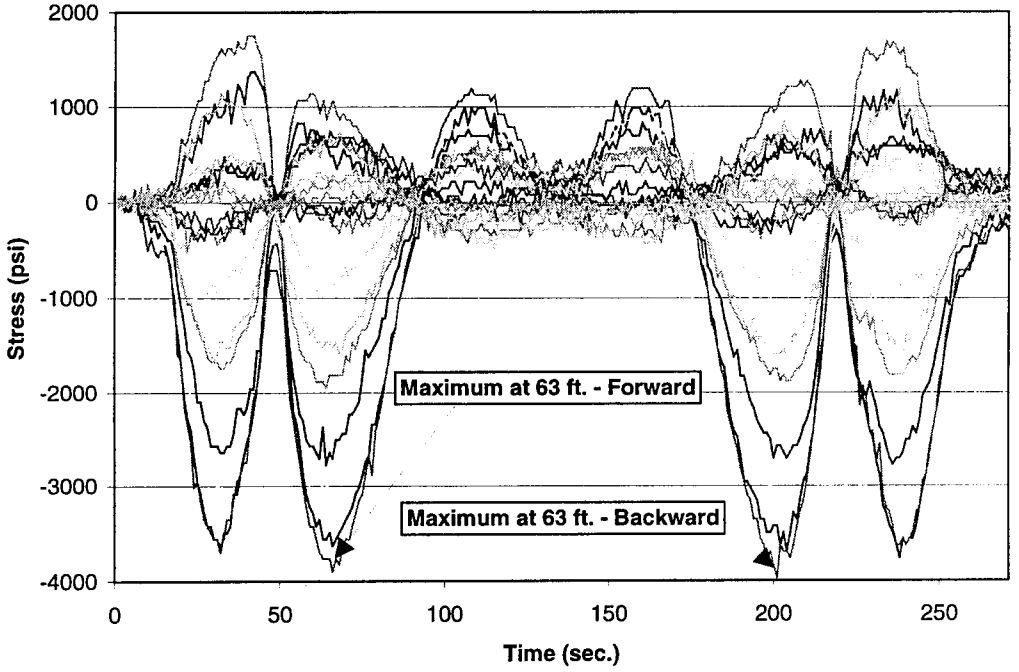

Figure 5.2 Stress vs. Time plot for Box #2, R-289_6-9-10.

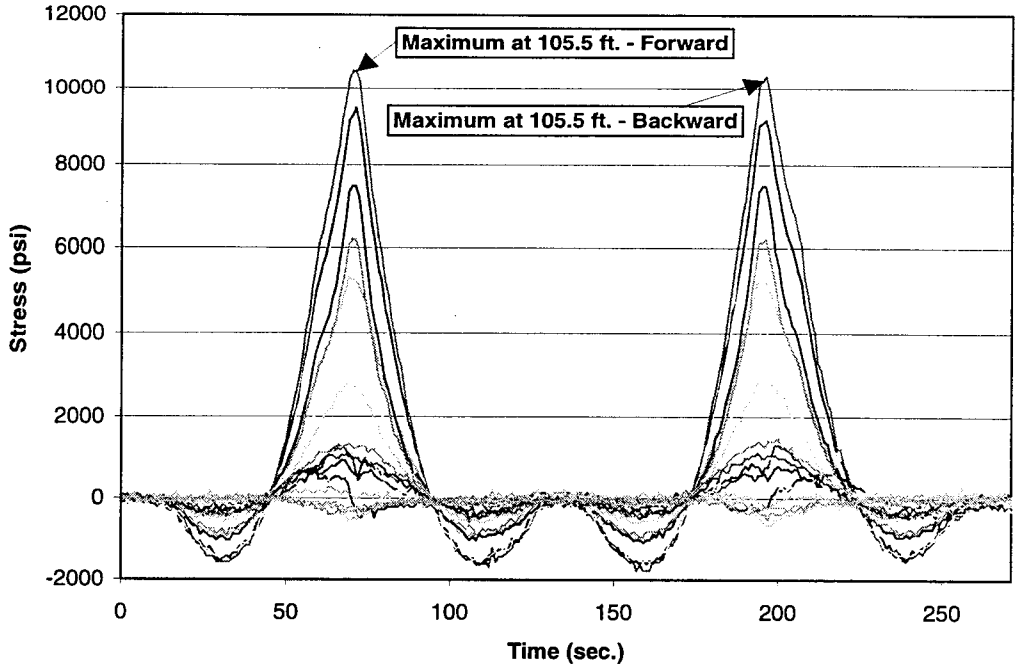

Figure 5.3 Stress vs. Time plot for Box #3, R-289_6-9-10.

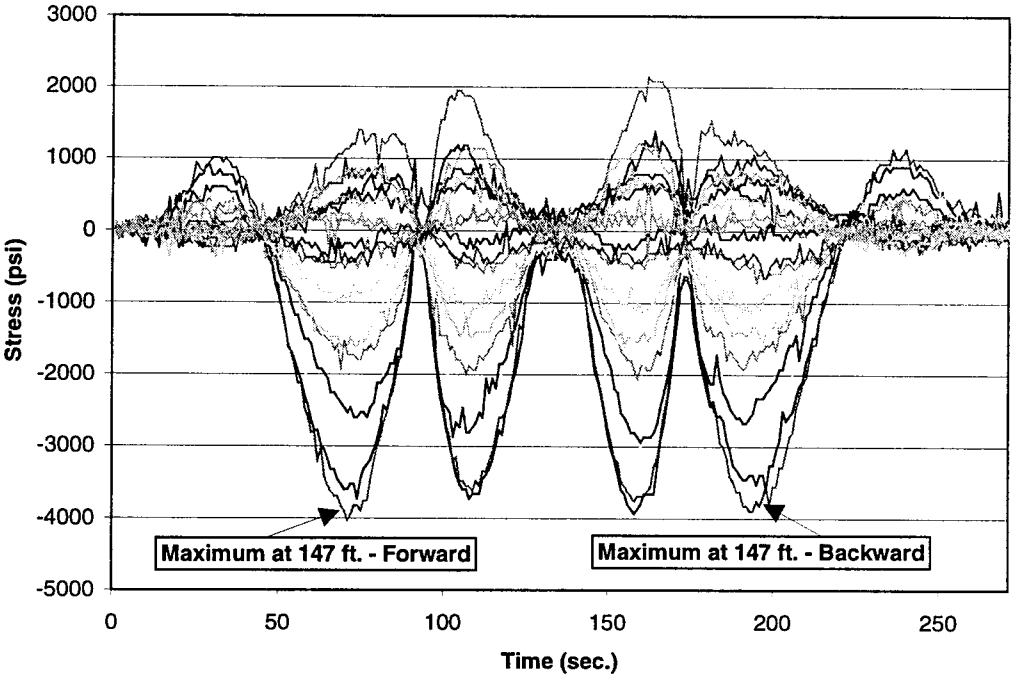

Figure 5.4 Stress vs. Time plot for Box #4, R-289_6-9-10.

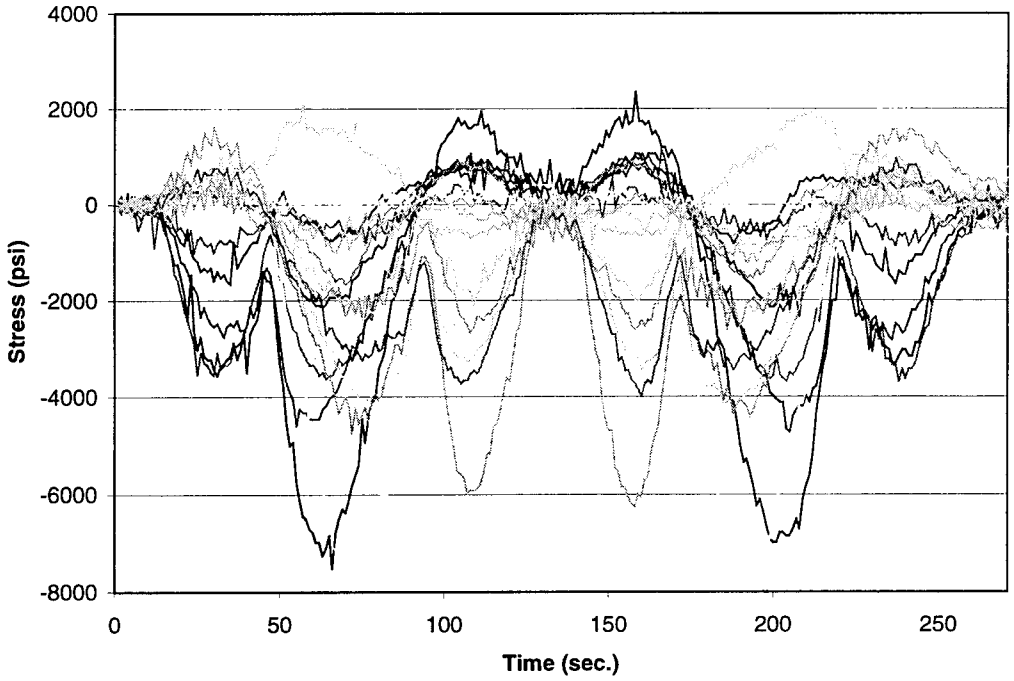

Figure 5.5 Stress vs. Time plot for Box #5, R-289_6-9-10.

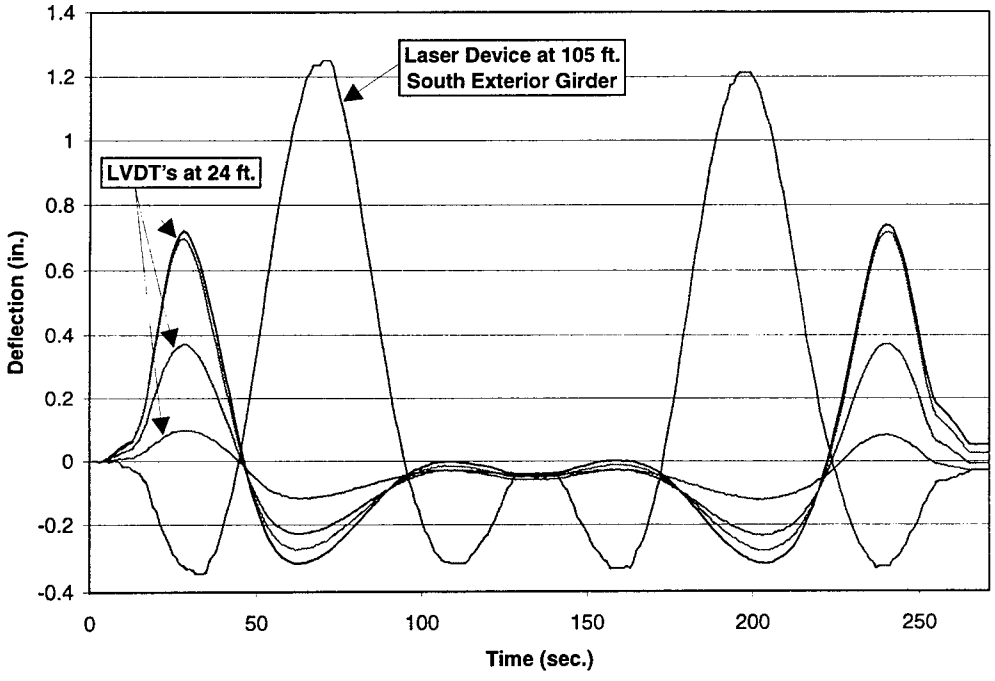

Figure 5.6 Deflection vs. Time plot, R-289_6-9-10.

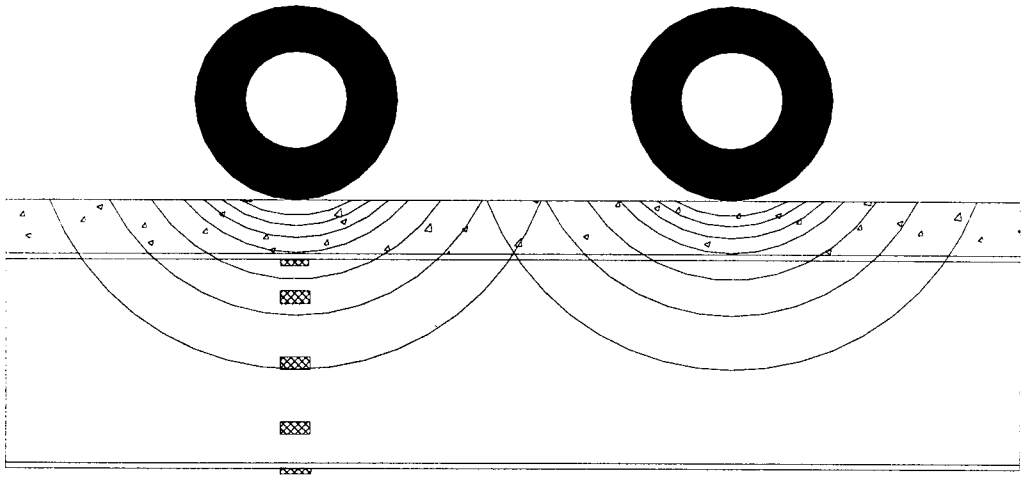

Figure 5.7 Local compressive zone due to wheel/slab contact stresses.

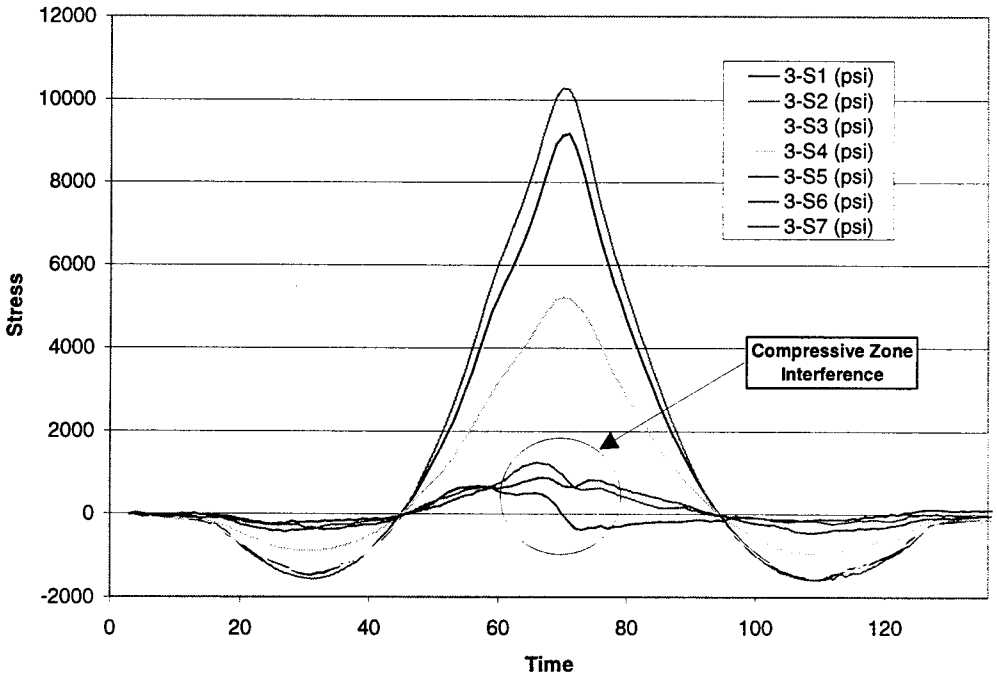

Figure 5.8 Effect of local compressive zone on stress histories.

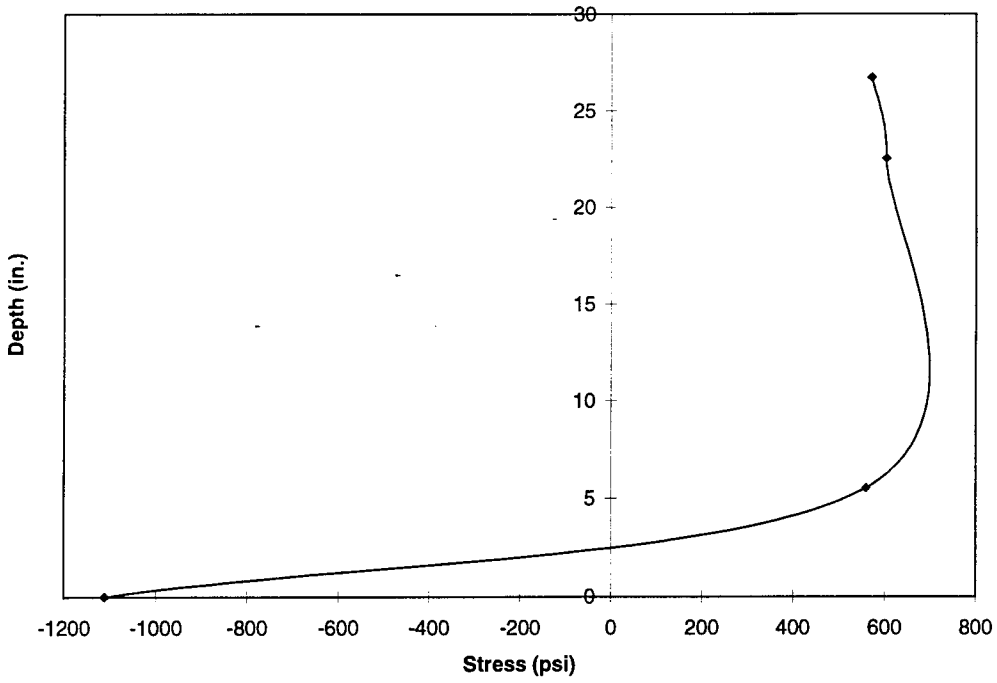

Figure 5.9 Stress distribution due to bearing restraint at 60 ft. with the truck at 105 ft.

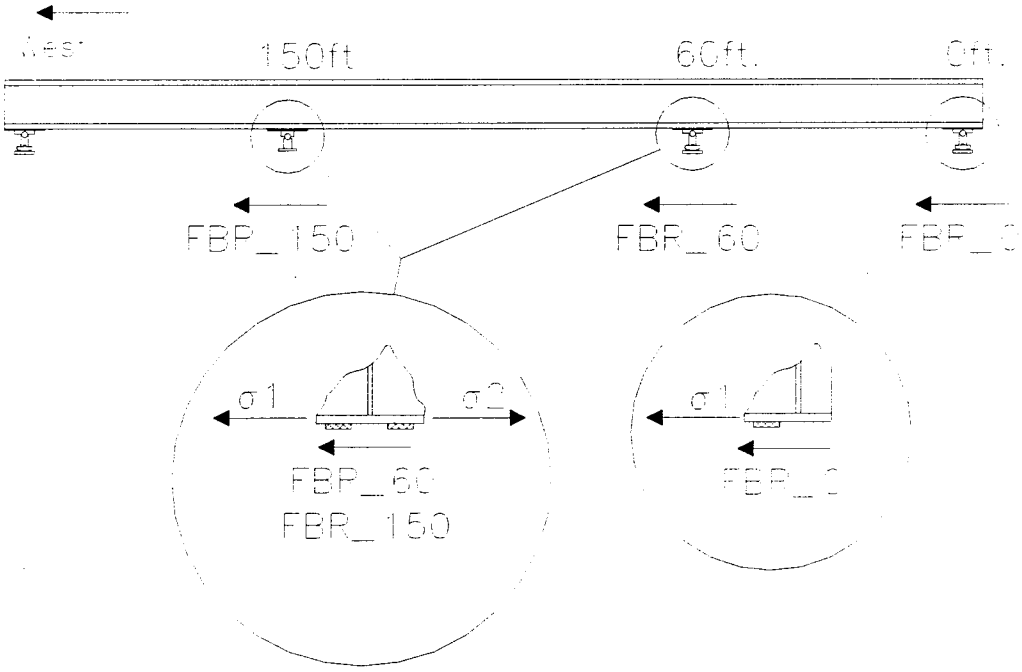

Figure 5.10 Positive sign convention for calculation of bearing restraint forces.

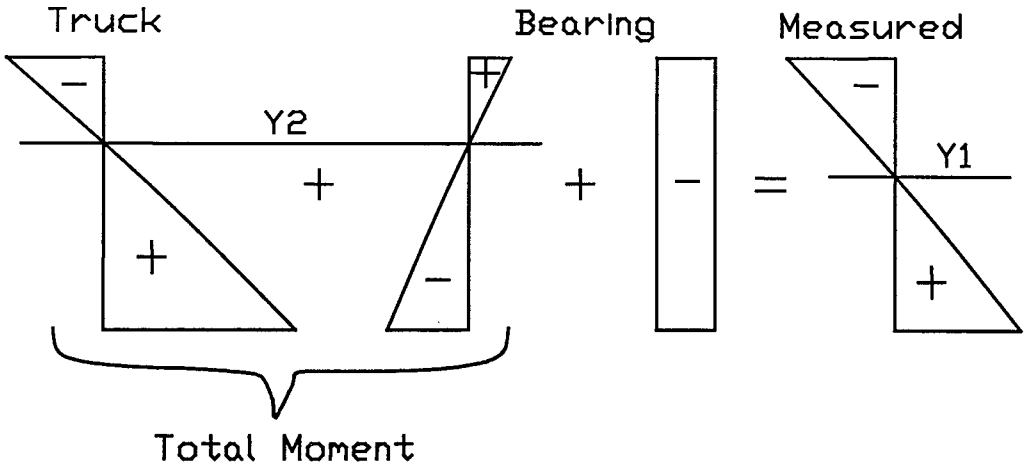

Figure 5.11 Superposition of stresses which make up the measured stress distribution.

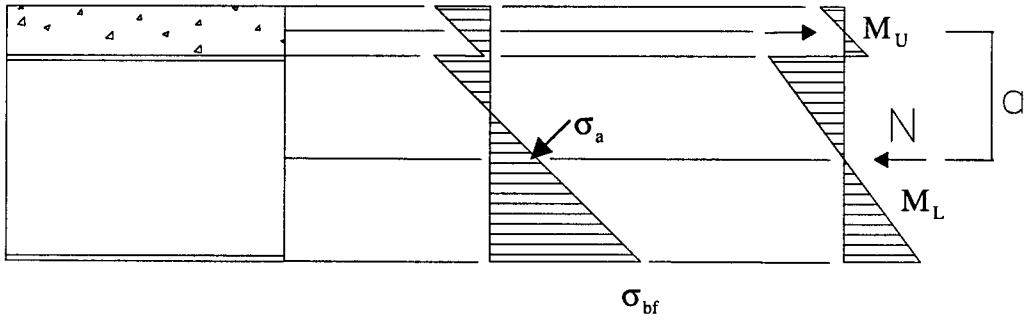

Figure 5.12 Breaking the measured bending moments into three components.

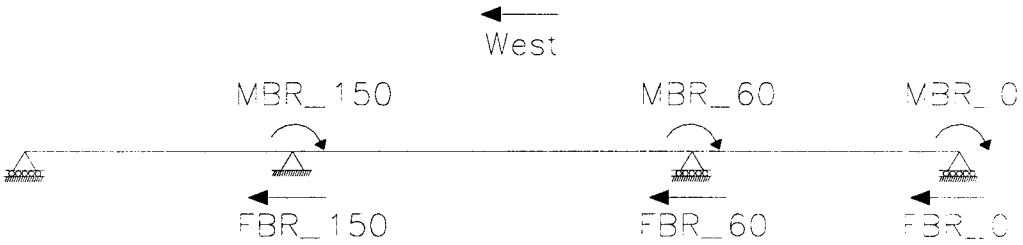

Figure 5.13 Positive sign convention for bearing forces and moments.

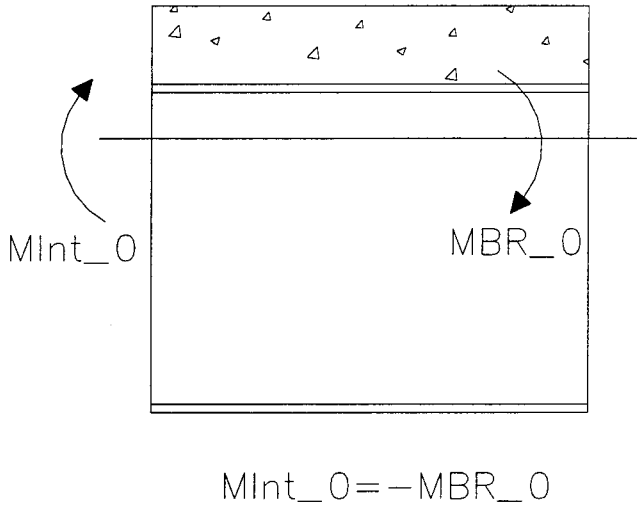

Figure 5.14 Calculation of internal moment at 0 ft.

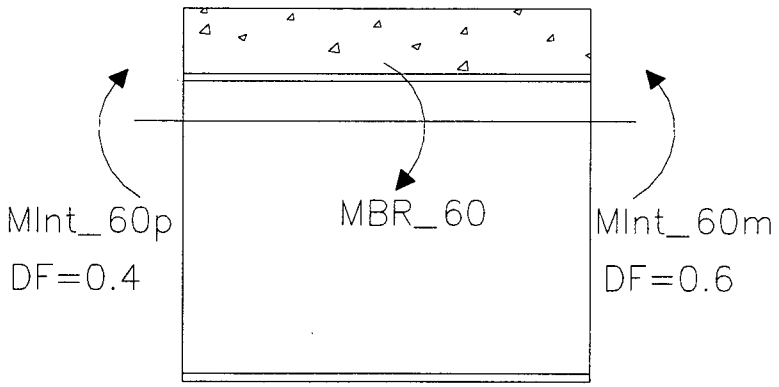

MInt_60m=0.6*MBR_60

MInt_60p=−0.4*−MBR_60

Figure 5.15 Calculation of internal moments at both sides of the 60 ft. bearings.

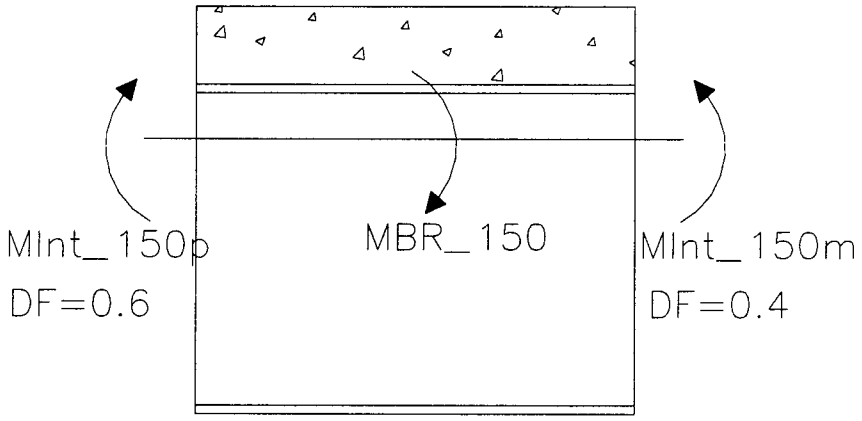

MInt_150m=0.4*MBR_150

MInt_150p=−0.6*−MBR_150

Figure 5.16 Calculation of internal moments at both sides of the 150 ft. bearings.

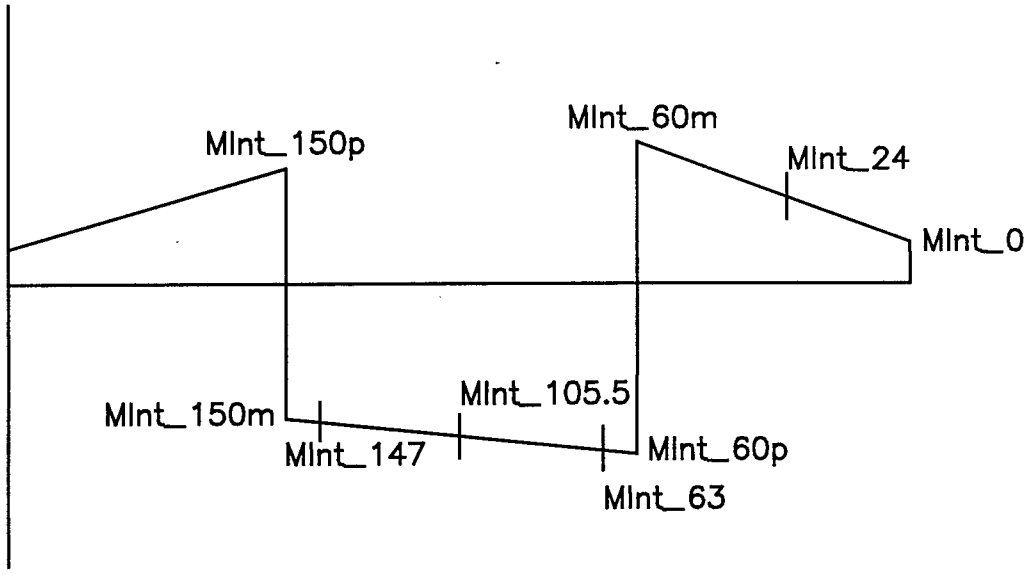

Figure 5.17 Moment diagram due to bearing restraint moments.

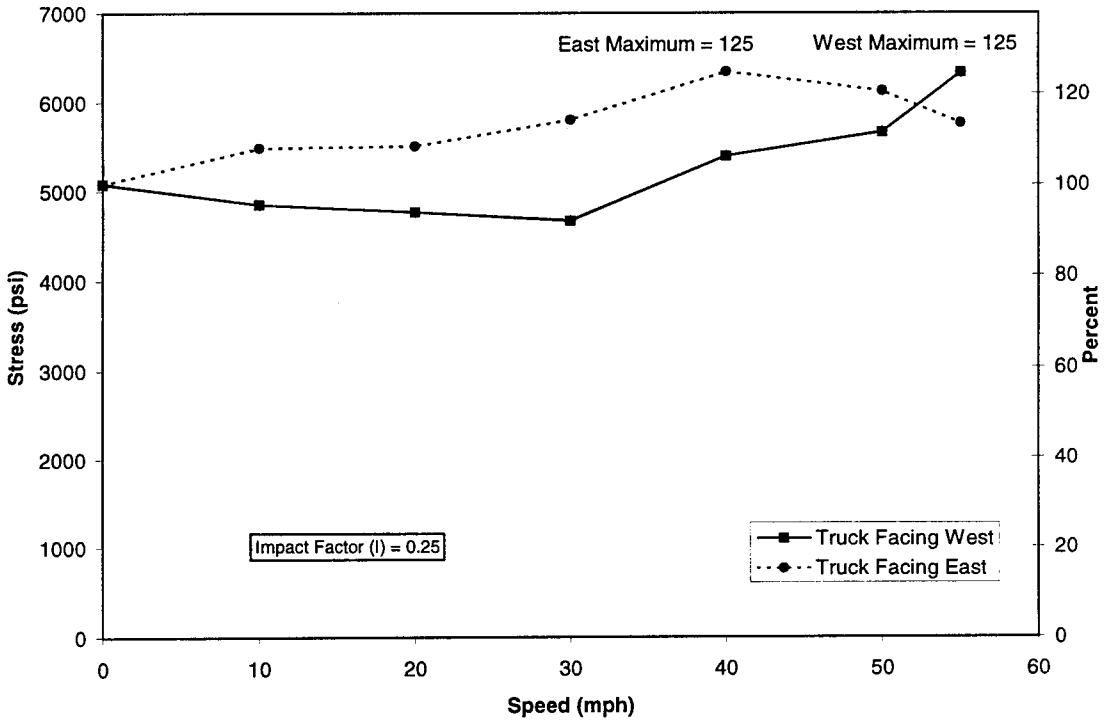

Figure 5.18 Results of the impact study.

CHAPTER 6

LOAD POSTING PLANS FOR DIAGNOSTIC FIELD TESTING

6.1 BACKGROUND

In order for an efficient load test to be conducted on a bridge structure, instrumentation plans requiring a minimum number of gages should be developed to test for each of the factors listed in below. For it to be effective, a load posting procedure needs to be developed that considers all of the enhancement factors. Frederick (1998) provides a derivation of this equation, which can be found in the following sections.

With the following load posting procedure, instrumentation plans are presented to accurately measure the contributions from the following factors:

(1) available live load capacity,

(2) actual impact,

(3) bearing restraint forces,

(4) actual lateral distribution of forces,

(5) actual longitudinal distribution of forces,

(6) contributions from barrier curbs, railings, and extra system components,

(7) actual section properties, and

(8) unintentional or additional composite action.

For a thorough field test, each factor listed above would need to be quantified. However, reliable postings can be developed with only portions of the above factors known. The following sections will show the gage instrumentation plans that are applicable and the calculations for posting with six different testing plans. The six testing plans, their objectives and level of effort vary according to the accuracy of load rating and factor information

desired. Finally, this chapter will conclude with examples showing how Bridge R-289, located in Franklin County, Missouri, can been rated with each testing plan at 24 ft, 60 ft, and 105 ft from the east abutment. These distances correspond to the maximum non-composite positive moment, maximum non-composite negative moment, and the maximum composite positive moment on the structure for the critical south exterior girder.

6.2 DETERMINATION OF ANALYTICAL POSTING

Before the bridge is to be tested, it needs to be inspected and analytically rated. The outcome of this process is a rating factor, which represents the ability of the bridge structure to resist the applied load (Frederick, 1998). The rating factor can be found from this simple equation:

$$\text{RatingFactor} = \frac{\text{Capacity} - \text{DeadLoadEffects}}{\text{LiveLoadEffects} + \text{Impact}} \tag{6.1}$$

Currently, any bridge in Missouri which is constructed, replaced or rehabilitated is rated using load factor design in accordance with national policy concerning the national Bridge Inventory. However, since allowable stress methods were used historically, there are still a large number of bridges in Missouri's inventory (such as bridge R-289) where the existing rating is based on allowable stress methods. Since the allowable stress method is the current method of record for bridge R-289, the following is in allowable stress format. The methods presented herein can be applied to the load factor method with little adjustment. The allowable stress rating used in posting calculations is set at 68% of the steel yield stress (MHTD, 1990). The following equation shows the allowable stress method used to determine the rating (Frederick, 1998):

$$Rating = \frac{\beta * \sigma_{Yield} - \sigma_{Deadload}}{\sigma_{L(1+I)}} * (TruckWeight) \tag{6.2}$$

where,

β = 75% for operating rating,
68% for Missouri posting rating,
55% for inventory rating,
σ_{yield} = Yield Stress,
$\sigma_{deadload}$ = Dead Load Stress, and
$\sigma_{L(1+I)}$ = Live Load Stress with Impact.

The analytical allowable stress posting equation can be determined with the following equation:

$$Analytical\_ASR\_Posting = \frac{(0.68 * F_y - \sigma_{DA})}{I_A * \left(\frac{M_{WL} * 12}{S_A}\right) * DF_A} * RVW \qquad (6.3)$$

where,
F_y = Yield Stress of Structural Steel (ksi),
σ_{DA} = Analytical Design Dead Load Stress (ksi),
I_A = Analytical Impact Factor,
S_A = Analytical Section Modulus with Design Dimensions (in^3),
DF_A = Analytical Distribution Factor,
RVW = Rating Vehicle Weight (tons), and
M_{WL} = Analytical Wheel Line Moment for RVW Truck (ft-kips).

6.3 POSTING UTILIZING EXPERIMENTAL PARAMETERS

When using data obtained from field testing, the stress equation listed in the previous section can be modified for use in posting. The equation is as follows:

$$ExpASPost = \frac{(0.68 * F_y - \sigma_{DE})}{(\frac{M_{RVW}}{M_{TRK}}) * (\frac{M_T * 12}{S_E}) * I_E} * RVW \qquad (6.4)$$

where,
σ_{DE} = Actual Dimensions Experimental Dead Load Stress (ksi),
I_E = Experimental Impact Factor,
S_E = Experimental Section Modulus (in^3),
DF_E = Experimental Distribution Factor,

M_T = Experimental Total Moment (ft-kips),
M_{TRK} = Analytical Truck Moment (ft-kips), and
M_{RVW} = Analytical RVW Truck Moment (ft-kips).

The experimental stress results are used to determine the experimental total moment M_T. The experimental posting load is usually less than the analytical rating. However, to justify raising the posted load, the attributes that tend to increase the capacity must be separated and quantified. To quantify the contributors to the additional capacity, Equation 6.4 is rewritten as:

$$ExpASPost = \frac{(0.68 * F_y - \sigma_{DE})}{I_E * \left[\frac{\frac{M_{RVW}}{M_{TRK}} * \frac{M_E}{M_{LE}} * \frac{M_{LE}}{DF_E} * \frac{M_T}{M_E} * 12}{\frac{S_E}{S_A^{ADIM}} * S_A^{ADIM}} \right] * DF_E} * RVW \qquad (6.5)$$

where,
M_E = Experimental Elastic Moment with Bearing Restraint Effects Removed (ft-kips),
M_{LE} = Experimental Elastic Moment Adjusted for Longitudinal Distribution (ft-kips), and
S_A^{ADIM} = Analytical Section Modulus with Actual Measured Dimensions (in^3).

The resulting equation is identical to Equation 6.4.

6.4 QUANTIFYING CONTRIBUTIONS TO EXPERIMENTAL RATING

As was derived in Frederick (1998), taking the ratio of the experimental allowable stress posting to the analytical allowable stress posting obtains the following generalized equation that can be used to show how each contributing factor listed in Section 6.1 changes the posting from the analytical calculations:

$$\frac{ExpASPost}{AnaASPost} = \left[\left(\frac{0.68F_Y - \sigma_{DE}}{0.68F_Y - \sigma_{DA}} \right) * \left(\frac{I_A}{I_E} \right) * \left(\frac{M_E}{M_T} \right) * \left(\frac{M_{LE}}{M_E} \right) * \left(\frac{DF_A}{DF_E} \right) * \left(\frac{M_{WL}}{\frac{M_{LE}}{DF_E} * \frac{M_{RVW}}{M_{TRK}}} \right) * \left(\frac{S_A^{ADIM}}{S_A} \right) * \left(\frac{S_E}{S_A^{ADIM}} \right) \right] \qquad (6.6)$$

The contribution from each factor is broken down as follows:

$\frac{0.68 * F_Y - \sigma_{DE}}{0.68 * F_Y - \sigma_{DA}}$ the calculation adjustment/correction of the design dead load versus the actual dead load computed with actual measured section dimemsions,

$\frac{I_A}{I_E}$ the adjustment for the experimental impact factor,

$\frac{M_E}{M_T}$ the adjustment for bearing restraint force effects,

$\frac{M_{LE}}{M_E}$ the adjustment for longitudinal redistribution of moment.

$\frac{DF_A}{DF_E}$ the adjustment for the experimental distribution factor,

$\frac{M_{WL}}{\frac{M_{LE}}{DF_E} * \frac{M_{RVW}}{M_{TRK}}}$ the adjustment for curbs, parapets, and railings,

$\frac{S_A^{ADIM}}{S_A}$ the adjustment for actual section dimensions for section modulus calculations, and

$\frac{S_E}{S_A^{ADIM}}$ the adjustment for unintentional composite action.

A detailed discussion and derivation of these factors can be found in Frederick (1998). Each testing plan in the following section will show how these factors are used to gain a better understanding of the experimental posting.

6.5 FIELD TESTING PLANS

Depending on the availability of funds, desired accuracy of the rating, and the time allowed for testing, different instrumentation plans can be used. The following list serves as a standard set of bridge test instrumentation plans that can be used to post existing slab on steel girder bridges. For a visual example of the testing plans, the reader will be shown

Bridge R-289 gage placements. Table 6.1 shows what factors each plan test can determine and what factors are lumped into a comprehensive factor. After the listing of the instrumentation plans, an example for Bridge R-289 will be discussed.

6.5.1 Test Plan I

The most simple instrumentation plan consists of gage placement such that the experimental impact factor and the experimental total moment can be used to post the bridge. This can theoretically be accomplished with one strain gage placed on the center of the bottom flange on the critical girder at the maximum moment longitudinal location as determined in analytical calculations. The implementation of Test Plan I for Bridge R-289 can be seen in Figure 6.1. However, this placement will not allow the individual quantification of the experimental section modulus, distribution factor, longitudinal redistribution of moment, contribution from curbs and railings, or the elastic moment with bearing restraint forces removed. Also note that the actual section dimensions and thus, the actual dead load stress can be calculated if the dimensions of the bridge are carefully measured by the testing crew. Thus, if measurements are made in the field, the dead load adjustment calculation can be made as well as the correction for the analytical section modulus with actual dimensions.

If the test is run according to the sound loading guidelines, the following can be calculated from the response in the gage:

$$(1) \qquad I_E = \frac{\sigma_0^{Dynamic}}{\sigma_0^{Static}} \tag{6.7}$$

where,

σ_0^{Static} = Measured static stress (psi), and

$\sigma_0^{Dynamic}$ = Largest measured dynamic stress (psi).

Note, testing for the "actual" impact factor is tedious and difficult. Unless there is sound justification for trying to lower the dynamic impact, it is recommended to use the design values.

(2) $$M_T = \frac{\sigma_0 * S_A}{12 * 1000} \tag{6.8}$$

where,

σ_0 = Measured Bottom Flange Stress (psi).

Note that the total moment can either be found using the analytical section modulus calculated with design dimensions or the analytical section modulus calculated with measured dimensions. Thus, Equation 6.5 reduces to the following:

Without S_A^{ADIM}

$$ExpASPost = \left[\frac{0.68 * F_Y - \sigma_{DE}}{I_E * \left(\frac{M_T * 12}{S_A} \right) * \left(\frac{M_{RVW}}{M_{TRK}} \right)} \right] * RVW \tag{6.9}$$

With S_A^{ADIM}

$$ExpASPost = \left[\frac{0.68 * F_Y - \sigma_{DE}}{I_E * \left(\frac{M_T^{ADIM} * 12}{S_A^{ADIM}} \right) * \left(\frac{RVW}{M_{TRK}} \right)} \right] * RVW \tag{6.10}$$

where,

M_T^{ADIM} = Total Moment with Measured Dimensions (ft-kips) (Note that the axial stress from bearing restraint is not removed).

The experimental posting can be calculated with either the actual dimension analytical section modulus or with just the analytical section modulus. The test plans that follow will be shown using the actual dimension analytical section modulus only, though it can be calculated with either.

With this testing plan, and assuming that the testing crew has measured the actual dimensions of the structure, the following factors can be determined for Equation 6.6:

(1) $$Dead\_Load\_Stress\_Adjustment = \frac{0.68 * F_y - \sigma_{DE}}{0.68 * F_y - \sigma_{DA}}$$

(2) $$Impact\_Adjustment = \frac{I_A}{I_E}$$

(3) $$Section\_Modulus\_Adjustment = \frac{S_A^{ADIM}}{S_A}$$

All of the other factors cannot be separated or quantified from this data. Thus, they are lumped into a comprehensive factor. With these adjustments, Equation 6.6 reduces to:

$$\frac{ExpASPost}{AnaASPost} = \left[\left(\frac{0.68F_Y - \sigma_{DE}}{0.68F_Y - \sigma_{DA}}\right) * \left(\frac{I_A}{I_E}\right) * \left(\frac{S_A^{ADIM}}{S_A}\right) * (Comp\_Factor)\right] \qquad (6.11)$$

It is noted that this testing plan could be used to load rate a bridge, though it is not advised due to the lack of redundancy in measuring stresses. The plan is mainly presented as a demonstration and to help develop the testing plans that follow.

6.5.2 Test Plan II

Test Plan I can be further enhanced by placing two additional gages in the web of the critical cross section. One gage should be placed near the quarter point of the web from the top of the bottom flange and the other gage should be placed near the midpoint of the girder. This will allow for an experimental verification of the section modulus and a more accurate

experimental total girder moment to be used in the posting calculations. An example of this test plan for Bridge R-289 can be seen in Figure 6.2.

From the responses in these three gages, the experimental section modulus and the experimental total moment can be calculated as follows. The derivation of this procedure can be found in Imhoff (1998). However, with this test plan the axial stress due to bearing restraint cannot be determined with the gage selection and thus has not been removed from this calculation.

(1) Find the experimental stress versus depth equation:

Assume that the gages are depicted as follows:

#1 – Bottom Flange

#2 – Quarterpoint of Web

#3 – Midpoint of Web

A table of the experimental maximum stress versus the distance from the bottom of the bottom flange can be developed similar to Table 6.2.

With the values obtained from Table 6.2, a linear regression can be applied to the data points to calculate the linear strain profile of the section, as shown in Figure 6.3. According to Imhoff (1998), this can be accomplished by solving the least squares analysis as follows.

$$\begin{bmatrix} \Sigma\sigma_i^2 & \Sigma\sigma_i \\ \Sigma\sigma_i & 3 \end{bmatrix} * \begin{Bmatrix} Slope \\ Intercept \end{Bmatrix} = \begin{Bmatrix} \Sigma(\sigma * d_i) \\ \Sigma d_i \end{Bmatrix} \tag{6.12}$$

Solving the matrix equation for the slope and the intercept and then writing the equation of the straight line yields the following:

$$Slope = \frac{3 * \Sigma(\sigma_i * d_i) - \Sigma\sigma_i * \Sigma d_i}{3 * \Sigma\sigma_i^2 - (\Sigma\sigma_i)^2} \tag{6.13}$$

$$Intercept = \frac{\Sigma(\sigma_i * d_i) - \Sigma\sigma_i^2 * slope}{\Sigma\sigma_i} \tag{6.14}$$

$$d = Slope * \sigma + Intercept \tag{6.15}$$

$$\sigma = \frac{1}{Slope} * d - \frac{Intercept}{Slope} \tag{6.16}$$

where,

Intercept = Neutral Axis from Bottom of Bottom Flange (in),
Slope = Slope of the Stress Profile,
d = Depth from Bottom of Bottom Flange (in), and
σ = Stress in Girder (psi).

(2) Calculate M_T

From the stress Equation 6.16, calculate the stresses at the bottom of the bottom flange and at the centroid (assumed here to be in the center of the steel girder) of the girder:

$$\sigma_0 = -\frac{Intercept}{Slope} \tag{6.17}$$

$$\sigma_{CG} = \frac{1}{Slope} * CG - \frac{Intercept}{Slope} \tag{6.18}$$

where,

CG = Center of Gravity (in).

Then, as shown in Figure 6.4 and discussed in Imhoff (1998) and Bakht (1990), the total moment can be calculated as follows:

$$M_L = \frac{(\sigma_0 - \sigma_{CG})}{12 * 1000} * S_{steel}^{ADIM} \tag{6.19}$$

$$M_U = \frac{(E_{conc} * I_{conc})}{(E_{steel} * I_{steel}^{ADIM})} * M_L \tag{6.20}$$

$$Na = \frac{(\sigma_{CG} * A_{steel}^{ADIM})}{12*1000}\left(\frac{d_{steel}^{ADIM}}{2} + Haunch^{ADIM} + \frac{d_{slab}^{ADIM}}{2}\right) \quad (6.21)$$

$$M_T^{Axial} = M_U + M_L + Na \quad (6.22)$$

where,

A_{steel}^{ADIM} = Area of Steel Girder using Measured Dimensions (in^2),
d_{steel}^{ADIM} = Depth of Steel Girder using Measured Dimensions (in),
$Haunch^{ADIM}$ = Depth of Haunch using Measured Dimensions (in),
E_{conc} = Modulus of Elasticity of Concrete (in^4),
E_{steel} = Modulus of Elasticity of Steel (in^4),
I_{conc} = Moment of Inertia of Concrete Slab (in^4),
I_{steel}^{ADIM} = Moment of Inertia of Steel using Measured Dimensions (in^4), and
M_T^{Axial} = The Total Moment with Axial from Bearing Restraint (ft-kips).

(3) Calculate S_E

The experimental section modulus can be calculated by finding the experimental moment of inertia and then dividing that by the intercept of the stress equation found earlier.

$$I_{Exp} = -(M_T^{Axial}) * Slope \quad (6.23)$$

$$S_E = \frac{I_{Exp}}{Intercept} \quad (6.24)$$

where,

I_{Exp} = Experimental Moment of Inertia (in^4).

With these factors taken into account, Equation 6.5 reduces to the following equation:

$$ExpASPost = \left[\frac{0.68 * F_Y - \sigma_{DE}}{I_E * \left(\frac{M_T^{Axial} * 12}{S_E} \right) * \left(\frac{M_{RVW}}{M_{TRK}} \right)} \right] * RVW \qquad (6.25)$$

With this testing plan the following factors can be determined for Equation 6.6:

(1) $Dead\_Load\_Stress\_Adjustment = \frac{0.68 * F_y - \sigma_{DE}}{0.68 * F_y - \sigma_{DA}}$

(2) $Impact\_Adjustment = \frac{I_A}{I_E}$

(3) $Section\_Modulus\_Adjustment = \frac{S_A^{ADIM}}{S_A}$

(4) $Additional\_Composite\_Adjustment = \frac{S_E}{S_A^{ADIM}}$

The remaining factors cannot be extracted from the data obtained from this test plan. Thus, the remaining factors are lumped into a single comprehensive factor. With these adjustments, Equation 6.6 reduces to:

$$\frac{ExpASPost}{AnaASPost} = \left[\left(\frac{0.68 F_Y - \sigma_{DE}}{0.68 F_Y - \sigma_{DA}} \right) * \left(\frac{I_A}{I_E} \right) * \left(\frac{S_A^{ADIM}}{S_A} \right) * \left(\frac{S_E}{S_A^{ADIM}} \right) * (Comp\_Factor) \right] \qquad (6.26)$$

It is noted that this testing plan produces a posting that is more accurate than the posting found from Test Plan I, due to the more accurate prediction of the bottom flange stress from the three gages on a cross section, not just a single gage.

6.5.3 Test Plan III

Test Plan III will give the same posting as Test Plan I, but it will also allow the determination of the experimental lateral distribution factor for the section in question. This plan consists of gage placement on the bottom flange of each girder at the maximized

longitudinal location as determined by the analytical analysis of the bridge. An example of this gage placement can be seen in Figure 6.5 for Bridge R-289. With these gages, the distribution factor can be determined as follows:

(1) Develop a table similar to Table 6.3 that lists the girder bottom flange stress versus the analytical section modulus for the respective section at a particular loading.

(2) Calculate the experimental distribution factor (DF_E)

$$DF_E = \frac{2*(\sigma_0^{critical} * S_{critical}^{ADIM})}{(\sigma_0^{critical} * S_A^{ADIM}) + \Sigma(\sigma_i^{noncritical} * S_i^{noncritical})} \tag{6.27}$$

With this testing plan, the posting equation is identical to Test Plan I and can be seen in Equation 6.28.

$$ExpASPost = \left[\frac{0.68 * F_Y - \sigma_{DE}}{I_E * \left(\frac{M_T^{ADIM} * 12}{S_A^{ADIM}} \right) * \left(\frac{M_{RVW}}{M_{TRK}} \right)} \right] * RVW \tag{6.28}$$

The following factors can be determined for Equation 6.6:

(1) $Dead\_Load\_Stress\_Adjustment = \frac{0.68 * F_y - \sigma_{DE}}{0.68 * F_y - \sigma_{DA}}$

(2) $Impact\_Adjustment = \frac{I_A}{I_E}$

(3) $Distribution\_Factor\_Adjustment = \frac{DF_A}{DF_E}$

(4) $Section\_Modulus\_Adjustment = \frac{S_A^{ADIM}}{S_A}$

These are the only factors that this testing plan can determine. Thus, Equation 6.6 reduces to the following with the remaining factors lumped into a comprehensive factor:

$$\frac{ExpASPost}{AnaASPost} = \left[\left(\frac{0.68F_Y - \sigma_{DE}}{0.68F_Y - \sigma_{DA}}\right) * \left(\frac{I_A}{I_E}\right) * \left(\frac{S_A^{ADIM}}{S_A}\right) * \left(\frac{DF_A}{DF_E}\right) * (Comp\_Factor)\right] \quad (6.29)$$

It is again noted that this testing plan produces the identical posting that Test Plan I would produce. However, the bridge structure would be better understood due to the testing of the experimental distribution factor.

6.5.4 Test Plan IV

Test Plan IV is simply the combination of the first three test plans. This will allow for a more accurate determination of the enhancement factors but will still have the same posting as in Test Plan II. A view of this testing plan for Bridge R-289 can be seen in Figure 6.6. Thus, the posting equation for this plan is:

$$ExpASPost = \left[\frac{0.68 * F_Y - \sigma_{DE}}{I_E * \left(\frac{M_T^{Axial} * 12}{S_E}\right) * \left(\frac{M_{RVW}}{M_{TRK}}\right)}\right] * RVW \quad (6.30)$$

With this testing plan, the following factors can be determined for Equation 6.6:

(1) $Dead\_Load\_Stress\_Adjustment = \frac{0.68 * F_y - \sigma_{DE}}{0.68 * F_y - \sigma_{DA}}$

(2) $Impact\_Adjustment = \frac{I_A}{I_E}$

(3) $Distribution\_Factor\_Adjustment = \frac{DF_A}{DF_E}$

(4) $Section\_Modulus\_Adjustment = \frac{S_A^{ADIM}}{S_A}$

(5) $Additional\_Composite\_Adjustment = \frac{S_E}{S_A^{ADIM}}$

These are the factors that can be determined with the gage placement for plan IV. Thus, with the remaining unknown factors lumped into a single comprehensive factor, Equation 6.6 reduces to:

$$\frac{ExpASPost}{AnaASPost} = \left[\left(\frac{0.68F_Y - \sigma_{DE}}{0.68F_Y - \sigma_{DA}}\right)*\left(\frac{I_A}{I_E}\right)*\left(\frac{S_A^{ADIM}}{S_A}\right)*\left(\frac{S_E}{S_A^{ADIM}}\right)*\left(\frac{DF_A}{DF_E}\right)*(Comp\_Factor)\right] \qquad (6.31)$$

This plan produces the same rating as Test Plan II. However, by utilizing this plan, the research team can gain valuable information about the factors listed in Equation 6.6. Thus, the behavior of the structure can be more carefully monitored and the bridge owner can determine what factors should be relied upon.

6.5.5 Test Plan V

Test Plan IV can further be enhanced by testing for and removing the bearing restraint forces so that the total moment can be found without the effects of bearing restraint. This gage placement is more difficult than previous tests and will require good engineering judgement. In general, gage placement needs to be developed to determine the bearing restraint forces at all bearings around the critical longitudinal cross section. The placement of these gages for Bridge R-289 can be seen in Figure 6.7. The gage layout can be developed by placing gages on each side of bearings, where applicable, on the center of the bottom flange at six inches from the bearing. Enough gages should be placed so that the following calculations can be accomplished for the critical cross section in question:

(1) Determine the bearing restraint forces:

The bearing restraint force calculations have been derived in Imhoff (1998). In general, a bearing force at an abutment can be calculated by:

$$BearingForce = -A_{bf} * \sigma_{bf} \tag{6.32}$$

where,

A_{bf} = Area of the Bottom Flange at the Bearing (in^2), and
σ_{bf} = Stress on the Bottom Flange at the Bearing (psi).

The bearing restraint force at a pier is slightly more difficult and requires gages on both sides of the bearing. The difference between the two stresses can be used to determine the bearing force as shown in the following equation:

$$BearingForce = \frac{(\sigma_{bf}^{two} - \sigma_{bf}^{one}) * A_{bf}}{CP} \tag{6.33}$$

where,

σ_{bf}^{two} = Stress on Left Side of Bearing (psi),
σ_{bf}^{one} = Stress on Right Side of Bearing (psi), and
CP = 2 if bottom flange is cover plated,
1 if not (Imhoff 1998).

(2) Remove axial stress:

The axial stress caused by the bearing restraint force should be found by cutting the full bridge at the cross section in question. Then, after summation of forces to obtain the bearing restraint at the cross section, the axial stress can be removed as follows. For a complete explanation of this, the reader is referred to Imhoff (1998):

$$\sigma_{axial} = \frac{NetBearingForce}{A_{comp}^{ADIM}} \tag{6.34}$$

where,

$$A_{comp}^{ADIM} = A_{Steel} + \frac{A_{conc}}{n} \text{ (in}^2\text{)}.$$

This axial stress can be removed from the stress equation as shown in Figure 6.8. The result can be seen in Equation 6.35.

$$\sigma = \frac{1}{Slope} * \frac{d}{2} - \frac{Intercept}{Slope} - \sigma_{axial} \tag{6.35}$$

(3) Calculate $M_T^{Axial\_Removed}$:

From Equation 6.35 the following stresses are calculated for axial stress removed:

$$\sigma_0^{Axial\_Removed} = -\frac{Intercept}{Slope} - \sigma_{axial} \tag{6.36}$$

and

$$\sigma_{CG}^{Axial\_Removed} = \frac{1}{Slope} * \frac{d}{2} - \frac{Intercept}{Slope} - \sigma_{axial} \tag{6.37}$$

Then, as shown in Figure 6.4, the total moment can be calculated as follows:

$$M_L^{Axial\_Removed} = \frac{(\sigma_0^{Axial\_Removed} - \sigma_{CG}^{Axial\_Removed})}{12*1000} * S_{steel}^{ADIM} \tag{6.38}$$

$$M_U^{Axial\_Removed} = \frac{(E_{conc} * I_{conc})}{(E_{steel} * I_{steel}^{ADIM})} * M_L^{Axial\_Removed} \tag{6.39}$$

$$N^{Axial\_Removed} a = \frac{(\sigma_{CG}^{Axial\_Removed} * A_{steel}^{ADIM})}{12*1000} * (\frac{d_{steel}^{ADIM}}{2} + Haunch^{ADIM} + \frac{d_{slab}^{ADIM}}{2}) \tag{6.40}$$

$$M_T^{Axial\_Removed} = M_U^{Axial\_Removed} + M_L^{Axial\_Removed} + N^{Axial\_Removed} a \tag{6.41}$$

where

$M_T^{Axial\_Removed}$ = The Total Moment without Axial from bearing restraint (ft-kips).

It is also beneficial with this gage placement to remove the bearing restraint moment from the total moment to obtain the elastic moment. The gage plan for Bridge R-289 will be used to describe this procedure. The procedure to calculate the elastic moment is as follows:

(1) Calculate the neutral axis for each section at the bearings:

Since inadequate gaging is available at the pier locations, the neutral axis at these locations should be analytically estimated with the measured dimensions.

(2) Calculate the bearing restraint moment at the bearings

The bearing restraint moment can be calculated at a particular section by simply multiplying the bearing restraint force by the depth of the neutral axis as shown in the following equation:

$$M_{BR} = BearingForce * \frac{d_{NA}}{12} \qquad (6.42)$$

where,

M_{BR} = Bearing Restraint Moment at a Section (ft-kips)

(3) Calculate the bearing restraint moment at the critical cross section

The calculation of bearing moments requires moment distribution of moment based on member and joint stiffness. The distribution of the moment can be calculated by taking the ratio of the member stiffness to the joint stiffness. For Bridge R-289, and assuming constant moment of inertia in all spans, the distribution can be calculated with the following equation:

$$Distribution = \frac{\left(\frac{E*I}{L}\right)}{\Sigma\left(\frac{E*I}{L}\right)} \tag{6.43}$$

Thus, a moment distribution factor of 0.4 should be used for the critical side of the pier for Bridge R-289 (Imhoff, 1998). Once the bearing restraint moments for both of the bearings on each side of the critical longitudinal section have been calculated, a straight line interpolation between the two values as shown in Figure 6.9 can be used to determine the bearing restraint moment at the critical section in question. For a centerline section, this is calculated as follows:

$$M_{BR}^{Critical\_Section} = \frac{M_{BR}^{Pier\#1} + M_{BR}^{Pier\#2}}{2} \tag{6.44}$$

where,

$M_{BR}^{Critical\_Section}$ = The Bearing Restraint Moment at the Critical Cross Section (ft-kips),

$M_{BR}^{Pier\#1}$ = The Bearing Restraint Moment at the First Pier Location (ft-kips), and

$M_{BR}^{Pier\#2}$ = The Bearing Restraint Moment at the Second Pier Location (ft-kips).

(4) Calculate the elastic moment at the critical cross section

The elastic moment with axial and bearing moment removed can then be calculated with the following equation:

$$M_E = M_T^{Axial\_Removed} - M_{BR}^{Critical\_Section} \tag{6.45}$$

where,

M_E = Elastic Moment.

With these calculations taken into effect, the posting Equation 6.5 reduces to the following equation:

$$ExpASPost = \left[\frac{0.68 * F_Y - \sigma_{DE}}{I_E * \left(\frac{M_T^{Axial\_Removed} * 12}{S_E} \right) * \left(\frac{M_{RVW}}{M_{TRK}} \right)} \right] * RVW \qquad (6.46)$$

With this testing plan, the following factors can be determined for Equation 6.6:

(1) $$Dead\_Load\_Stress\_Adjustment = \frac{0.68 * F_y - \sigma_{DE}}{0.68 * F_y - \sigma_{DA}}$$

(2) $$Impact\_Adjustment = \frac{I_A}{I_E}$$

(3) $$Distribution\_Factor\_Adjustment = \frac{DF_A}{DF_E}$$

(4) $$Bearing\_Restraint\_Adjustment = \frac{M_E}{M_T}$$

(5) $$Section\_Modulus\_Adjustment = \frac{S_A^{ADIM}}{S_A}$$

(6) $$Additional\_Composite\_Adjustment = \frac{S_E}{S_A^{ADIM}}$$

This plan can test for all of the factors listed previously except for the longitudinal redistribution of moment and the effects from the curbs and parapets. These two remaining factors are lumped into a comprehensive factor. With these adjustments, Equation 6.6 becomes:

$$\frac{ExpASPost}{AnaASPost} = \left[\left(\frac{0.68F_Y - \sigma_{DE}}{0.68F_Y - \sigma_{DA}} \right) * \left(\frac{I_A}{I_E} \right) * \left(\frac{S_A^{ADIM}}{S_A} \right) * \left(\frac{S_E}{S_A^{ADIM}} \right) * \left(\frac{DF_A}{DF_E} \right) * \left(\frac{M_E}{M_T} \right) * (Comp\_Factor) \right] \qquad (6.47)$$

It is noted that this testing plan produces better results than Test Plan IV because of the removal of the effects of bearing restraint. It also gives the bridge owner a more complete look at the factors that effect the load rating on the bridge.

6.5.6 Test Plan VI

The final test plan to be introduced is Test Plan VI. This plan, if implemented correctly, can determine each of the factors listed previously. However, the rating will be no different than the rating obtained from testing plan V.

This plan is the same as Test Plan V except that it requires gages to accurately determine the experimental elastic moment diagram for the critical span being tested on the bridge. For continuous multi-span bridges, this gage placement consists of three gages for each negative moment cross section to determine the elastic moment as was determined in plan V for the critical section. An example of Test Plan VI can be seen for Bridge R-289 in Figure 6.10. For Bridge R-289, this includes determining the elastic moments at both pier locations and at the critical location as determined in Test Plan V.

It is important to note that the gages used to determine the elastic moment at the negative moment sections cannot be placed over the piers because of interference from the bearings and diaphragms. Thus, placement of these gages should be at a distance of approximately the depth of the steel girder away from the bearing.

To calculate the elastic longitudinal adjustment, the following procedure is used:

(1) Calculate the elastic moments for the three sections to construct the moment diagram.

This is the exact same procedure as enumerated in testing plan V. Therefore, a discussion of the method will not be listed. Once these three

elastic moments are calculated, plot them on a graph similar to Figure 6.11 with the analysis moment diagram of the load test truck. This plot will be used later in the example of Bridge R-289. Note that the elastic moments for the negative section are at a distance of approximately the depth of the steel girder away from the pier. This should be adjusted by using a linear extrapolation between the critical section and the negative section in question.

(2) Calculate the Statical Moments

As discussed in Frederick (1998), the statical moments can be calculated with the following equations:

$$STAT_A = M_C^2 - (1-\alpha) * M_C^1 - (\alpha) * M_C^3 \quad (6.48)$$

$$STAT_E = M_E^2 - (1-\alpha) * M_E^1 - (\alpha) * M_E^3 \quad (6.49)$$

where,

$STAT_A$ = Statical Moment for Load Truck Moment (ft-kips),
$STAT_E$ = Statical Moment for Experimental Data (ft-kips),
M_C = Analysis Load Truck Moment at Sections (ft-kips), and
α = Percentage of Length.

(3) Calculate the elastic longitudinal adjustment moment:

The calculation of the elastic longitudinal adjustment moment can be accomplished with the following equation:

$$M_{LE} = \frac{STAT_E}{STAT_A} * M_C^2 \quad (6.50)$$

As noted earlier, even with these calculations, the load posting equation is still the same as the equation listed in Test Plan V and rewritten below:

$$ExpASPost = \left[\frac{0.68 * F_Y - \sigma_{DE}}{I_E * \left(\frac{M_T^{Axial\_Removed} * 12}{S_E} \right) * \left(\frac{M_{RVW}}{M_{TRK}} \right)} \right] * RVW \tag{6.51}$$

With this testing plan, all of the factors listed in Section 6.4 can be determined as follows:

(1) $Dead\_Load\_Stress\_Adjustment = \dfrac{0.68 * F_y - \sigma_{DE}}{0.68 * F_y - \sigma_{DA}}$

(2) $Impact\_Adjustment = \dfrac{I_A}{I_E}$

(3) $Distribution\_Factor\_Adjustment = \dfrac{DF_A}{DF_E}$

(4) $Bearing\_Restraint\_Adjustment = \dfrac{M_E}{M_T}$

(5) $Curb/Railing\_Adjustment = \dfrac{M_{WL}}{\frac{M_{LE}}{DF_E} * \frac{M_{RVW}}{M_{TRK}}}$

(6) $Section\_Modulus\_Adjustment = \dfrac{S_A^{ADIM}}{S_A}$

(7) $Longitudinal\_Adjustment = \dfrac{M_{LE}}{M_E}$

(8) $Additional\_Composite\_Adjustment = \dfrac{S_E}{S_A^{ADIM}}$

This plan completely quantifies the enhancement factors available in experimental load testing. Thus, Equation 6.6 can be written as:

$$\frac{ExpASPost}{AnaASPost} = \left[\left(\frac{0.68F_Y - \sigma_{DE}}{0.68F_Y - \sigma_{DA}} \right) * \left(\frac{I_A}{I_E} \right) * \left(\frac{M_E}{M_T} \right) * \left(\frac{DF_A}{DF_E} \right) * \left(\frac{M_{LE}}{M_E} \right) * \left(\frac{M_{WL}}{\frac{M_{LE}}{DF_E} * \frac{M_{RVW}}{M_{TRK}} * \frac{RVW}{LTVW}} \right) * \left(\frac{S_A^{ADIM}}{S_A} \right) * \left(\frac{S_E}{S_A^{ADIM}} \right) \right] \tag{6.52}$$

This testing plan produces the best rating while detailing each factor that leads to the enhanced load rating calculated in Equation 6.51. This allows for easy removal of the factors that the bridge owner does not want to rely upon and the use of the remaining factors to load rate the structure.

6.6 USING TESTING PLANS ON BRIDGE R-289

The testing plans that were discussed in the previous section will be shown by example in the this section. This will include a load posting for the maximum non-composite positive moment section, the maximum non-composite negative moment section, and the maximum composite positive moment section for the critical south exterior girder. Only the calculations for the maximum composite positive moment section will be shown. The remaining results are presented in Table 6.7.

As discussed in Frederick (1998), the critical loading vehicle for this bridge was the H20. Thus, testing run (R_289-6-8-33) with the test truck weight at 29.93 tons is used for this example. The values used for the posting calculations below can be found in Table 6.4.

6.6.1 Analytical Posting

Frederick (1998) provides a complete discussion concerning the analytical posting (using past MoDOT inputs) of Bridge R-289. The posting for Bridge R-289 is calculated using Equation 6.3 as follows:

$$Analytical\_ASR\_Posting = \frac{(0.68*(36ksi)-15.24ksi)}{1.23*\left(\frac{\left(525ft-kips/2\right)*12}{343.0in^3}\right)*1.09}*20tons = 15.0tons$$

6.6.2 Test Plan I – Bridge R-289

The layout for Test Plan I for Bridge R-289 can be seen in Figure 6.1. From this, the bottom flange gage for the critical cross section was monitored and the maximum stress applied to this gage during the critical run was found to be:

$$\sigma_0 = 8662 \text{ psi}$$

The experimental impact factor was determined from several runs with a different loading vehicle. The experimental impact factor calculated by Imhoff (1998) for the bridge will be used. It is equal to:

$$I_E = 1.25$$

The experimental moment is calculated with the actual dimensions from Table 6.4 and Equation 6.8 as follows:

$$M_T^{ADIM} = \frac{(8662\,psi) * (365in^3)}{12000} = 263.5\,ft - kips$$

Using the experimentally measured dead load stress, the experimental posting is calculated from Equation 6.10 as follows:

$$ExpASPost = \frac{0.68 * (36ksi) - 13.77ksi}{1.25 * \left(\frac{263.5kip - ft * 12}{365in^3}\right) * \left(\frac{529.1kip - ft}{736kip - ft}\right)} * 20tons = 1.376 * 20 = 27.51tons$$

The denominator of the above calculation contains a ratio of the maximum moment at 105 ft for the H20 truck versus the 29.93 ton load testing vehicle. As discussed in Frederick (1998), this ratio is used to adjust the response from the 29.93 ton truck into equivalent H20 response. From this, the following adjustment factors listed in Equation 6.11 are calculated below:

(1) $$Dead\_Load\_Stress\_Adjustment = \frac{0.68 * 36ksi - 13.77ksi}{0.68 * 36ksi - 15.24ksi} = 1.159$$

(2) $$Impact\_Adjustment = \frac{1.23}{1.25} = 0.984$$

(3) $$Section\_Modulus\_Adjustment = \frac{365in^3}{343in^3} = 1.064$$

(4) $$Comprehensive\_Factor = \frac{\left(27.51tons/15tons\right)}{(0.984*1.159*1.064)} = 1.511$$

Thus, with this testing plan for R-289, it can be seen that the experimental impact actually lowers the load rating by the factor listed above because the experimental value is higher than the analytical. The experimental dead load stress and the actual dimension analytical section modulus factors act to enhance the posting. The origin of the remainding enhancement cannot be determined with the information from a single strain gage and, thus, is lumped into the comprehensive factor. This factor contributes 50% additional enhancement to the capacity for this testing plan. If lumping this enhancement is not desireable, further testing would be suggested.

6.6.3 Test Plan II – Bridge R-289

Test Plan II provides for further enhancement of the posting for R-289 by allowing the calculation of the experimental total moment and the experimental section modulus. The gage placement for Bridge R-289 can be seen in Figure 6.2. Table 6.5 lists the values of the maximum stresses for this gage placement scheme. Solving matrix Equation 6.12 for the slope and the intercept yields:

Slope = -0.0032

Intercept = 28.59 in

Thus, Equation 6.16 can be written as:

$$\sigma = -312.5 * d + 8934.4$$

The experimental total moment can be calculated with the use of Equations 6.17 through 6.22 as shown below.

$$\sigma_0 = 8934.4\,psi$$

$$\sigma_{CG} = \sigma_{13.37"} = 4755.9\,psi$$

$$M_L = \frac{(8934.4\,psi - 4755.9\,psi)}{12\,{}^{in}/_{ft} * 1000\,{}^{lbs}/_{kip}} * 220in^3 = 76.61\,ft - kips$$

$$M_U = \frac{(3.6ksi) * (1107in^4)}{29ksi * (2941in^4)} * M_L = 3.58\,ft - kips$$

$$Na = \frac{(4755.9\,psi * 25.97in^2)}{12\,{}^{in}/_{ft} * 1000\,{}^{lbs}/_{kip}} * \left(13.37in + 3.36in + \left(\frac{6in}{2}\right)\right) = 203.1\,ft - kips$$

$$M_T^{Axial} = 76.61\,ft - kips + 3.58\,ft - kips + 203.10\,ft - kips = 283.29\,ft - kips$$

Finally, the experimental section modulus can be calculated by using the equations listed in Test Plan II as follows:

$$I_{Exp} = -(283.29\,ft - kips) * (-0.0032\,{}^{in}/_{psi}) * 12\,{}^{in}/_{ft} * 1000\,{}^{lbs}/_{kip} = 10{,}878.3in^4$$

$$S_E = \frac{10{,}878.3in^4}{28.59in} = 380.5in^3$$

With this information, the load posting can be calculated as in Equation 6.25:

$$ExpASPost = \left[\frac{0.68 * 36ksi - 13.77ksi}{1.25 * \left(\frac{283.29\,ft - kips * 12\,{}^{in}/_{ft}}{380.5in^3}\right) * \left(\frac{529.1\,ft - kips}{736\,ft - kips}\right)}\right] * 20tons = 1.334 * 20tons = 26.68tons$$

The factors contribution to this posting are:

(1) $Dead\_Load\_Stress\_Adjustment = 1.159$

(2) $Impact\_Adjustment = 0.984$

(3) $Section\_Modulus\_Adjustment = 1.064$

(4) $Additional\_Composite\_Adjustment = \frac{380.5in^3}{365in^3} = 1.042$

(5) $Comprehensive\_Factor = \frac{\left(26.68tons/15tons\right)}{(0.984*1.159*1.064*1.042)} = 1.407$

This plan used three strain gages to develop the load posting whereas Test Plan I only utilized one gage. Thus, more information can be determined from this plan.

6.6.4 Test Plan III – Bridge R-289

The layout for Bridge R-289 for Test Plan III can be seen in Figure 6.5. This layout will help to determine the lateral distribution factor for the section in question. Table 6.6 gives the bottom flange stresses and the corresponding section modulus for each girder at the critical longitudinal location. The lateral distribution is:

$$DF_E = \frac{2*(8662psi*343in^3)}{(8662psi+933psi)*343in^3+(6296+2951)*389in^3} = 0.863$$

Regardless of this calculation, the posting is still equal to the posting of Test Plan I. However, the factors that effect the load rating of the bridge can be more carefully defined with this testing plan. The factors that can be determined are:

(1) $Dead\_Load\_Stress\_Adjustment = 1.159$

(2) $Impact\_Adjustment = 0.984$

(3) $Distribution\_Factor\_Adjustment = \frac{1.09}{0.863} = 1.263$

(4) $Section\_Modulus\_Adjustment = 1.064$

$$(5)\ Comprehensive\_Factor = \frac{\left(27.51 tons / 15 tons\right)}{(0.984 * 1.159 * 1.064 * 1.263)} = 1.197$$

As can be seen above, the lateral distribution factor contributes to about 27% of the enhancement of the posting over the analytical value. It can also be seen that the comprehensive factor drops to about 20% compared to about 40% for Test Plan II. Thus, for Bridge R-289, it appears that the lateral distribution factor plays a major role in the increased experimental posting capacity. However, there is still about 20% of the extra capacity that cannot be separately quantified with this plan.

6.6.5 Test Plan IV – Bridge R-289

As discussed earlier, Test Plan IV is simply a conglomeration of the previous three plans. This is accomplished to more accurately determine the factors that effect the load rating. Note that the posting will still be the same as obtained in Test Plan II and shown below:

$$ExpASPost = \left[\frac{0.68 * 36 ksi - 13.77 ksi}{1.25 * \left(\frac{283.29 ft - kips * 12 in/ft}{380.5 in^3}\right) * \left(\frac{529.1 ft - kips}{736 ft - kips}\right)}\right] * 20 tons = 1.334 * 20 tons = 26.68 tons$$

The factors contribution to this posting are:

(1) $Dead\_Load\_Stress\_Adjustment = 1.159$

(2) $Impact\_Adjustment = 0.984$

(3) $Distribution\_Factor\_Adjustment = 1.263$

(4) $Section\_Modulus\_Adjustment = 1.064$

(5) $Additional\_Composite\_Adjustment = \frac{380.5 in^3}{365 in^3} = 1.042$

$$(6)\ Comprehensive\_Factor = \frac{\left(26.68 tons / 15 tons\right)}{(0.984 * 1.159 * 1.064 * 1.042 * 1.263)} = 1.114$$

This plan works to effectively determine the enhancement factors for the bridge and only leaves about 11% of the enhancement grouped into the comprehensive factor.

6.6.6 Test Plan V – Bridge R-289

Testing plan V can further build on testing plan IV by removing the bearing restraint factors in the posting equation. The testing plan for Bridge R-289 can be seen in Figure 6.7. The bearing forces need to be calculated for three locations. The forces that need to be calculated and the sign convention are illustrated in Figure 6.12. The following bearing stresses were taken from the field test data for the bearing force calculations:

$$\sigma^{0ft} = -13.6 psi$$

$$\sigma^{59.5ft} = -3223.9 psi$$

$$\sigma^{60.5ft} = -5054.9 psi$$

$$\sigma^{149.5ft} = -6635.5 psi$$

$$\sigma^{150.5ft} = -4142.0 psi$$

The bearing force for the abutment bearing can be calculated using Equation 6.32 as follows:

$$BearingForce^{0ft} = \frac{-(-13.6 psi)}{1000 lbs/kip} * (0.64 in * 9.96 in) = 0.087 kips$$

The remaining bearing forces over the piers can be calculated using Equation 6.33 as follows:

$$BearingForce^{60ft} = \frac{(-3223.9 psi - (-5054.95 psi))}{2 * 1000 lbs/kip} * (0.64 in * 9.96 in + \frac{5}{8} in * 12 in) = 12.70 kips$$

$$BearingForce^{150ft} = \frac{(-6635.5 psi - (-4142.0 psi))}{2 * 1000 lbs/kip} * (0.64 in * 9.96 in + \frac{5}{8} in * 12 in) = -17.30 kips$$

Summing the axial forces at 105.5 feet, the axial force acting at the critical section is:

$$\sigma_{axial} = -\frac{12.70kips - 0.087kips}{\left(25.97in^2 + \left(\frac{61.5in * 6in}{8}\right)\right)} = -177.5psi$$

Taking the stress equation found in Plan II from Equation 6.16 and removing the axial stress yields:

$$\sigma = 8934.4 - 312.5d - (-177.5psi) = 9111.9 - 312.5d$$

After axial has been removed, the procedure used to calculate total moment in Test Plan V is as follows:

$$\sigma_0^{Axial\_Removed} = 9111.9psi$$

$$\sigma_{CG}^{Axial\_Removed} = \sigma_{13.37"}^{Axial\_Removed} = 4933.8psi$$

$$M_L^{Axial\_Removed} = \frac{(9111.9psi - 4933.8psi)}{12^{in}/_{ft} * 1000^{lbs}/_{kip}} * 220in^3 = 76.6ft - kips$$

$$M_U^{Axial\_Removed} = \frac{(3.6ksi) * (1107in^4)}{(29ksi * (2941in^4)} * M_L^{Axial\_Removed} = 3.58ft - kips$$

$$Na^{Axial\_Removed} = \frac{(4933.8psi * 25.97in^2)}{12^{in}/_{ft} * 1000^{lbs}/_{kip}} * \left(13.37in + 3.36in + \left(\frac{6in}{2}\right)\right) = 210.67ft - kips$$

$$M_T^{Axial\_Removed} = 76.6ft - kips + 3.58ft - kips + 210.67ft - kips = 290.85ft - kips$$

The effects of the bearing restraint moment need to be removed from the experimental data. The bearing restraint moments at each pier are:

$$M_{BR}^{60} = \frac{12.7kips * (24.38in)}{12^{in}/_{ft}} = 25.8ft - kips$$

$$M_{BR}^{150} = \frac{-17.3kips * (20.76in)}{12^{in}/_{ft}} = -29.93ft - kips$$

Assuming constant stiffness in all spans, the moment distribution calculated from Equation 6.43 for Bridge R-289 is:

$$Distribution^{90ft-span} = \frac{\frac{1}{90ft}}{(\frac{1}{90ft}+\frac{1}{60ft})} = 0.4$$

The bearing restraint moment at 105.5 feet can then be linearly interpolated between the bearing moments at 60 feet and 150 feet as follows:

$$M_{BR}^{105} = \frac{(-29.93ft-kips)*0.4+(-25.8ft-kips)*0.4}{2} = -11.15ft-kips$$

Thus, removing the bearing moment from the total moment with the axial removed yields the following elastic moment:

$$M_E^{Critical\_Section} = M_T^{Axial\_Removed} - M_{BR}^{105} = 301.85ft-kips$$

The Test Plan V posting can then be obtained from Equation 6.45 as shown:

$$ExpASPost = \left[\frac{0.68*36ksi-13.77ksi}{1.25*\left(\frac{290.85ft-kips*12\,in/ft}{380.5in^3}\right)*\left(\frac{529.1ft-kips}{736ft-kips}\right)}\right]*20tons = 1.299*20tons = 26.0tons$$

The factors can then be calculated as follows:

(1) $Dead\_Load\_Stress\_Adjustment = 1.159$

(2) $Impact\_Adjustment = 0.984$

(3) $Distribution\_Factor\_Adjustment = 1.263$

(4) $Bearing\_Restraint\_Adjustment = \frac{301.85}{290.85} = 1.038$

(5) $Section\_Modulus\_Adjustment = 1.064$

$$(6)\ Additional\_Composite\_Adjustment = \frac{380.5in^3}{365in^3} = 1.042$$

$$(7)\ Comprehensive\_Factor = \frac{\left(26.0tons/15tons\right)}{(0.984*1.159*1.064*1.042*1.263*1.038)} = 1.046$$

This will be the best posting obtained in field testing. However, this testing plan still has about 5% that is not separated in specific factors. Test Plan VI can provide the same rating with all of the factors separated and quantified by the calculations.

6.6.7 Test Plan VI – Bridge R-289

The final testing plan is a comprehensive plan that will fully describe the behavior of the bridge rating procedure. This testing plan for Bridge R-289 can be seen in Figure 6.10. The gages across the depth of the section, to measure the negative moment, would theoretically be located directly over the piers. However, due to the interference with the bearings and diaphragms, these gages were placed at a distance of three feet from the centerline of the bearing.

The first step is to calculate the total moments at all three cross sections that are heavily gaged in Figure 6.10. Note that the 105.5 feet location has already been calculated for in Test Plan V. The results for the other sections are as follows:

For the 63 ft location:

$$\sigma_{axial} = -\frac{12.70kips - 0.087kips}{\left(41.12in^2 + \left(\frac{61.5in*6in}{8}\right)\right)} = -146.6psi$$

Taking the maximum stresses from the three gages at 63 feet, solving the matrix Equation 6.12, and removing the axial stress from the stress Equation 6.16 yields:

$$\sigma = -2981.4 + 116.3*d - (-146.6psi) = -2834.8 + 116.3*d$$

After axial has been removed, the procedure used to calculate total moment in Test Plan V is as follows:

$$\sigma_0^{Axial\_Removed} = -2834.8\,psi$$

$$\sigma_{CG}^{Axial\_Removed} = \sigma_{14.01"}^{Axial\_Removed} = -1206.6\,psi$$

$$M_L^{Axial\_Removed} = \frac{(-2834.8\,psi - (-1206.6\,psi))}{12\,{}^{in}/_{ft} * 1000\,{}^{lbs}/_{kip}} * 413in^3 = -56.0\,ft-kips$$

$$M_U^{Axial\_Removed} = \frac{(3.6ksi) * (1107in^4)}{(29ksi * (5781in^4)} * M_L^{Axial\_Removed} = -1.33\,ft-kips$$

$$Na^{Axial\_Removed} = \frac{(-1206.6\,psi * 41.1in^2)}{12\,{}^{in}/_{ft} * 1000\,{}^{lbs}/_{kip}} * \left(14.01in + 3.36in + \left(\frac{6in}{2}\right)\right) = -84.20\,ft-kips$$

$$M_T^{Axial\_Removed} = -56.0\,ft-kips - 1.33\,ft-kips - 84.2\,ft-kips = -141.5\,ft-kips$$

For the 147 ft location:

$$\sigma_{axial} = -\frac{12.70kips - 0.087kips}{\left(41.12in^2 + \left(\frac{61.5in * 6in}{8}\right)\right)} = -146.6\,psi$$

Taking the maximum stresses from the three gages at 147 feet, solving the matrix Equation 6.12, and removing the axial stress from the stress Equation 6.16 yields:

$$\sigma = -3390.6 + 156.25 * d - (-146.6\,psi) = -3244.0 + 156.25 * d$$

After axial has been removed, the procedure used to calculate total moment in plan V is used as follows:

$$\sigma_0^{Axial\_Removed} = -3244.0\,psi$$

$$\sigma_{CG}^{Axial\_Removed} = \sigma_{14.01"}^{Axial\_Removed} = -1056.5\,psi$$

$$M_L^{Axial\_Removed} = \frac{(-3244.0\,psi - (-1056.5\,psi))}{12\,{}^{in}/_{ft} * 1000\,{}^{lbs}/_{kip}} * 413in^3 = -75.29\,ft-kips$$

$$M_U^{Axial\_Removed} = \frac{(3.6ksi)*(1107in^4)}{(29ksi*(5781in^4)} * M_L^{Axial\_Removed} = -1.79ft - kips$$

$$Na^{Axial\_Removed} = \frac{(-1056.5psi*41.1in^2)}{12^{in}/_{ft}*1000^{lbs}/_{kip}} * \left(14.01in + 3.36in + \left(\frac{6in}{2}\right)\right) = -73.71ft - kips$$

$$M_T^{Axial\_Removed} = -75.29ft - kips - 1.79ft - kips - 73.71ft - kips = -150.79ft - kips$$

For the 105.5 ft location

$$M_T^{Axial\_Removed} = 76.6ft - kips + 3.58ft - kips + 210.67ft - kips = 290.85ft - kips$$

The total moments for both the 63 feet location and the 147 feet location need to be linearly extrapolated to the pier locations of 60 feet and 150 feet, respectively. This procedure yields the following:

$$M_T^{60} = \frac{290.85ft - kips + 141.5ft - kips}{42ft} * (45ft) - 290.85ft - kips = 172.4ft - kips$$

$$M_T^{150} = \frac{290.85ft - kips + 150.79ft - kips}{42ft} * (45ft) - 290.85ft - kips = 182.3ft - kips$$

Then, the bearing restraint moments at each pier need to be calculated as in the following:

$$M_{BR}^{60} = \frac{12.7kips*(24.38in)}{12^{in}/_{ft}} = 25.8ft - kips$$

$$M_{BR}^{150} = \frac{-17.3kips*(20.76in)}{12^{in}/_{ft}} = -29.93ft - kips$$

The elastic moments at 60 feet, 105.5 feet, and 150 feet can now be calculated as follows:

$$M_E^{60} = 172.4ft - kips + 0.4*25.8ft - kips = 182.72ft - kips$$

$$M_E^{105} = 290.85ft - kips - (-11.15ft - kips) = 301.85ft - kips$$

$$M_E^{150} = 182.3ft - kips + 0.4*29.93ft - kips = 194.27ft - kips$$

The elastic moments above can be plotted against the 29.93 ton truck global moment as shown in Figure 6.11. From this, the statical moments can be determined as follows:

$$STAT_A = 736\,ft-kips - 0.5*-453.9\,ft-kips - 0.5*-449.1\,ft-kips = 1187.5\,ft-kips$$

$$STAT_E = 301.85\,ft-kips - 0.5*-182.72\,ft-kips - 0.5*-194.27\,ft-kips = 490.345\,ft-kips$$

Finally, the longitudinal adjustment moment can be calculated as follows:

$$M_{LE}^{105} = \frac{490.345\,ft-kips}{1187.5\,ft-kips} * 736\,ft-kips = 304.4\,ft-kips$$

The posting equation is identical to Test Plan V and can be seen below:

$$ExpASPost = \left[\frac{0.68*36ksi - 13.77ksi}{1.25*\left(\frac{290.85\,ft-kips*12\,{}^{in}/_{ft}}{380.5in^3}\right)*\left(\frac{529.1\,ft-kips}{736\,ft-kips}\right)}\right]*20tons = 1.305*20tons = 26.0tons$$

From the previous calculations, all of the enhancement factors can be calculated. They are listed below:

(1) $Dead\_Load\_Stress\_Adjustment = 1.159$

(2) $Impact\_Adjustment = 0.984$

(3) $Distribution\_Factor\_Adjustment = 1.263$

(4) $Bearing\_Restraint\_Adjustment = \frac{301.85}{290.85} = 1.038$

(5) $Longitudinal\_Adjustment = \frac{304.04\,ft-kips}{301.85\,ft-kips} = 1.007$

(6) $Curb\,/\,Railing\_Adjustment = \frac{525\,ft-kips/2}{\frac{304.4\,ft-kips}{0.863}*\frac{529.1\,ft-kips}{736\,ft-kips}} = 1.038$

(7) $Section\_Modulus\_Adjustment = 1.064$

$$(8)\ Additional\_Composite\_Adjustment = \frac{380.5in^3}{365in^3} = 1.042$$

As can be seen above, this testing plan produces the most reliable rating available with the total amount of contribution from each factor determined. This process was also repeated for the 24 ft location and the 60 ft location. The results of this can be seen in Table 6.7.

6.7 SUMMARY OF RESULTS

Though the actual testing of Bridge R-289 included 95 strain gages placed in strategic locations across the bridge, the bridge could be accurately posted with only 17 gages, as was done for plan VI. Note that plans I, II, and II in Table 6.7 leave large comprehensive factors (shaded). Thus, these plans are not ideal for when the origin of the contributions is important. However, they could be used to quickly determine the condition of a structure, get an estimate of the behavior, or when the lumped sum of the contributors is adequate. The last three gage plans are more ideal for accurate testing where the factors that effect the load rating can be determined. Frederick (1998) presents a thorough discussion of the factors and their behavior for different types of sections and scenarios.

6.7.1 General Observations

Table 6.8 presents the analytical and experimental posting capacities for three sections along the length (24 ft, 63 ft, and 105.5 ft) for the interior and exterior girders. The contributing factors are also shown for the results of the Test Plan VI data. It is worthwhile to examine this table, for there are differences that are evident for different type sections. The individual contributor quantities are shown along with the product of all contributions near the bottom. The last row in the table illustrates the additional capacity found through field testing after removing the effects of differences in the dead load stress calculations.

This represents the true additional capacity that one can obtain from careful inspection (measuring dimensions) and field testing. The Dead Load Stress factor has little to do with field testing and is only a clerical adjustment.

6.7.2 Impact Factor Ratio

The impact factor ratio is relatively ineffective in altering the capacity. Measured values were near identical to design values. However, if the impact factor is to be used for increasing the capacity, special care needs to be used to ensure the load-speed-truck configurations represent expectations on the structure. Measuring for dynamic impact is a tricky task and, most likely, the cost of doing so will not be worth the benefit. Therefore, usually one would use the design impact value and the ratio in the field testing equation would be 1.0.

6.7.3 Measured Section Dimensions

The measured section dimensions are slightly larger than the nominal design values (roughly 4%). This is expected since manufacturers tend to be on the heavy side of tolerances to assure acceptance. This benefit can be obtained simply by field measurements and field testing is not necessary.

6.7.4 Unaccounted System Stiffness

The unaccounted system stiffness represents the contributions from the curbs, railings, and possibly extra concrete material. It varies between an additional capacity of 12% to 28% over that of the analytical rating.

6.7.5 Lateral Load Distribution

The lateral distribution ratio is considered conservative for steel girder bridges. The results confirm this belief. The increase is due to a better sharing of the load between girders than the AASHTO equations predict. This contributor has great potential for increasing the safe load carrying capacity of existing bridges.

6.7.6 Bearing Restraint Effects

The bearing restraint effects are relatively small. The maximum effect is an 8% increase for the exterior girder at 63 ft. The average increase is only 4%. After testing more bridges, if this trend continues, maybe the owner can set a fixed reduction in experimental capacity to account for the bearing restraint effects and not spend the time and money performing higher level tests.

6.7.7 Longitudinal Distribution Factor

The longitudinal distribution effects vary depending on the section location. It is clear that the results show that the analysis procedures do a fairly good job at estimating the expected longitudinal distribution in the positive moment regions (ratio near 1.0). At the negative pier section, it seems the experimental response is less than that predicted by analysis procedures. This can be a result of using a prismatic analysis while the bridge is acting at least slightly nonprismatic.

6.7.8 Unintended or Additional Composite Action

The 24 ft section is a noncomposite positive moment section in the first span. The analytical ratings are 17 tons and 21 tons for the interior and exterior girders, respectively. The same experimental capacities are 35 tons and 48 tons after dividing the totals by the

Experimental Dead Load Stress factor. This represents a 105% and 128% increase over the analytical posting (bottom row). However, a large reason for this increase is that the section is behaving partially composite with the deck slab (30% increase due to Unintended Composite Action). If the bridge owner does not think this composite action is reliable, the capacity increase drops to 56% for the exterior and 75% for the interior girders. Having the ability to separate and quantify the unintended composite action is a great benefit of the procedures.

The 63 ft section is at the interior pier under negative bending. The section is designed noncomposite, yet is acting partially composite according to the experimental results (39% and 29% increase in capacity at the exterior and interior girders). The total increases for these girders are 142% and 164% after removing the Dead Load Stress effects. This increase decreases to 74% and 105% after removing the benefits of the unintended composite action.

The 105.5ft section was designed composite. Therefore, the Unintended Composite Action factor is near 1.0.

6.8 SUPERPOSITION OF TESTS FOR MULTI-LANE PRESENCE

Bridge R-289 is posted for one-lane of traffic, yet it has a 20 ft wide clear width. Thus, according to policy, it may have two traffic lanes. To consider removing the one-lane restriction, superposition of diagnostic tests can be used. Figure 6.13 illustrates two truck positions used here to demonstrate the experimental rating for two lanes.

The experimental load rating will be calculated for the 105.5 ft exterior girder to demonstrate the superposition. Test run R_289_6-8-33 is the data for the truck next to the

South curb. Test run R_289_6-8-36 is the data for the truck 4 ft north of centerline. This configuration allows a 2 ft distance between the truck tires.

The superposition of stresses for the 105.5 ft exterior girder position is shown in Table 6.9. They are simply the addition of the stresses for the two loading conditions. From Equation 6.12:

Slope = -0.0026

Intercept = 28.46 in

Thus, Equation 6.16 can be written as:

$$\sigma = -375 * d + 10673$$

The experimental total moment is calculated with the use of Equations 6.17 through 6.22 as shown below.

$$\sigma_0 = 10673 psi$$

$$\sigma_{CG} = \sigma_{13.37"} = 5659 psi$$

$$M_L = \frac{(10673 psi - 5659 psi)}{12 \,{}^{in}/_{ft} * 1000 \,{}^{lbs}/_{kip}} * 220 in^3 = 91.9 ft - kips$$

$$M_U = \frac{(3.6 ksi) * (1107 in^4)}{29 ksi * (2941 in^4)} * M_L = 4.3 ft - kips$$

$$Na = \frac{(5659 psi * 25.97 in^2)}{12 \,{}^{in}/_{ft} * 1000 \,{}^{lbs}/_{kip}} * \left(13.37 in + 3.36 in + \left(\frac{6 in}{2} \right) \right) = 241.6 ft - kips$$

$$M_T^{Axial} = 91.9 ft - kips + 4.3 ft - kips + 241.6 ft - kips = 337.8 ft - kips$$

The experimental section modulus is calculated by using the equations listed in Test Plan II as follows:

$$I_{Exp} = -(337.8ft - kips) * (-0.0026 {}^{in}/_{psi}) * 12 {}^{in}/_{ft} * 1000 {}^{lbs}/_{kip} = 10{,}946in^4$$

$$S_E = \frac{10{,}946in^4}{28.46in} = 384.6in^3$$

The experimental distribution factor is calculated as before, except the multiplier of 2 is replaced by 4 since there are 4 wheel lines in the experimental results. The superimposed stresses across the girders at 105.5 ft are shown in Table 6.10. The distribution factor is:

$$DF_E = \frac{4 * (10469psi * 343in^3)}{(10469psi + 7760psi) * 343in^3 + (10321 + 9011) * 389in^3} = 1.043$$

The bearing forces for the abutment bearing and piers can be calculated by superimposing the stresses at the bearing locations:

$$BearingForce^{0ft} = 0.61kips$$

The remaining bearing forces over the piers can be calculated using Equation 6.33 as follows:

$$BearingForce^{60ft} = 13.1kips$$

$$BearingForce^{150ft} = -14.6kips$$

Summing the axial forces at 105.5 feet, the axial force acting at the critical section is:

$$\sigma_{axial} = -\frac{13.1kips + 0.61kips}{\left(25.97in^2 + \left(\frac{61.5in * 6in}{8}\right)\right)} = -190psi$$

Taking the stress equation found in Plan II from Equation 6.16 and removing the axial stress yields:

$$\sigma = 10673 - 375d - (-190psi) = 10863 - 375d$$

After axial has been removed, the procedure used to calculate total moment in Test Plan V is as follows:

$$\sigma_0^{Axial\_Removed} = 10863 psi$$

$$\sigma_{CG}^{Axial\_Removed} = \sigma_{13.37"}^{Axial\_Removed} = 5849 psi$$

$$M_L^{Axial\_Removed} = \frac{(10863 psi - 5849 psi)}{12\,{}^{in}/_{ft} * 1000\,{}^{lbs}/_{kip}} * 220 in^3 = 91.9 ft - kips$$

$$M_U^{Axial\_Removed} = \frac{(3.6 ksi) * (1107 in^4)}{(29 ksi * (2941 in^4)} * M_L^{Axial\_Removed} = 4.3 ft - kips$$

$$Na^{Axial\_Removed} = \frac{(5849 psi * 25.97 in^2)}{12\,{}^{in}/_{ft} * 1000\,{}^{lbs}/_{kip}} * \left(13.37 in + 3.36 in + \left(\frac{6 in}{2}\right)\right) = 249.7 ft - kips$$

$$M_T^{Axial\_Removed} = 91.9 ft - kips + 4.3 ft - kips + 249.7 ft - kips = 346 ft - kips$$

The effects of the bearing restraint moment need to be removed from the experimental data. The bearing restraint moments at each pier are:

$$M_{BR}^{60} = \frac{13.1 kips * (24.38 in)}{12\,{}^{in}/_{ft}} = 26.6 ft - kips$$

$$M_{BR}^{150} = \frac{-14.6 kips * (20.76 in)}{12\,{}^{in}/_{ft}} = -25.2 ft - kips$$

Assuming constant stiffness in all spans, the moment distribution calculated from Equation 6.43 for Bridge R-289 is:

$$Distribution^{90 ft\_span} = \frac{\frac{1}{90 ft}}{(\frac{1}{90 ft} + \frac{1}{60 ft})} = 0.4$$

The bearing restraint moment at 105.5 feet can then be linearly interpolated between the bearing moments at 60 feet and 150 feet as follows:

$$M_{BR}^{105} = \frac{(-25.2 ft - kips) * 0.4 + (-26.6 ft - kips) * 0.4}{2} = -10.36 ft - kips$$

Thus, removing the bearing moment from the total moment with the axial removed yields the following elastic moment:

$$M_E^{Critical\_Section} = M_T^{Axial\_Removed} - M_{BR}^{105} = 357\,ft - kips$$

The Test Plan V posting can then be obtained from Equation 6.45 as shown:

$$ExpASPost = \left[\frac{0.68 * 36ksi - 13.77ksi}{1.25 * \left(\frac{337.9\,ft - kips * 12\,{}^{in}/_{ft}}{384.5in^3} \right) * \left(\frac{529.1\,ft - kips}{736\,ft - kips} \right)} \right] * 20tons = 1.13 * 20tons = 22.6tons$$

The factors can then be calculated as follows:

(1) $Dead\_Load\_Stress\_Adjustment = 1.159$

(2) $Impact\_Adjustment = 0.984$

(3) $Distribution\_Factor\_Adjustment = 1.046$

(4) $Bearing\_Restraint\_Adjustment = \frac{357}{346} = 1.032$

(5) $Section\_Modulus\_Adjustment = 1.064$

(6) $Additional\_Composite\_Adjustment = \frac{384.6in^3}{365in^3} = 1.054$

(7) $Comprehensive\_Factor = \frac{\left(22.6tons/15tons \right)}{(0.984 * 1.159 * 1.064 * 1.054 * 1.043 * 1.032)} = 1.094$

These factors were determined using Test Plan V. Assuming the same Longitudinal Distribution factor of 1.007, the remaining System factor can be determined. Table 6.11 presents the results of the two-lane superposition results.

6.9 EXPERIMENTAL POSTING DECISIONS

If Bridge R-289 is to remain a single-lane structure, a rational load posting would be the total experimental load post capacity after removing the effects of bearing restraint forces. From Table 6.8:

$$Field\_Test\_Posting = \frac{26tons}{1.038} = 25tons$$

If Bridge R-289 is to be opened to two lanes of traffic, the bearing restraint effects should be removed from the total experimental load post capacity. From Table 6.11:

$$Field\_Test\_Posting = \frac{22.6tons}{1.032} = 21.9tons$$

The field test procedures have documented and justified the removal of the restricted loading for a single lane structure. However, Missouri has an axle weight tolerance which results in posting single unit vehicles at 23 tons. Therefore, the two lane capacity, although raised significantly, does not quite get up to 23 tons.

This analysis was for the single unit (H20) vehicle. This bridge is also posted for combination vehicles. Thus, to complete the recommendations for a new posting level, these procedures would need to be evaluated against the combination vehicle truck.

Table 6.1 Contributing Factors for Testing Plans

Factor	Plan I	Plan II	Plan III	Plan IV	Plan V	Plan VI
Impact Factor	Yes	Yes	Yes	Yes	Yes	Yes
Experimental Dead Load	Yes	Yes	Yes	Yes	Yes	Yes
Actual Dimensions	Yes	Yes	Yes	Yes	Yes	Yes
Unintended or Additional Composite	No	Yes	No	Yes	Yes	Yes
Lateral Distribution	No	No	Yes	Yes	Yes	Yes
Bearing Restraint	No	No	No	No	Yes	Yes
Longitudinal Distribution	No	No	No	No	No	Yes
Unaccounted System Stiffness	No	No	No	No	No	Yes

Table 6.2 Cross-Section Stress versus Distance

Gage #	Distance from Bottom of Bottom Flange (in)	Stress (psi)
1	0	σ_1
2	d_2	σ_2
3	d_3	σ_3

Table 6.3 Bottom Flange Stresses versus Analytical Section Modulus

Girder	Analytical Section Modulus	Bottom Flange Stress
Critical	S_A^{ADIM}	$\sigma_0^{critical}$
$NonCritical_i$	S_i^{ADIM}	$\sigma_i^{noncritical}$
↓	↓	↓
$NonCritical_{(n-1)}$	$S_{(n-1)}^{ADIM}$	$\sigma_{(n-1)}^{noncritical}$

Table 6.4 Values for 105.5' Critical Cross Section

Property	South Exterior	South Interior	North Interior	North Exterior
S_A	343.0 in^3	389.0 in^3	389.0 in^3	343.0 in^3
S_A^{ADIM}	365.0 in^3	N/A	N/A	N/A
S_{steel}^{ADIM}	220.0 in^3	N/A	N/A	N/A
d_{steel}	26.74 in	N/A	N/A	N/A
I_{steel}^{ADIM}	2941 in^4	N/A	N/A	N/A
A_{steel}^{ADIM}	25.97 in^2	N/A	N/A	N/A
σ_{DA}	15.24 psi	N/A	N/A	N/A
σ_{DE}	13.77 psi	N/A	N/A	N/A
M_{H20}	529.1 ft-kips	N/A	N/A	N/A
M_{TRK}	736.0 ft-kips	N/A	N/A	N/A
Haunch	3.36 in	N/A	N/A	N/A
Slab	6.00 in	N/A	N/A	N/A

Table 6.5 Stress Values for Plan II

Gage #	Distance from Bottom of Bottom Flange (d)	Stress (σ)
1	0"	8662.0 psi
2	4.89"	7682.9 psi
3	13.39"	4650.5 psi

Table 6.6 Bottom Flange Stresses for Lateral Distribution Factor Calculation

Girder	Analytical Section Modulus	Bottom Flange Stress
South Exterior	343 in^3	8662 psi
South Interior	389 in^3	6296 psi
North Interior	389 in^3	2951 psi
North Exterior	343 in^3	993 psi

Table 6.7 Results of Test Plans on Bridge R-289

Location		Experimental Posting	Impact	Dead Load	Actual Dimensions	Additional Composite	Lateral Distribution	Bearing Restraint	Longitudinal Distribution	Curbs & Railings
Plan I	24'	42.96 tons	1.016	1.162	1.033			2.048		
	60'	102.10 tons	0.984	1.981	1.022			2.616		
	105.5'	27.51 tons	0.984	1.159	1.064			1.511		
Plan II	24'	42.56 tons	1.016	1.162	1.033	1.313		1.545		
	60'	100.74 tons	0.984	1.981	1.022	1.382		1.868		
	105.5'	26.68 tons	0.984	1.159	1.064	1.042		1.407		
Plan III	24'	42.96 tons	1.016	1.162	1.033		1.020		2.007	
	60'	102.10 tons	0.984	1.981	1.022		1.122		2.332	
	105.5'	27.51 tons	0.984	1.159	1.064		1.263		1.188	
Plan IV	24'	42.56 tons	1.016	1.162	1.033	1.313	1.020		1.515	
	60'	100.74 tons	0.984	1.981	1.022	1.382	1.122		1.665	
	105.5'	26.68 tons	0.984	1.159	1.064	1.042	1.263		1.106	
Plan V	24'	40.9 tons	1.016	1.162	1.033	1.313	1.020	1.054		1.381
	60'	91.4 tons	0.984	1.981	1.022	1.382	1.122	1.082		1.396
	105.5'	26.00 tons	0.984	1.159	1.064	1.042	1.263	1.038		1.046
Plan VI	24'	40.9 tons	1.016	1.162	1.033	1.313	1.020	1.054	1.059	1.302
	60'	91.4 tons	0.984	1.981	1.022	1.382	1.122	1.082	1.139	1.226
	105.5'	26.00 tons	0.984	1.159	1.064	1.042	1.263	1.038	1.007	1.039

Table 6.8 Results of Test Plan VI on Bridge R-289

Section	24 ft Exterior	24 ft Interior	63 ft Exterior	63 ft Interior	105.5 ft Exterior	105.5 ft Interior
Analytical Posting	17.2 tons	21.0 tons	19.1 tons	25.2 tons	15.0 tons	21.0 tons
Experimental Posting	40.9 tons	59.4 tons	91.4 tons	152 tons	26.0 tons	42.5 tons
Experimental Dead Load Stress	1.162	1.242	1.981	2.282	1.159	1.364
Impact Factor	1.016	1.016	1.000	1.000	0.984	0.984
Measured Section Dimensions	1.033	1.033	1.022	1.025	1.064	1.087
Unaccounted System Stiffness	1.120	1.280	1.224	1.098	1.045	1.204
Lateral Load Distribution	1.186	1.238	1.125	1.436	1.264	1.216
Bearing restraint Effects	1.054	1.009	1.082	1.022	1.038	1.012
Longitudinal Distribution	1.059	1.043	1.139	1.248	1.007	0.928
Unintended or Additional Composite Action	1.313	1.301	1.392	1.286	1.042	1.008
Product Totals	2.37	2.83	4.78	6.05	1.73	2.02
Product Totals Without Dead Load Adjustment	2.05	2.28	2.42	2.64	1.50	1.48

Table 6.9 Superposition of Multi-lane Stress Values

Gage #	Distance from Bottom of Bottom Flange (d)	Stress (σ)
1	0"	10469 psi
2	4.89"	9301 psi
3	13.39"	5535 psi

Table 6.10 Multi-Lane Superimposed Bottom Flange Stresses for Lateral Distribution Factor Calculation

Girder	Analytical Section Modulus	Bottom Flange Stress
South Exterior	343 in^3	10469 psi
South Interior	389 in^3	10321 psi
North Interior	389 in^3	9011 psi
North Exterior	343 in^3	7760 psi

Table 6.11 Results of Multi-Lane Rating on Bridge R-289

Section	105.5 ft Exterior
Analytical Posting	15.0 tons
Experimental Posting	22.6 tons
Experimental Dead Load Stress	1.159
Impact Factor	0.984
Measured Section Dimensions	1.064
Unaccounted System Stiffness	1.086
Lateral Load Distribution	1.046
Bearing restraint Effects	1.032
Longitudinal Distribution	1.007
Unintended or Additional Composite Action	1.054
Product Totals	1.51
Product Totals Without Dead Load Adjustment	1.30

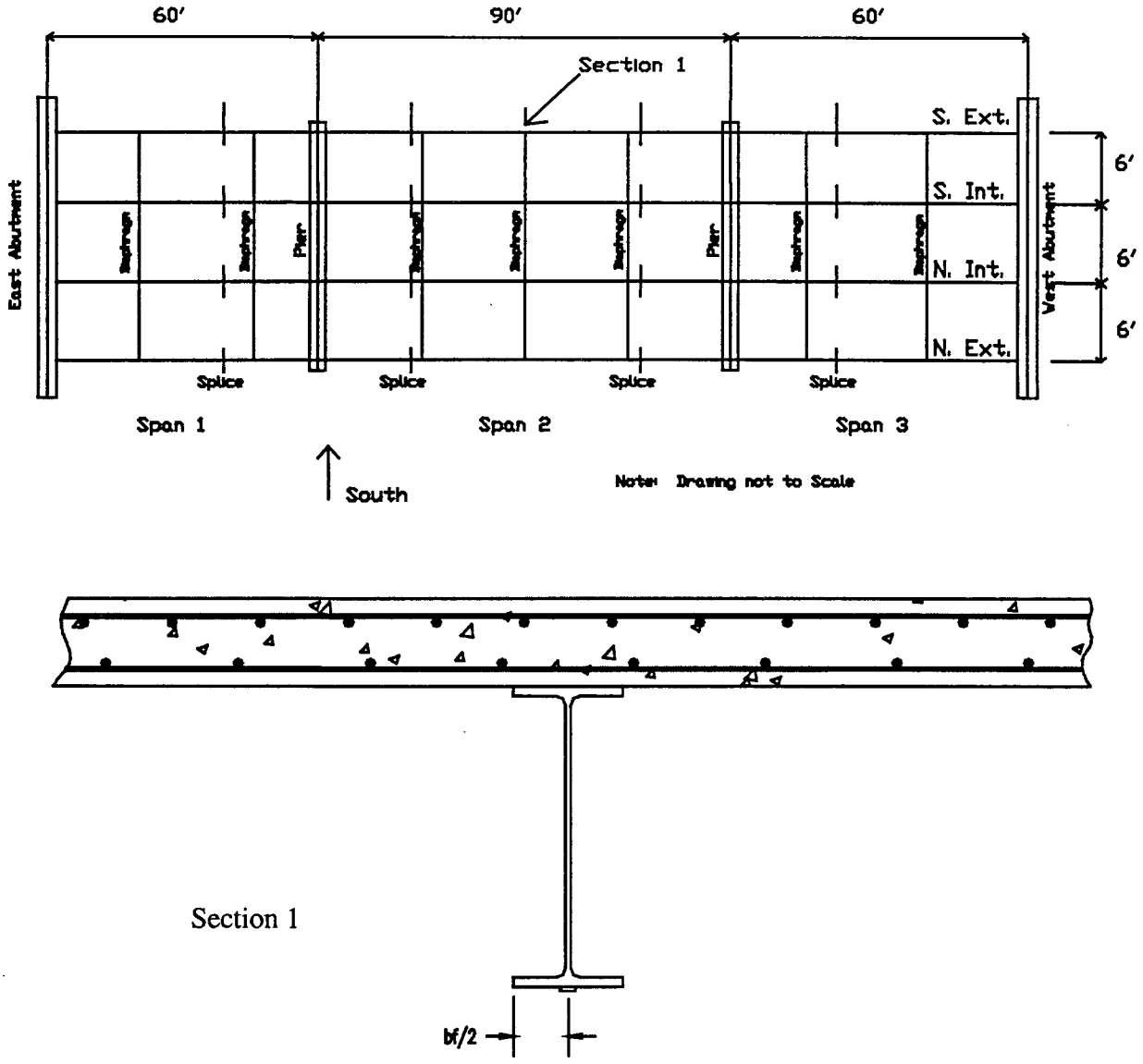

Figure 6.1 Testing Plan I for R-298

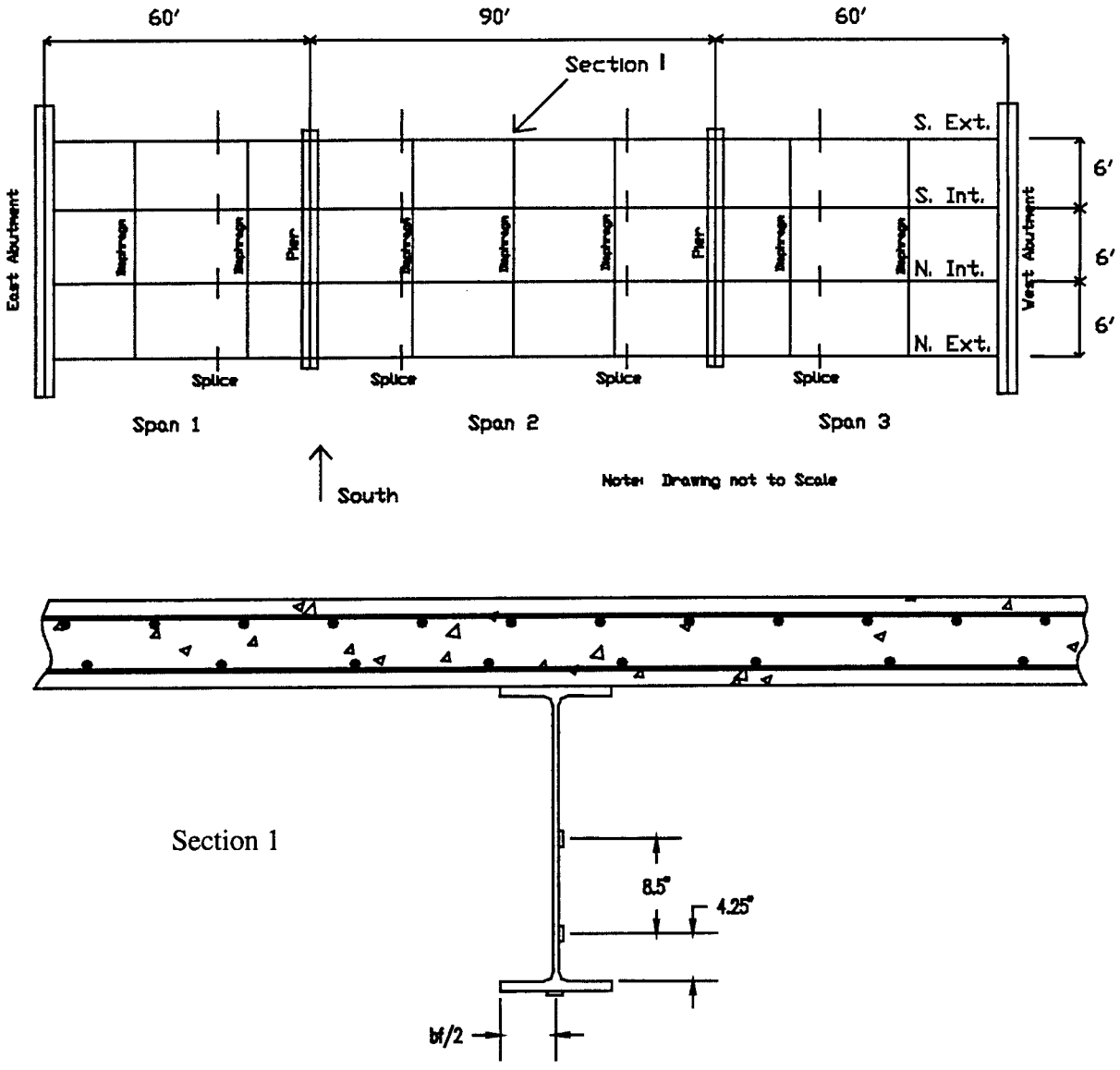

Figure 6.2 Testing Plan II for Bridge R-289

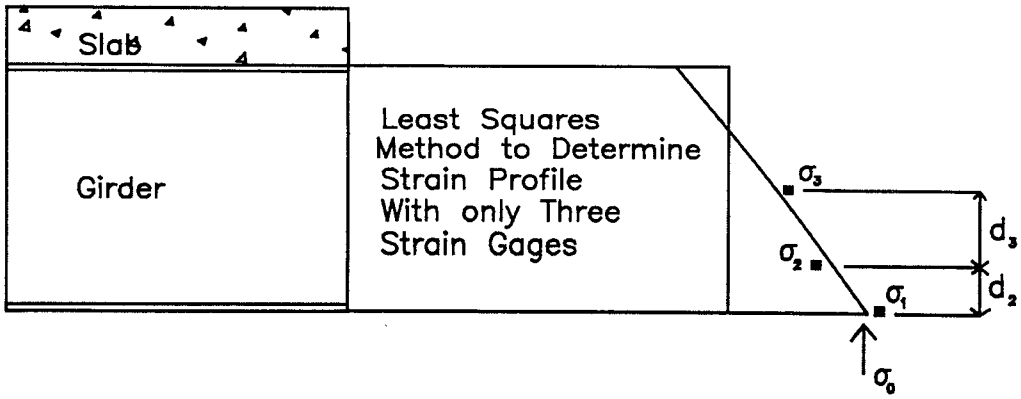

Figure 6.3 Three Gage Profile with Least Squares Method

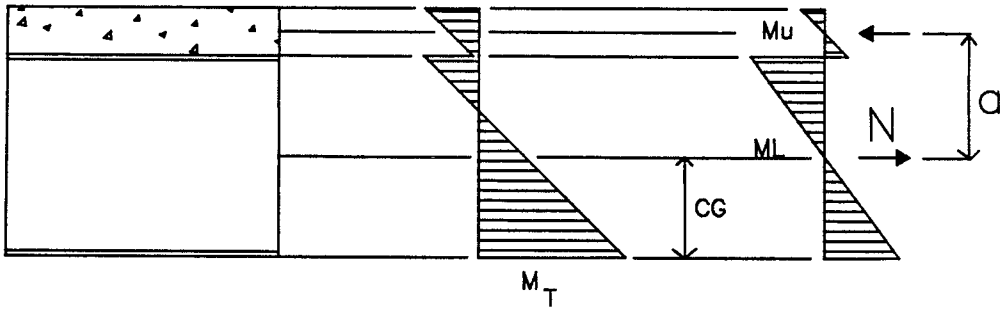

Figure 6.4 Total Moment (Courtesy of Imhoff (1998))

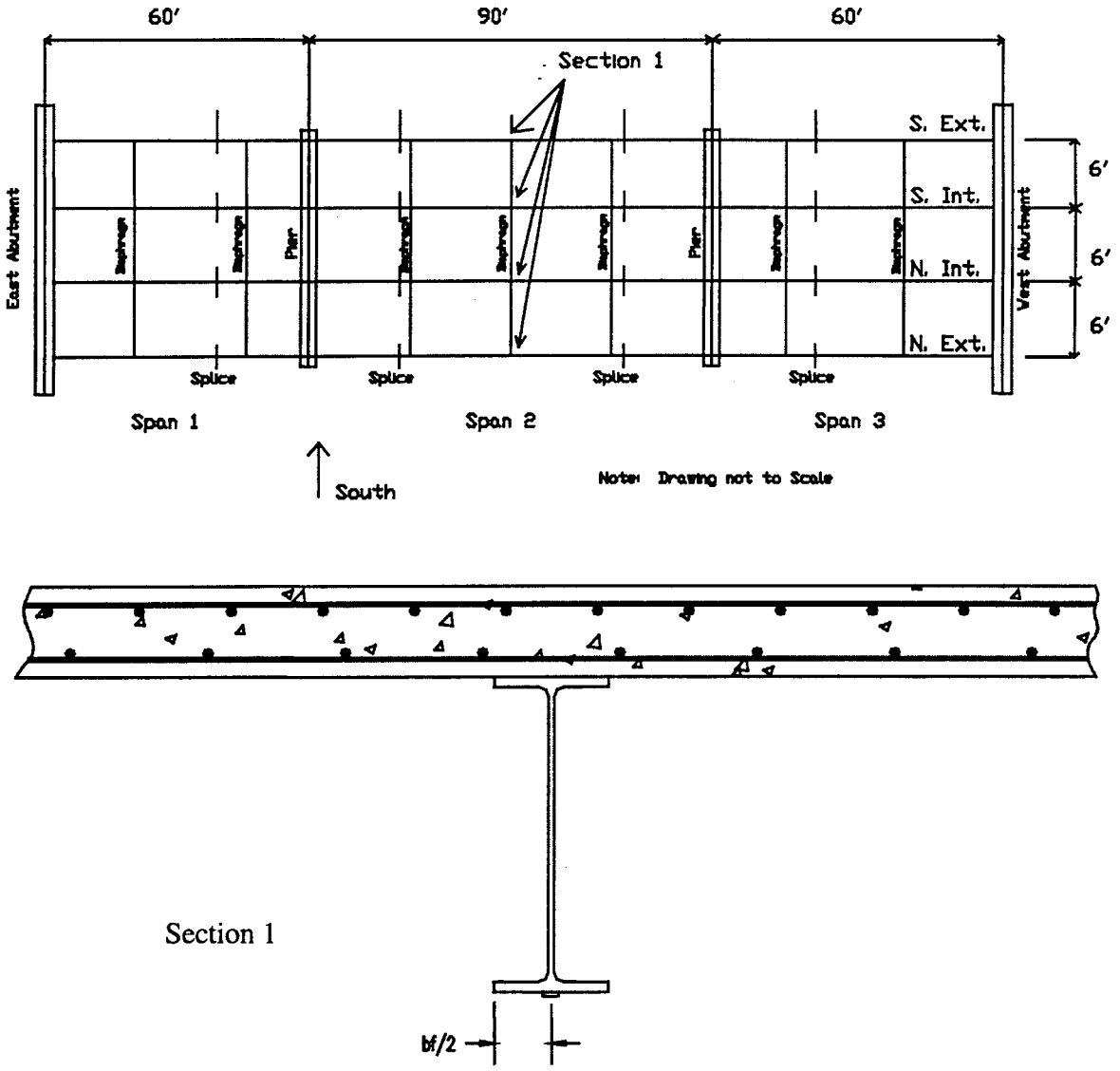

Figure 6.5 Testing Plan III for Bridge R-289

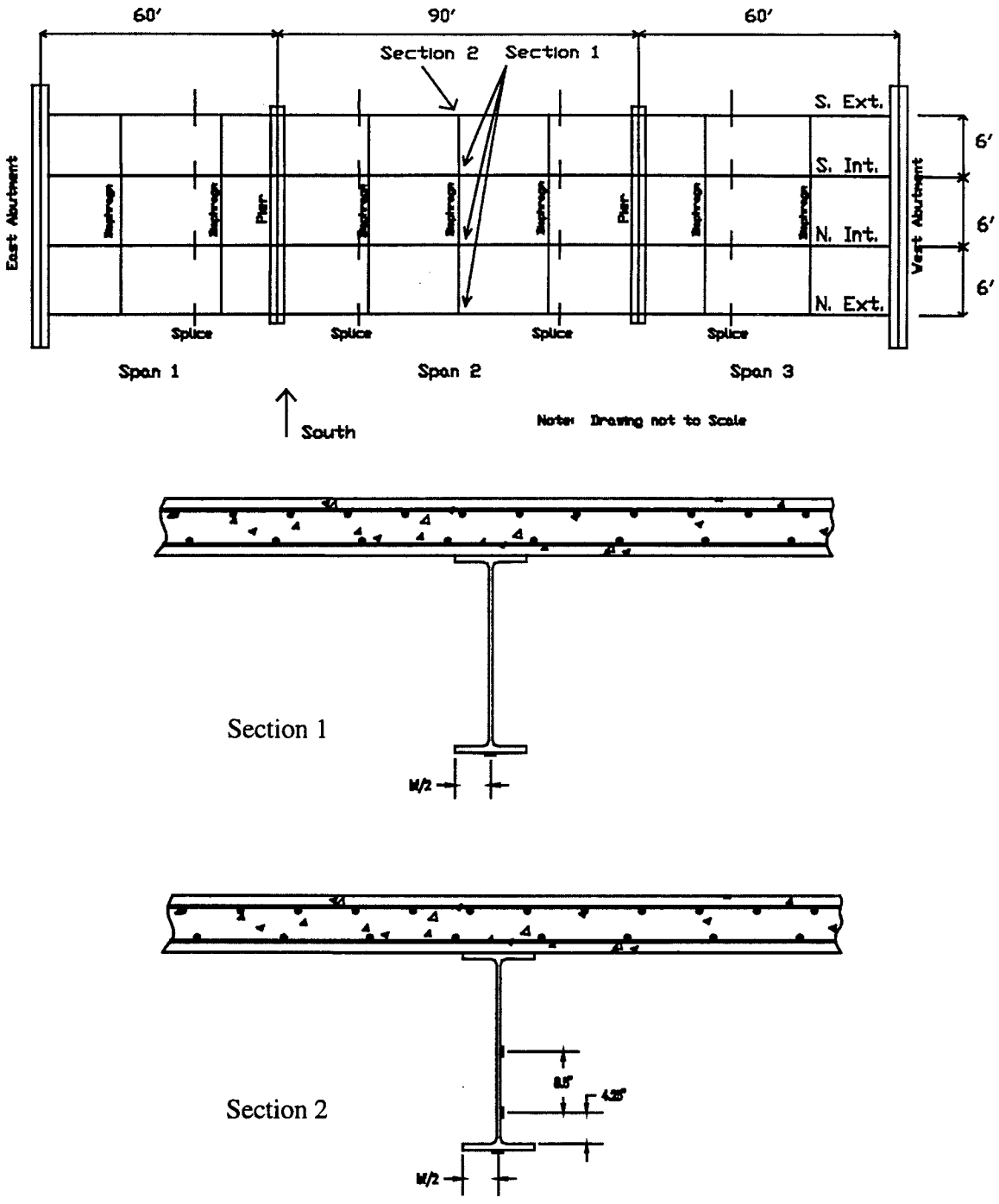

Figure 6.6 Testing Plan IV for Bridge R-289

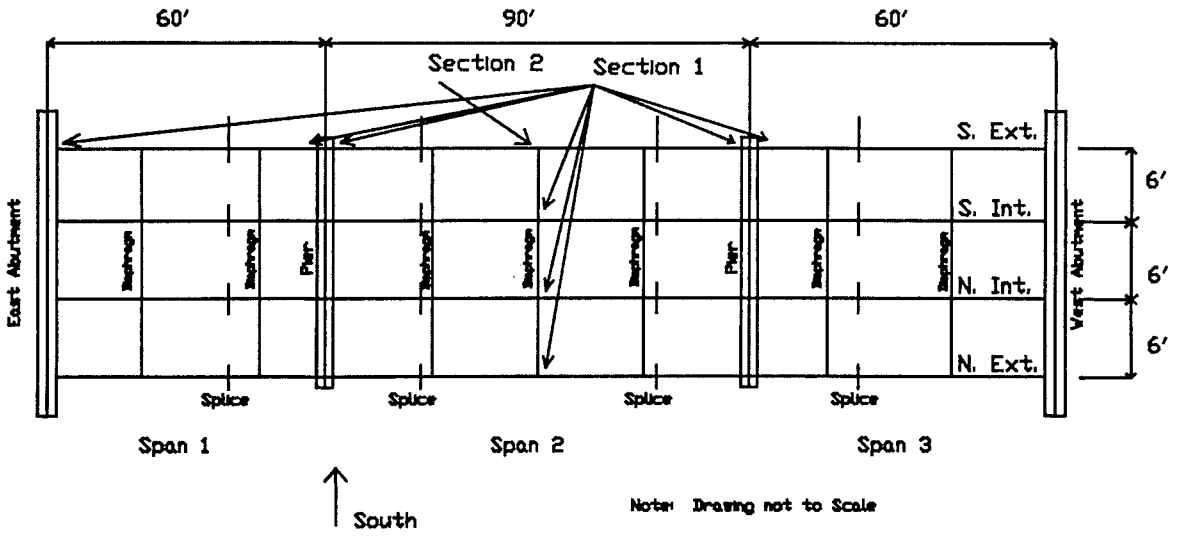

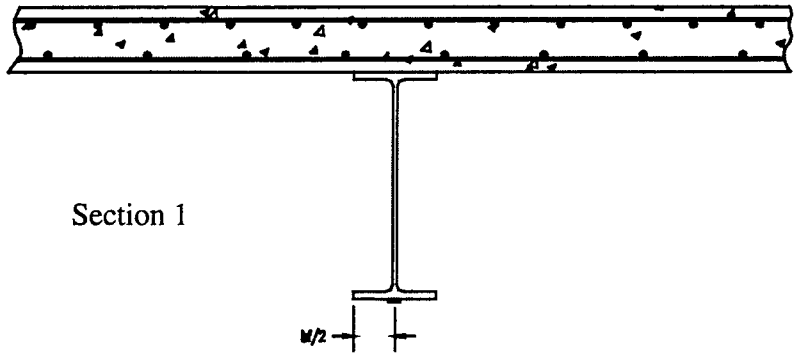

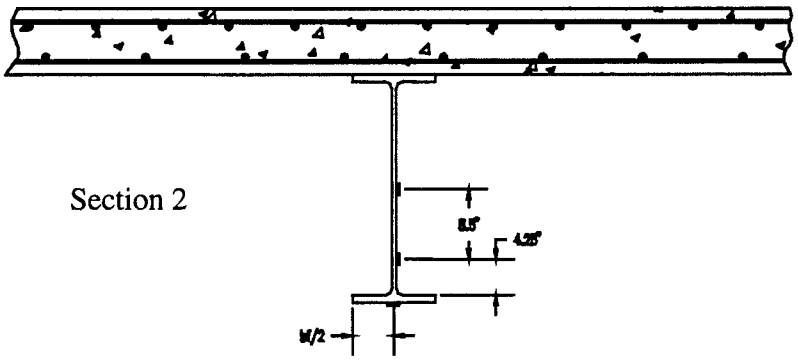

Figure 6.7 Testing Plan V for Bridge R-289

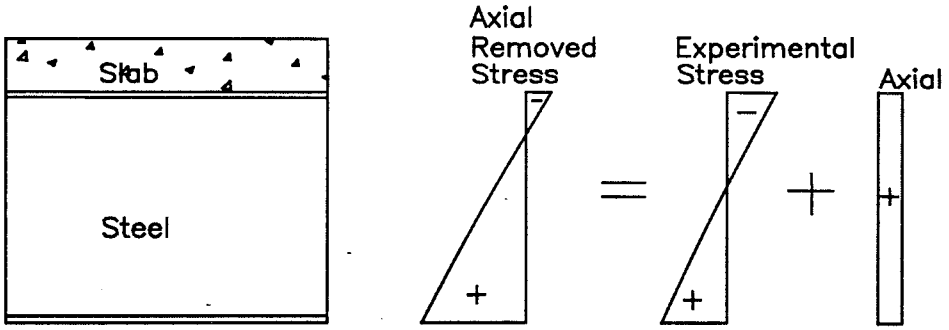

Figure 6.8 Removal of Axial Stress

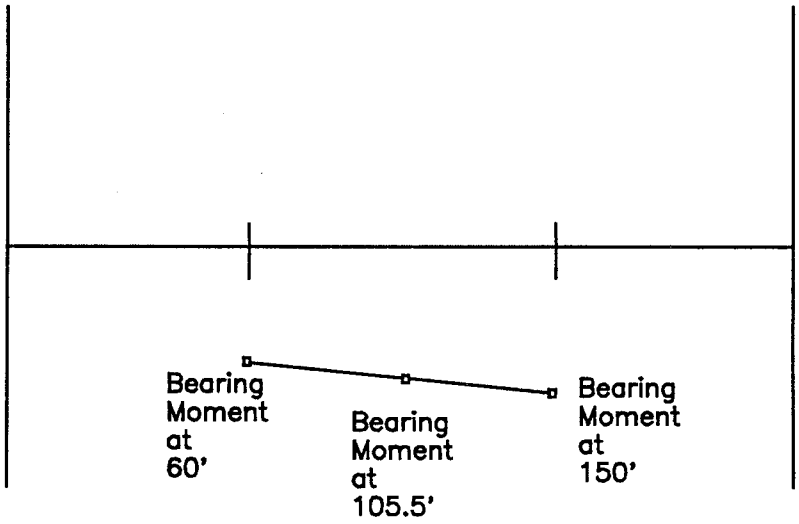

Figure 6.9 Linear Interpolation of Bearing Moment

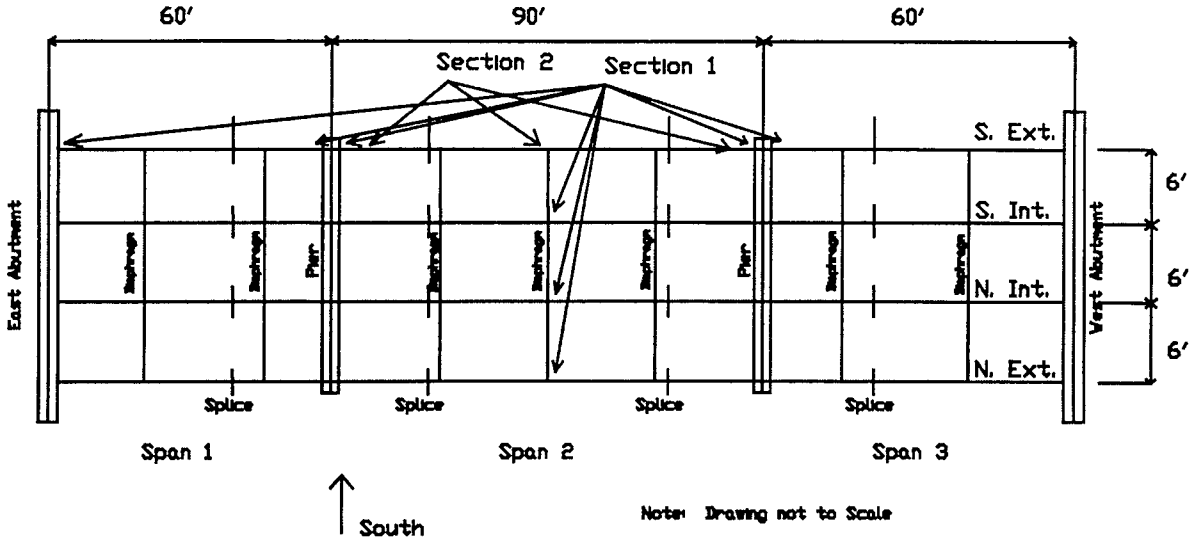

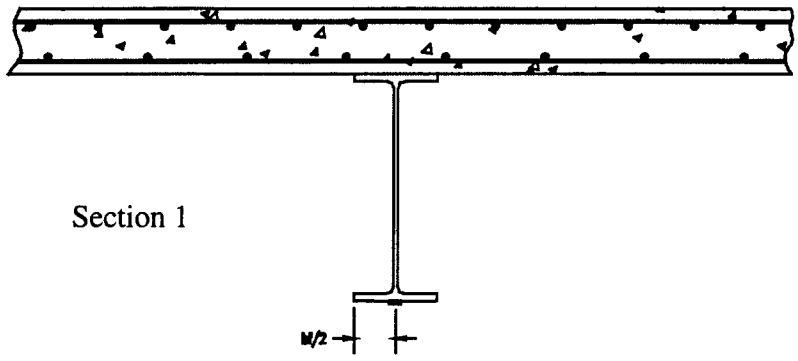

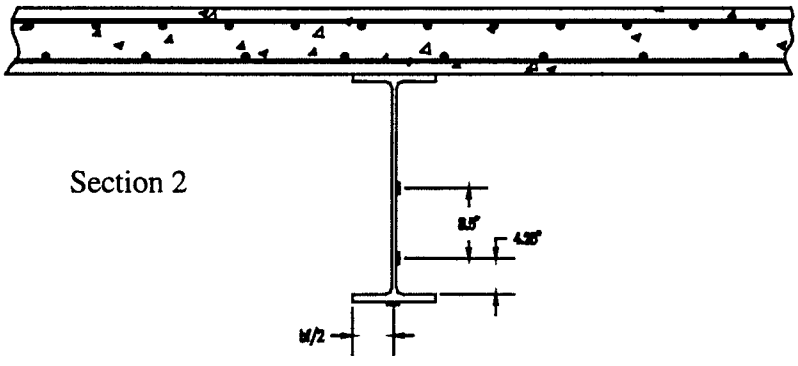

Figure 6.10 Testing Plan VI for Bridge R-289

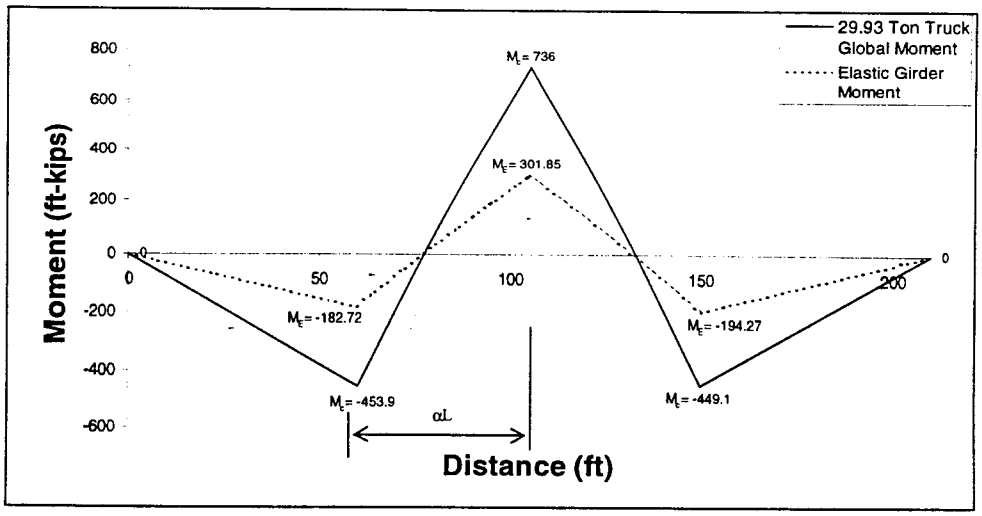

Figure 6.11 Elastic Moments versus Global Truck Moments

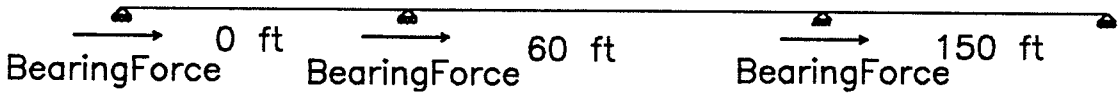

Figure 6.12 Bearing Restraint Force Sign Convention

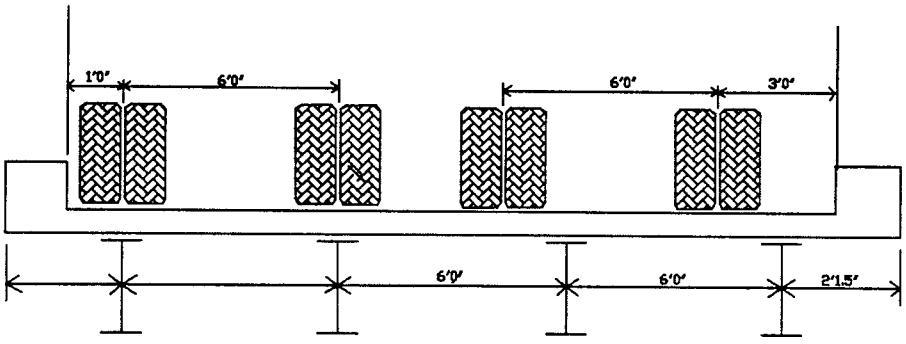

Figure 6.13 Multi-Lane Superposition for Two-Lane Rating

REFERENCS AND BIBLIOGRAPHY

AASHTO [1996], *Standard Specifications for Highway Bridges*, Sixteenth Edition, American Association of State Highway and Transportation Officials, Washington, D.C.

AASHTO [1994], Manual for Conditions Evaluation of Bridges, American Association of State Highway and Transportation Officials, Washington, D.C.

AASHTO [1989], *Guide Specifications for Strength Evaluation of Existing Steel and Concrete Bridges*, American Association of State Highway and Transportation Officials, Washington, D.C.

AASHTO [1983], *Manual for Maintenance and Inspection of Bridges*, American Association of State Highway and Transportation Officials, Washington, D.C.

ANSYS [1997], *Users Manual*, Version 5.3, SAS IP, Inc.

Bakht, B. and Jaeger, L.G. [1990], *Bridge Testing – A Surprise Every Time*, Journal of Structural Engineering, Volume 116, No. 5, May.

Bakht, B. [1988a], *Testing of an Old Short Span Slab-on-Girder Bridge*, Structural Research Report SRR-88-01, Research and Development Branch, Ministry of Transportation, Downsview, Ontario, June.

Bakht, B. [1988b], *Observed Behavior of a New Medium Span Slab-on-Girder Bridge*, Structural Research Report SRR-88-02, Research and Development Branch, Ministry of Transportation, Downsview, Ontario, June.

Bakht, B. [1988c], *Ultimate Load Test of a Slab-on-Girder Bridge*, Structural Research Report SRR-88-03, Research and Development Branch, Ministry of Transportation, Downsview, Ontario, July.

Bakht, B. and Jaeger, L. G. [1982], *The Grillage Analogy in Bridge Analysis*, Canadian Journal of Civil Engineering, Vol. 9, 224-235.

Bakht, B. and Csagoly, P.F. [1979], *Bridge Testing*, Structural Research Report SRR-79-10, Research and Development Branch, Ministry of Transportation, Downsview, Ontairo, August.

Barker, M.G. and Hartnagel, B.A. [1997], *Longitudinal Restraint Response of Existing Girder Bridge Bearings*, Report 97-4, MCHRP, Missouri Department of Transportation, May.

Barker, M.G., Koenig, David, Magruder, L [1994], *Load Rating Steel and Concrete Girder Bridges in Missouri,* Missouri Cooperative Highway Research Program, Report 91-1, University of Missouri Columbia, February.

Barker, M. G. [1990], *The Shakedown Limit State of Slab-on-Girder Bridges*, Doctoral Thesis, University of Minnesota, June.

Beckwith, T.F., and Maragoni, R.D. [1990], *Mechanical Measurements – Fourth Edition*, Addison-Wesley Publishing Company, Reading, Massachusetts.

Burgess, N.T. [1989], *Quality Assurance of Welded Construction*, Applied Science, London, New York, NY.

Chajes, M., Mertz, D., Reichelt, G., and Reid, J. [1995], *Bridge Strength Evaluation Based on Field Tests,* Probabilistic Mechanics.

Frederick, T.L. [1998], *Experimental Load Rating of an Existing Slab on Girder Bridge*, Master's Thesis, University of Missouri, Columbia, August.

Frederick, T.L. [1997], *Development of Bridge Load Test System*, Undergraduate Honors Report, University of Missouri, Columbia, May.

Guedelhoefer, O., Kritzler, R., Pinjarkar, S., and Smith, B. [1990], *Nondestructive Load Testing For Bridge Evaluation and Rating*, National Cooperative Highway Research Board Project 12-28(13) Final Report. Willowbrook, Illinois.

Hahin, C., South, J.M., Mohammadi, J, and Polepeddi, R.K. [1993], *Accurate and RapidDetermination of Fatigue Damage in Steel Bridges*, Journal of StructuralEngineering, January.

Hewlett Packard [1997], *HP 54602B User and Service Guide.*

Hopwood, T. [1996], *Determining Bridge Inspection Requirements for Fatigue Damage Using Reliability*, Proceedings of the Specialty Conference, ASCE, New York, NY.

Imhoff, C.M. [1998a], *Testing and Modeling of Bridge R-289*, Master's Thesis, University of Missouri, Columbia, August.

Imhoff, C.M. [1998b], *Field Testing of State Bridge R-289: Presentation of Data and Results*, Results Volume, University of Missouri,.

Imhoff, C.M. [1997], *Development of an Electro-Optical Deflection Measurement Device for Use in Bridge Field Testing*, Undergraduate Honors Report, University of Missouri, Columbia, May.

Keeling, C. [1997], *Bridge Field Testing of an Existing Steel Girder Bridge*, Master's Thesis, University of Missouri, Columbia, May.

Koenig, D. [1992], *Rating and Posting Practices for Steel Slab on Girder Bridges*, Master's Thesis, University of Missouri Columbia, August.

Labview [1997], *Users Manual*, Version 4.1.

Laman, J.A. [1996], Probabilistic Fatigue Models for Bridge Evaluation, Proceedings of the Specialty Conference, ASCE, New York, NY.

Lichtenstein, A.G. [1993], *Bridge Rating Through Nondestructive Testing*, Final Draft, NCHRP Project 12-28(13)A, Transportation Research Board, National Research Council, Washington D.C., June.

Lichtenstein, A.G. [1990], *Nondestructive Load Testing for Bridge Evaluation and Rating*, Final Report, NCHRP Project 12-28(13), Transportation Research Board, National Research Council, Washington D.C., February.

McDaniel, W.T. [1998], *Field Test of Bridge R-289 By Utilizing University of Missouri Field Test Unit*, Master's Thesis, University of Missouri Columbia, August.

Measurements Group, Inc. [1993], *Micro-Measurement Division Catalogue*, Raleigh, North Carolina.

Missouri Highway and Transportation Department [1990], *Bridge Inspection Rating Manual Inventory and Appraisal Program*, Bridge Division and Maintenance and Traffic Division, Jefferson City Missouri.

National Instruments [1997], *Instrumentation Reference and Catalogue*, Austin, Texas.

NCHRP [1998], *Manual for bridge Rating Through Load Testing*, Research Results Digest HRD 234, Transportation Research Board, National Research Council, Washington D.C.

New York State Department of Transportation [1992], *Bridge Inspection Rating Manual*, Bridge Division and Maintenance and Traffic Division, Albany, New York.

Schrage, S. [1998], *Laser Referenced Deflection Measuring System for Bridge Field Testing*, Undergraduate Honors Thesis, University of Missouri, Columbia, May.

Schulz, J.L. [1993], *In Search of Better Load Ratings*, Civil Engineering, September.

Sulzen, L.M. [1997], *Data Acquisition System for Bridge Field Testing*, Undergraduate Honors Thesis, University of Missouri, Columbia, May.

Tarhini, K.M., Mabsout, M., and Kobrosly, M. [1995], *Effect of Sidewalks and Railings on Wheel Load Distribution in Steel Girder Bridges*, Computing in Civil Engineering, New York, New York,.

Telex [1997], *Operating Instructions: Professional Wireless Intercom System*, Litho USA.

Tripplite [1997], *Omnipower 2000 Owner's Manual.*

Xanthakos, P.P. [1994], *Theory and Design of Bridges*, John Wiley & Sons, Incorporated, Canada.